University of Southampton

Faculty of Engineering and Physical Sciences

Engineering

Optimisation of off-road motorcycle suspensions

by

Felipe Vasquez Stuardo

Thesis for the degree of Doctor of Philosophy

July 2020

University of Southampton

Abstract

Faculty of Engineering and Physical Sciences

Engineering

Thesis for the Degree of Doctor of Philosophy

Optimisation of off-road motorcycle suspensions

by Felipe Vasquez Stuardo

Off-road motorcycles are built for commuting, recreation and racing on roads with significant irregularities and elevation changes. The suspension system absorbs large impulses from the road making transit on these terrains comfortable and handleable. Development of calculation and assessment procedures of suspension characteristics have the potential to improve performance of modern suspensions designed by empirical methods, leading to safer, more enjoyable and faster motorcycles. With this motivation, in this thesis we determine calculation and assessment procedures for the optimisation of off-road motorcycles suspensions.

We begin by determining appropriate performance metrics. To this end we examine the literature for performance indices, we pre-select seven from the literature and propose two for comparison. We compare them with a three degree-of-freedom model under impulsive and continuous excitations representative of off-road. We find that the best suited metrics for performance assessment are the fourth order generalised mean for the accelerations and eighth order generalised mean for the contact forces.

Second, we develop a procedure to estimate contact forces for experimental assessment, motivated by the absence of such a method in the literature. To this end, we derive an overdetermined system of inverse dynamics equations of the motorcycle in the plane. We add a set of constraints to include knowledge of the solution in particular situations. We arrange the problem to solve it efficiently with a non-negative least squares solver and verify the estimations using data from a virtual experiment. We test it with experimental data measured on a motocross track. We find that the estimated contact forces vary consistently with the track, and conclude that is an appropriate tool for performance comparisons.

Third, we develop a suitable rider model for the estimator. We consider a passive model, as the literature suggests and we compare it against a basic model derived assuming the fundamental motion of the rider. When tested with experimental data the basic rider yields more realistic than the passive one, providing evidence that passiveness is not a valid assumption for rider modelling and we provided an alternative model for estimation of forces.

Fourth, we calculate an optimal suspension to understand its characteristics. To this end, we investigate methods to calculate optimal suspensions to select a suitable one, we apply it to a

cross motorcycle, where we optimised stiffness and damping in whoops, braking and acceleration using a sophisticated motorcycle model. We use a multiobjective genetic algorithm to obtain the Pareto fronts. We analyse the correlations between suspension parameters and performance finding that performance in whoops significantly correlated to eight of the ten design variables established, while braking and acceleration are correlated to four each. Also we find that there is conflict between performance in whoops, and braking and accelerating, while not among these two.

Declaration of Authorship

I, Felipe Vasquez Stuardo, declare that the thesis entitled *Optimisation of off-road motorcycle suspensions* and the work presented in the thesis are both my own, and have been generated by me as the result of my own original research. I confirm that:

- this work was done wholly or mainly while in candidature for a research degree at this University;
- where any part of this thesis has previously been submitted for a degree or any other qualification at this University or any other institution, this has been clearly stated;
- where I have consulted the published work of others, this is always clearly attributed;
- where I have quoted from the work of others, the source is always given. With the exception of such quotations, this thesis is entirely my own work;
- I have acknowledged all main sources of help;
- where the thesis is based on work done by myself jointly with others, I have made clear exactly what was done by others and what I have contributed myself;
- parts of this work have been published as:
  - Vasquez F., Lot R., Rustighi E., Pegoraro R.(2020) Tyre force estimation for off-road motorcycles *Mechanical Systems and Signal Processing, under review*
  - Vasquez F., Lot R., Rustighi E. (2019) Off-road motorcycle tyre force estimation. *Journal of Physics: Conference Series 1264 012020*

Signed: .....

Date: .....

Table of Contents

List of Figures

Acknowledgements

First, I would like to acknowledge my supervisors Roberto and Emiliano, for contributing with ideas that led the course of the thesis, for solving dead-ends, for corrections of texts, and dealing with the paperworks. Also for the contact made with WP Suspension GmbH. From this company, I would like to acknowledge Roberto Pegoraro, Alexander Brenner and Bert Meyer, for the experimental data provided. To BecasChile for the scholarship number 72170605 provided to fund the PhD.

Additionally, I would like to acknowledge the support given by friends and family. Freddy Paiva, Paulo Flores and Mario Razeto who motivated me to study abroad; Ricardo Rojas who introduced me into motorsport suspensions; Neto, Alex Pomeri, Cristian Sanchez and Cesar Rojas, for showing me the motorcycle passion; Orval, Pinto, Rodolfo, Adolfo and Jorge who gave me support in the hard times; Aldo, Maria Elena and Jaime, for the good times when I visited home, and lending me motorcycles; Eduardo, Canales, Anibal, Rafael and Benjamin for hosting me around Europe; to Richard, Carolina, Carina, Reyna, Felix and Loreto, for Chilean atmosphere in Southampton; Patrick, Francesco, Zohra, Horacio, Ulises, Rodolfo, Andrea, Joan, Yann, Hynek, Roberto, Gerardo, Noel, Miika and Eirini for the laughs and good times in Southampton; Nikos, for the nice conversations; Thanasis, for the music and company; Guru Ander for help in Matlab; and Angelis for the many insights we had together. To my mother, for being always present even in the distance and her endless love; Nacho, for coming to Europe every summer to visit me and for giving me an itunes account, with which I could work for hours undistracted. Nico, for always being attentive in how I was, and for giving joy when I visited home. Rosa, for being worried on the distance and treated me with love when I visited home. To Berto, Rosa, Alber y Javi for receiving me at your place and making me feel at home at the other side of the world. Your support, allowed me to finish the thesis on time. Lastly, to Elena, for opening my mind, for showing me how to enjoy life, and for the endless patience and support throughout the thesis. Your love has been endless, I want to continue sharing it.

CHAPTER 1

Introduction

1.1 Motivation

Off-road motorcycles are built for commuting, recreation and racing on roads with significant irregularities and elevation changes. Their suspension system absorbs large impulses from the road, making transit on these terrains comfortable and handleable. Due to the central role played by this system in the overall performance of the motorcycle, the question arises naturally, how to optimise off-road motorcycle suspensions?

Modern suspensions systems are designed by empirical methods which have, at least, two limitations. First, there is limited theoretical understanding on the relationships between design variables and performance of the system. Classical vibration theory provides only qualitative foundations, since it is limited by the strong non-linearities existing in the system, such as large displacements of the chassis, and non-linear forces arising from rider commands, detachments, stopping rubbers, and purpose built non-linear stiffness and damping. Therefore, development is conducted by experienced engineers over existing designs. Second, testing relies mainly on the feedback of the rider. He/she has to assess the performance of the motorcycle by sensing vibration isolation, road grip, and overall behaviour. This sensing is inherently subjective since it depends on rider's previous experience and driving skills. Therefore, testing is usually conducted by experienced riders such as retired race drivers.

Development of calculation and assessment procedures, have the potential to improve performance of current suspensions, leading to safer, more enjoyable and faster motorcy-

cles.

1.2 Literature review

Development of suspension systems requires the definition of performance indices, since they define the sense in which the suspension is optimal. Performance, considered as the global behaviour of the vehicle, describes its comfort and handling capabilities [2–5]

On one hand, comfort describes the vibration isolation between road and chassis [4]. Chassis accelerations are assessed by methodologies suggested by national and international standards [6–9]. For example, ISO 2631-1 [6] which is widely adopted [10–14], suggests a basic evaluation method consisting on the root mean square value (rms) of the frequency-weighted accelerations. The frequency-weighting is performed by a filter, included in the standard, to take into account human-body sensitivity. It also suggests a method to assess severe vibration consisting on the fourth order mean (rms4) times the sampling period to the power of one fourth. Simpler methodologies are also widely used to assess chassis accelerations, such as the rms of the (un-weighted) accelerations [2, 15–20] the maximum acceleration [21–23] and the standard deviation [24, 25].

On the other hand, handling describes the lateral and longitudinal capabilities of the vehicle. The direct approach to assess handling is by considering standardised manoeuvres, each of which has specific indices [26–28]. The indirect approach, is by considering the normal force, since any longitudinal or lateral manoeuvre depends on this force. The latter is commonly assessed by the rms of the contact forces or tyre deformations [2, 16, 18, 19, 21, 29] and also by the standard deviation [24, 25, 30].

Additionally, the working space of the suspension is also considered. Some authors consider it as an objective [16, 18, 24, 30–32], others as a constraint [21, 23] and others include it implicitly in the stiffness description [33].

Development of suspension systems also requires understanding of the fundamental dynamics of the motorcycle. The most basic model able to capture chassis accelerations, wheel load variations and suspension stroke is the single-wheel-station model [2], also known as quarter-car model [4], which consist on two masses connected by the suspension system between them, and by a spring to the ground. The system is excited by a vertical displacement of the road which has a power spectral density (psd) modelled as a power function by ISO 8608 [1]. This representation has been widely used [2, 19, 29, 31, 34–37] as well as a double slope psd for improved matching with experimental data [34, 35, 37]. An analytical expression for optimal stiffness and damping as a function of the relative importance between comfort, road holding and working space [2], demonstrate the conflict between comfort and handling, described by other authors [4, 24, 38], and the conflict between comfort and working space, also described by other authors [31, 39].

Inclusion of non-linearities into the model makes derivation of general analytical solutions cumbersome and can only be found for particular cases. For example, by considering the asymmetric behaviour of the damper, i.e. different behaviour in compression than extension [20, 38, 40], it can be shown that it improves performance with respect to linear damping [34]. Also, by considering the progressivity of the damper, i.e. force as a power function of the velocity [38], it can be shown that actually linearity is a reasonable choice [39].

Enhancing the model to include front and rear dynamics, allows to detect front and rear wheel interactions as well as pitch-bounce interaction. The de-coupling between front and rear single-wheel-stations occur if the radius of gyration of pitch inertia squared, equals the product of the distances from front and rear wheels to centre of mass. This is quantified by the coupling mass [2] or equivalently the dynamic index [4, 5]. With typical vehicle parameters, the condition is nearly met, therefore, considering single-wheel-station model for optimisations is a reasonable choice. Moreover, it has been shown that without the condition being met, the interaction between front and rear tyre compressions is small [29]. Regarding pitch-bounce interaction, it has been shown that if the stiffness ratio (front suspension stiffness times its distance to centre of mass over rear suspension stiffness times its distance to centre of mass) is close to one, pitch motion over the rider is reduced which is beneficial for comfort [4]. Additionally, it has been shown that if front and rear are decoupled together with bounce and pitch, the vibration is unpredictable, and therefore is a situation to avoid [4].

Optimisations of realistic models, which include large displacements and rotations, and non-linear description of forces, requires numerical solutions. The basic formulation, is a single objective optimisation, in which the objectives are weighted into a single one such as in [22, 41]. Non-linear damper forces are easily included in this procedure such as bilinear [16], exponential [14] or B-spline [41]. Although the solution has a low computational cost, it is difficult to select the weights [42] and it gives no insight into the relation between design variables and performance indices [30]. The advanced formulation is multi-objective optimisation, which minimises the objectives simultaneously without requiring weighting. The set of solutions is the Pareto-optimal set, also called Pareto front, in which each solution improves at least one objective function and worsens at least one of the others. The advantage of this formulation is that multiple variables can be optimised for several situations simultaneously, as seen for example in [24, 25, 42]. Additionally, all the optimal solutions are known, as well as their relation to the objective function.

For simple to medium complexity problems, iterative algorithms are well suited to solve optimisations. They move towards the minima by knowing explicitly, or approximating, the first and possibly the second derivatives of the objective function. They are efficient in finding the minima, but they could get trapped in local minima [12]. For complex problems, heuristic algorithms are used, and in particular in vehicle dynamics, genetic

algorithms are widely used [16,21,22,24,42,43]. They consist of a population being reproduced iteratively, allowing the best fitted individuals to reproduce to the next generation, leading towards the optimal solution. The advantage of these algorithms is that they approach the global minima efficiently, however, it requires a large computational effort, convergence to the minimum is not guaranteed and progress after approaching the global minima is not efficient.

Experimental testing relies on the rider's feedback. For a broader insight into the motorcycle's behaviour, this feedback could be complemented with measurements of the variables correlated to performance. Accelerations can be measured directly by accelerometers, while contact forces are not easily measurable. Direct measurement of the contact forces by force transducers is expensive and used only for vehicle development. For applications in production vehicles, estimators are used instead [44]. Estimators for two-wheeled vehicles have been developed for lateral dynamics [45, 46] assuming on-road conditions, while force estimators assuming off-road conditions, is an open topic. Development of an estimator, requires to manipulate a set of equations and solve for the forces. Since it is a multibody problem [47], the set of equations is cumbersome to deal with by hand, and instead can be done symbolically, for example in MBSymba [48, 49].

The estimator requires knowledge of the rider force over the motorcycle. The rider drives in standing position, where arms and legs provide significant vibration isolation to the mass of the rider [50], which contributes significantly to the overall dynamics of the motorcycle [51]. Motorcycle rider models have been developed assuming a seated position, since they consider on-road driving and focus has been put on control strategies [51–53]. Rider models in standing position are found in similar activities, such as off-road cycling [50, 54] and horse riding [55]. The basic configuration in these models consists of one or more masses attached by passive elements (spring-damper) to the base (bicycle or horse). The masses are excited by vertical and possibly pitch motion of the base, from where the forces are retrieved.

Summarising, improvement and optimisation of suspensions performance requires calculation and assessment procedures that have not been developed for off-road motorcycles. For example, the design process requires an appropriate definition of performance for these motorcycles, and knowledge of the relationships between variables and performance. The former needs to be selected from the existing indices, while the latter can be obtained through a multiobjective optimisation, which in turn, requires an off-road motorcycle model that is not available. Additionally, objective methodologies for experimental testing of these motorcycles are non existent, requires development of an estimator which addresses the peculiarities of off-road, and a rider model for which only ideas from other activities are present.

the calculation procedure of an optimal suspension. The understanding of the character-

istics of an optimal suspension, as well as the relations between variables and performance can guide the design process as well help on in-field tuning

onsidering the importance of a procedure to assess performance experimentally for in-field testing and fine tuning of suspensions

1.3 Aims and objectives

The aim of this thesis is to determine calculation and assessment procedures for the optimisation of off-road motorcycle suspensions.

In particular, the objectives of this thesis are to:

- define and recommend performance metrics,
- develop an estimator of contact forces for the experimental assessment of performance,
- develop a rider model pertinent for the estimator,
- understand the characteristics of optimal suspensions and the influence of variables on performance.

1.4 Contributions of the thesis

The contributions of this thesis to the state-of-art are fourfold.

- First, the recommendation of fourth-order-average (rms4) of frequency-weighted or non-weighted chassis accelerations and the eight-order-average (rms8) of the contact forces as pertinent criteria for performance of off-road motorcycles.
- Second, the development of an estimator of the contact forces for these motorcycles, which considers in-plane dynamics and generic forces of the rider acting over foot-peg and handlebar.
- Third, the development of an elementary rider model in standing position to be used in the estimator and evidence that the rider executes significant active actions.
- Fourth, a procedure to optimise suspensions in these motorcycles, together with a description of the optimal set of suspensions on whoops, braking and acceleration for a cross motorcycle, as well as the correlations between design variables and performance in these situations. Additionally, the inference that whoops performance is in conflict with that of braking and accelerating, and that these two are not in conflict.

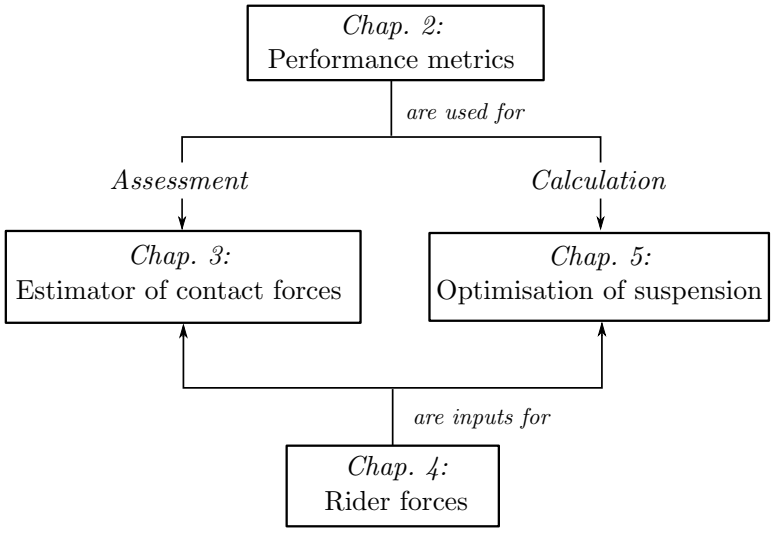

Figure 1.5.1: Thesis organisation

1.5 Outline of the thesis

In this thesis, we present tools for two areas of suspension development: experimental assessment and design calculations, which are supplemented by two complementary chapters as summarised in Figure 1.5.1. We begin defining meaningful metric of performance in Chapter 2. To this end, we examine the literature and compare pre-selected indices using a three-degree-of-freedom model excited by representative conditions of off-road.

We continue by presenting the experimental assessment procedure in Chapter 3. Here, we address the problem of measurement of contact forces. In particular, we present an inverse dynamics model of the motorcycle and a set of constraints which together form the estimator equations. Additionally, we present a signal processing procedure with which is possible to obtain an estimation of the contact forces only from kinematic measurements. In this estimator, the forces of the rider are required, for which we develop a model in Chapter 4.

Next, we present tools for design calculations in Chapter 5. In particular, we present an optimisation procedure. To this end, we investigate suitable methods for optimisation, apply the relevant one to a particular class of motorcycle for which we use the rider model of Chapter 4 and a forward dynamics motorcycle model (different from the model of Chapter 3), and analyse the relations between the optimal solutions.

Lastly, in Chapter 6, we summarise the analysis performed throughout the thesis, we highlight the contributions to the state-of-art, and suggest future work.

CHAPTER 2

Definition of the performance criteria

The definition of the performance criteria is essential to our study. It defines the sense in which the motorcycle is optimal and defines the quantities that we seek to measure and improve throughout this thesis. Therefore, it is necessary to search for meaningful quantities that capture the essence of performance of off-road motorcycles.

In this chapter, we determine appropriate metrics to assess performance in these motorcycles. To this end, a review of performance criteria used in vehicle dynamics is presented. Relevant indices are pre-selected and compared under continuous and impulsive excitations, to conclude with a selection of performance metrics for off-road motorcycles.

2.1 Review of performance indices used in vehicle dynamics

In this section, we present a brief review of performance metrics used in vehicle dynamics. We begin by defining performance, comfort and handling, next, we review comfort indices followed by handling indices, and we conclude by pre-selecting seven indices and proposing two more, for comparison in the next section.

The measurement of performance aims to correlate the subjective perception that the driver has of a vehicle to a physical variable that can be measured objectively. There are different definitions of performance depending on the authors, and even within one book. As an example of this, we examine Road and Off-road Vehicle System Dynamics Handbook [3] edited by G. Mastinu and M. Ploechl. In Chapter 29; "ride comfort and road holding", K. Popp refers to *vehicle performance* as a criterion to assess longitudinal

motion of a vehicle, in opposition to driving stability, a criterion to assess lateral motion, and *ride comfort* and safety, a criterion to assess vertical motion. Similarly, in Chapter 34; "dynamics of off-road vehicles", J. Wong, refers to *performance* as the ability to overcome motion resistance, negotiate a slope and other longitudinal motion conditions, which is different to *handling*, which refers to steering response to driver commands, and *ride quality*, which refers to vibration isolation. Differently, in Chapter 31; "active and semi-active suspension control", D. Hrovat, refers to *performance* in terms of *ride comfort* (good vibration isolation), vehicle *handling* (good road holding to increase safety, control and stability) and suspension stroke. In a similar way, in Chapter 37; "subjective and objective evaluations of car handling and ride", G. Gim indicates that *handling* and *ride performances* are grouped in five capabilities: straightability, steerability, controlability, stability, and comfortability. Furthermore, in Chapter 36; "vehicle comfort", K. Siebertz describes *comfort* in terms of vibrations, ergonomics and climate (temperature, moisture, radiation and air speed). Although, more examples can be found, the five given here help to illustrate that performance, handling and comfort do not have a unique meaning.

In this thesis we will refer to performance as a description of the global behaviour of a vehicle (as Hrovat and Gim) and to handling as a description of longitudinal and lateral capabilities of the vehicle. On the other hand, we will use the term comfort to refer to vibration isolation of the driver, instead of ride quality, ride comfort or ride as used by some authors.

Next, we present a review of the main comfort and handling indices used in vehicle dynamics.

2.1.1 Performance indices used to assess comfort

While driving a vehicle, the human body is exposed to vibrations from multiple sources, such as road, engine and aerodynamics. The suspension system, together with the tyres and the seat, aim to mitigate vibration transmission from the road, since exposure to lower vibration accelerations correlates with a greater comfort. It is reasonable then, to assess the effectiveness of a suspension system in providing comfort by evaluating the accelerations received by the driver.

The representation of the accelerations with a single index is not trivial. It requires considering factors such as driver receiving vibrations in more than one point (gluteus, back, feet and hands), in more than one direction (6-axis), and the frequency dependency with which human perceive vibrations. To represent these vibration accelerations into a single index, international standards recommend methodologies which take into account these factors. For example, ISO 2631-1 [6] treats the evaluation of human exposure to whole-body vibrations, while ISO 5349-1 [7] treats exposure to hand vibrations. Moreover, some countries have their own standards to evaluate human vibrations, such as Germany, which

has VDI 2057 [9], and United Kingdom, which has BS 6841 [8]. Considering that in vehicle dynamics all of these standards are equivalent in providing an objective measurement that correlates to the subjective evaluation of passengers [56], we only summarise the methodology provided by ISO 2631-1, since it is the most commonly adopted.

The basic methodology of this standard is to use the weighted root mean square (rms) acceleration,

$$\Phi_{a_w} = \mathrm{rms}(a_w(t)) = \left(\frac{1}{T} \int_0^T a_w^2(t) dt \right)^{1/2}, \tag{2.1.1}$$

where, $a_w(t)$ is the weighted acceleration over time, and T, the duration of the measurement. The weighted acceleration is calculated by applying frequency-weightings curves that are dependent on the position (seated, standing and recumbent) and on the aim of the evaluation (health, comfort and perception, or motion sickness) [6]. The applicability of this method is bounded to non-severe vibrations.

In order to detect severe vibrations, two criteria are given. The first is if the crest factor cf is larger than nine,

$$cf = \frac{\max(|a_w(t)|)}{\Phi_{a_w}} > 9. \tag{2.1.2}$$

The second is if the ratio between VDV (defined next) and Φ_{a_w} normalised by the fourth root of the measurement time is larger than 1.75. In the absence of a name in the standard, we will refer to it as severity ratio r,

$$r = \frac{VDV}{T^{1/4} \Phi_{a_w}} > 1.75. \tag{2.1.3}$$

In the case of severe vibrations, one of the following two indices should be determined as well. The running rms,

$$a_w(t_0) = \left[\frac{1}{\tau} \int_{t_0-\tau}^{t_0} a_w^2(t) dt \right]^{1/2}, \tag{2.1.4}$$

where, τ is the time-width of the running window, and t_0 is the instantaneous time of observation, or the fourth power Vibration Dose Value (VDV),

$$\mathrm{VDV} = \left(\int_0^T a_w^4(t) dt \right)^{1/4}, \tag{2.1.5}$$

where, T is the sampling time. This standard, ISO 2631, has been used in [10–14, 57]; BS 6841 in [58–60]; and VDI 2057 in [24].

These are not the only indices used for comfort evaluation in vehicle dynamics. Sim-

pler ones, such as rms, maximum value (max) and standard deviation (std), of the (unweighted) accelerations have been also used. For example, the rms of accelerations,

$$\Phi_a = \text{rms}(a(t)) = \left(\frac{1}{T} \int_0^T a^2(t) dt \right)^{1/2}, \tag{2.1.6}$$

has been used in [15–18], while the maximum value,

$$a_M = \max(|a(t)|), \tag{2.1.7}$$

has been used in [21–23], and the standard deviation, in [30].

A peculiar set of indices have been used for the analysis of off-road motorcycles suspensions by Vliet [33]. He derived them to analyse the deterministic response of a single-degree of freedom motorcycle, to a sinusoidal road and to a landing. For the stationary response, he considers a linear combination of the vertical displacement transmissibility at the natural frequency ω_n and at eight times the natural frequency $8\omega_n$,

$$V_s = a_1 \frac{z_{\omega_n}}{z_0} + a_2 \frac{z_{8\omega_n}}{z_0}, \tag{2.1.8}$$

where, z_0 is the road amplitude, and a_1 and a_2 are scalar weights. For the transient response, he considers the peak force F_{max} transmitted to the chassis with respect to a theoretical optimal force F_{opt},

$$V_t = \frac{F_{max}}{F_{opt}}. \tag{2.1.9}$$

The optimal force was defined as the constant force, that doing mechanical work along the complete suspension stroke in the first compression, would dissipate all the kinetic energy of the system at the moment of impact. From conservation of energy law he shows it to be

$$F_{opt} = \frac{mv^2}{2l_{max}}. \tag{2.1.10}$$

In his single-degree-of-freedom model used for analysis, this force is proportional to the chassis acceleration, and also it is the contact force with the ground, therefore, is an assessment of comfort and road holding simultaneously. However, since the intention of Vliet is to measure “shock isolation” of the motorcycle, we consider it as a measure of comfort.

2.1.2 Performance indices used to assess handling

Multiple indices have been defined to assess handling since vehicles can perform multiple longitudinal and lateral manoeuvres. In order to provide a common basis for comparison, some driving manoeuvres have been standardised, for example severe lane-change and obstacle avoidance in ISO 3888:2018, braking in a turn in ISO 7975:2019, and power-off reaction of a vehicle in a turn in ISO 9816:2018. Each of these manoeuvres are assessed by diverse metrics, which results in a large number of indices representing handling. For example handling metrics in motorcycles include steering torque to roll angle, steering torque to yaw rate and yaw rate to roll rate [26], maximum steering torque to roll rate and maximum steering torque to yaw rate [27], lane change roll index [28] and braking distance [61] among others.

Handling is also assessed indirectly by the normal tyre forces, usually referred to as road holding. The basis for this approach is that any lateral or longitudinal manoeuvre requires a tangential force on the tyre, which essentially depends on the normal force. In this way, handling can be measured by a single index. This index, is a common criterion for ride safety, since it determines the available braking and lateral guidance forces required to avoid accidents.

Indices used to assess road holding are mainly the rms [16, 18, 21, 41, 62] and less frequently the std [24,30] of the normal force or tyre radial deformation. A different approach, is measuring the flying time of the wheel, which is defined as the sum of time intervals Δt in which the normal load on the wheel N has been null [63].

$$\text{flyt} = \sum \Delta t_{N=0} \tag{2.1.11}$$

2.1.3 Performance indices used to assess other aspects

There is a third aspect which is also relevant in the design of suspension systems, which is the suspension stroke. This is because the maximum stroke of the suspension produced with the expected excitations, must lie within the available space.

The way in which this aspect is included into optimisations is not unique. On the one hand, some authors consider the stroke as an objective (or part of an objective) to minimise [16,18,24,30,32]. On the other hand, other authors include the maximum stroke as a constraint of the optimisation [21, 23]. A third approach consists of including the stroke directly in the physical model used in the optimisation [33]. Specifically, the rubber stop at the end of the stroke is included as a high stiffness spring which limits the maximum stroke as in the real world. Suspension configurations that reach the maximum stroke are detected indirectly by the large accelerations that are generated when the rubber stop is reached.

2.1.4 Summary and pre-selection of indices

Summarising, performance is assessed by comfort and handling metrics. Both are subjective perceptions of the rider that are correlated to objective measurements. On the one hand, comfort correlates with vibration accelerations on the rider or chassis, which are assessed by simple statistical metrics such as rms, std or max, or according to standards (ISO 2631, BS 6841, VDI 2057, among others) that use frequency-weighted accelerations to consider rider perception. On the other hand, handling correlates to several driving parameters and is assessed directly or indirectly. Directly, handling is assessed by the behaviour of the vehicle in specific manoeuvres, usually standardised, each of which is measured by diverse variables. Indirectly, handling is assessed by road holding, which is measured by the normal force on the tyres. In both cases, the statistical metrics used to describe the normal force are rms, std or max, and in a different approach, the total flying time.

In order to select appropriate metrics to assess performance, we choose some of the reviewed indices for comparison, as follows, On the one hand, for comfort, we compare five indices. First, we choose Vliet's indices [33], Equations 2.1.8 and 2.1.9, since they have been used for the same purpose as this study. Second and third, we choose metrics from a standard. Considering that every standard is equally representative [64], we choose ISO 2631 because of its availability. From this standard, we consider the rms of the frequency-weighted accelerations, Equation 2.1.1, since it is the basic method. For severe vibrations, we modify the VDV, Equation 2.1.5, to compare it in the same scale as the rms by considering the nth order generalised mean definition. The nth order generalised mean of a signal $x(t)$, which we refer to as rms-n because of its relation to the rms, is defined as

$$\text{rms-}n\,(x(t)) = \left(\frac{1}{T}\int_0^T x(t)^n dt\right)^{1/n}, \tag{2.1.12}$$

where, with $n = 1$, we obtain the mean value; with $n = 2$, the rms; with $n = \infty$, the maximum value; and with $n = -\infty$, the minimum value, to name some. In this way, by dividing VDV by the fourth root of the measurement time, we modify it to a fourth order generalised mean,

$$\text{rms4}(a_w(t)) = \left(\frac{1}{T}\int_0^T a_w^4(t) dt\right)^{1/4}, \tag{2.1.13}$$

which is the index we use for comparison.

As fourth and fifth indices, we choose to compare the rms and rms4 of the un-weighted accelerations, to study the effect of the frequency-weighting. In this way, the comfort indices to be compared are Vliet$\{V_s$ or $V_t\}$, rms(a_w), rms4(a_w), rms(a), and rms4(a).

On the other hand, for handling, we choose to measure it indirectly by road holding, since it allows to consider implicitly multiple manoeuvres with a single index. For road holding, we choose to compare four indices. First, we choose the rms of the contact forces since it is the most commonly used. Second, we choose the time spent flying, flyt, because in off-road the loss of contact is recurrent, and no discussion is found in the literature relating statistical index with the loss of contact. In addition to these two indices, we decide to consider other generalised orders of mean. Orders closer to one tend to capture the central tendency of data, while higher and lower orders tend to capture the extreme values. Since we are interested in capturing both, the average and peak values of forces, we choose to include the rms4 and the rms8 of the contact forces in the comparison as well. These indices are not found in the vehicle dynamics literature, but we think they could provide a better approximation to the average and peak values, than the rms. In this way, the handling indices to be compared are rms(N), rms4(N), rms8(N), and flyt(N).

2.2 Methodology to compare pre-selected indices

In this section, we describe the methodology used to compare the indices pre-selected in Section 2.1.4. In particular, we require to test if the indices are able to condense accelerations and contact forces without losing three features of interest: vibration isolation, impacts and detachments. First, we take into account vibration isolation between road and rider to assess comfort properly. Second, we consider impacts from road excitation and maximum compressions of tyre, suspension, and rider, since these impacts reduce comfort and could injury the rider. Third, we consider tyre detachments since they reduce handling capabilities. These three features depend on the road excitations and suspension parameters. Therefore, to test the indices we calculate them under several driving conditions and a range of suspension parameters to verify if the changes are captured. In the following, we explain the motorcycle representation, next, the driving situations taken into account, and lastly, the suspension considered.

2.2.1 Motorcycle dynamics model

We test the indices using the simplest motorcycle model able to capture the features of interest. In order to capture vibration isolation between road and chassis, as well as the maximum compression (bottoming) of the suspension, we need to consider sprung and unsprung mass displacements independently. In the same way, to capture vibration isolation between chassis and rider, which is significant in off-road riding [50], as well as rider bottoming, we need to consider chassis and rider displacement independently. The remaining phenomena of interest, namely, tyre detachments, and impacts from road excitation and tyre bottoming, can be captured with an appropriate tyre force description.

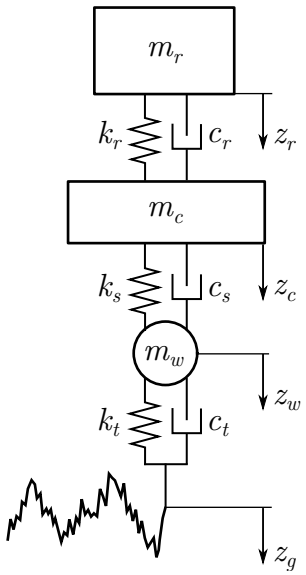

Figure 2.2.1: Three degree of freedom motorcycle model. Subindices r, c, w , s , t and g refer to rider, chassis, wheel, suspension tyre and ground respectively. The suspension of the rider represents the muscular action of legs and arms.

Consequently, a formulation with three vertical degrees of freedom and three bodies, Figure 2.2.1, is a reasonable choice to test the indices.

The equations of motion of this system are:

$$m_r \ddot{z}_r = -f_r + m_r g, \tag{2.2.1}$$

$$m_c \ddot{z}_c = -f_s + f_r + m_c g, \tag{2.2.2}$$

$$m_w \ddot{z}_w = -f_t + f_s + m_w g, \tag{2.2.3}$$

where, m and z refer to mass and downward displacements, subindices r, c and w refer to rider, chassis, and wheel, f_r, f_s, f_t are rider, suspension and tyre forces, respectively.

The forces acting on this system are considered as follows. On the one hand, suspension and tyres forces are well known to be passive and non linear [4, 5, 38]. To simplify the representation, we consider linear dampers since this simplification does not deteriorate significantly the ability to capture vibration isolation, impacts and detachments. Similarly, the stiffnesses are considered linear in the working range. On the other hand, the rider force is a combination of active and passive elements. Of these, the passive elements have been modelled as linear springs and dampers in off-road cycling and horse riding [50,54,55], which are similar activities. Contrarily, the active element, consisting of the contraction of leg and arms muscles, has been neglected in these studies. This assumption is reasonable for small amplitude excitations, however it might not hold for larger ones. Nonetheless, due to the lack of further information in the literature in similar activities, we disregard it. In this way, the elastic and damping forces f^l in the working range are linear, and

described as,

$$f_r^l = k_r(z_r - z_c) + c_r(\dot{z}_r - \dot{z}_c), \tag{2.2.4}$$
$$f_s^l = k_s(z_c - z_w) + c_s(\dot{z}_c - \dot{z}_w), \tag{2.2.5}$$
$$f_t^l = k_t(z_w - z_g) + c_t(\dot{z}_w - \dot{z}_g). \tag{2.2.6}$$

Notice that compressions have been defined positive.

In order to capture impacts due to bottoming (bottom of the working range), we add a harder stiffness at the maximum compression. This is done by an elastic force which is activated when the relative displacement between corresponding bodies exceed the maximum compression. The activation is modelled by a saturation function $s(.)$, which is one for positive arguments and null for negative ones. Details of the function are described in Appendix A.1. In this way, the bottoming forces f^b are,

$$f_r^b = n_r^b k_r(z_r - z_c - z_{rM})s(z_r - z_c - z_{rM}), \tag{2.2.7}$$
$$f_s^b = n_s^b k_s(z_c - z_w - z_{sM})s(z_c - z_w - z_{sM}), \tag{2.2.8}$$
$$f_t^b = n_t^b k_t(z_w - z_g - z_{tM})s(z_w - z_g - z_{tM}), \tag{2.2.9}$$

where, n^b is a bottoming factor that amplifies the stiffness of the working range and subindex M refers to maximum value.

Additionally, on suspension and rider forces we add a harder stiffness in extension to capture the maximum extension end. Reaching this end can make the wheel to be lifted by the chassis, and the chassis by the rider, which in turn, can result in wheel detachment. To activate these extension forces f^e, we also use a saturation function,

$$f_r^e = n_r^e k_r(z_r - z_c)s(-(z_r - z_c)), \tag{2.2.10}$$
$$f_s^e = n_s^e k_s(z_c - z_w)s(-(z_c - z_w)), \tag{2.2.11}$$

where, n^e, is the analogous of n^b for extension.

Lastly, an extension force does not exist in the tyre, therefore when the tyre reaches maximum extension, detachment occurs. To activate the tyre force only in compression, a saturation function is applied to the entire force. In this way, the total forces are,

$$f_r = f_r^l + f_r^b + f_r^e, \tag{2.2.12}$$
$$f_s = f_s^l + f_s^b + f_s^e, \tag{2.2.13}$$
$$f_t = (f_s^l + f_s^b)s(z_w - z_g), \tag{2.2.14}$$

which results in tri-linear characteristics for stiffness and linear for damping, as seen in Figure 2.2.2.

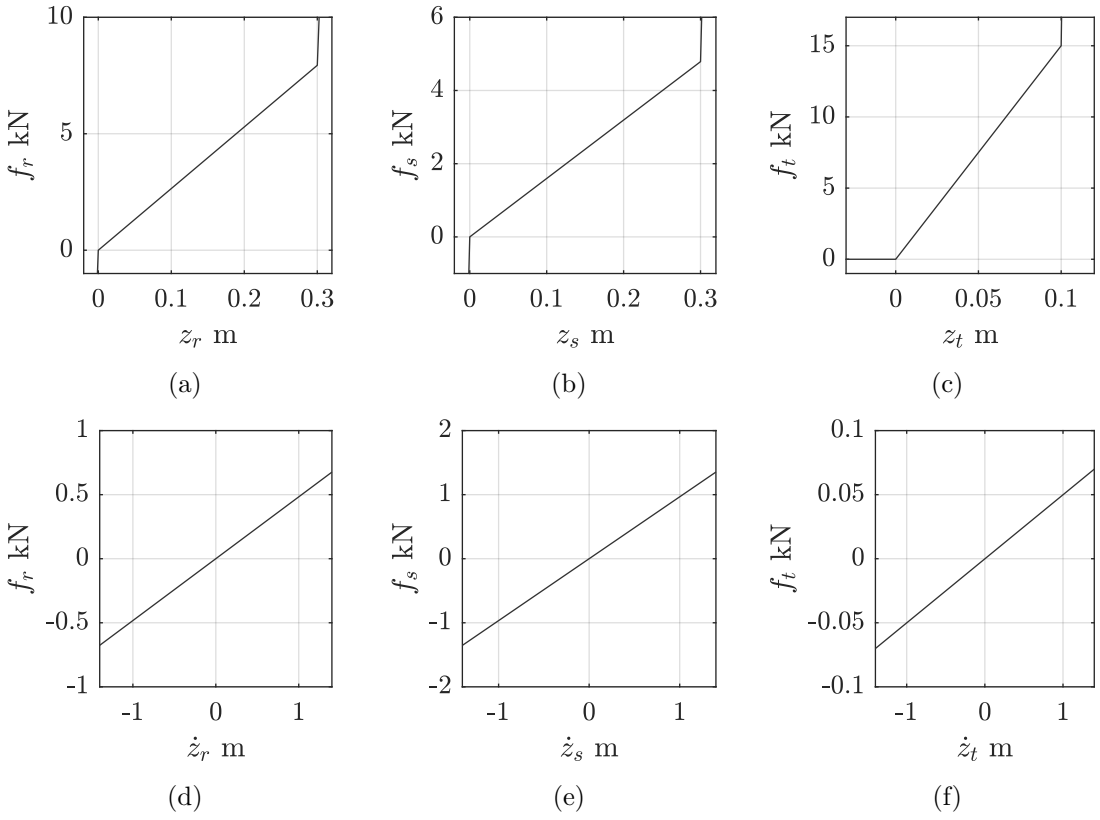

Figure 2.2.2: Rider, suspension and tyre forces. (a), (b), and (c) show f_r, f_s, and f_t forces (Equations 2.2.12 to 2.2.14) under compression and zero velocity, while (d), (e), (f) show f_r, f_s, and f_t forces under a velocity and zero compression. z_r, z_s and z_t are rider, suspension and tyre compressions. Parameters: $k_r = 26464$ N/m, $k_s = 15961$ N/m, $k_t = 150000$ N/m; $c_r = 47536$ Ns/m, $c_s = 966$ Ns/m, $c_t = 483$ Ns/m; $n^b = n^e = 50$. Details on sources in Appendix A.3.

2.2.2 Definition of driving situations

The driving situations need to represent the typical range of excitation of an off-road motorcycle, which we define based on two sources. The first one, Durbin et al. [65], indicates that typical off-road riding conditions include open desert, sand dunes, motocross tracks, mountains and other trails, and that typical mean and maximum speeds are around 10 m/s and 20 m/s. The second one, is experimental data measured on a motocross track provided by WP Suspension GmbH (details of measurement are explained in Chapter 3), Figure 2.2.3. It can be seen that the signals consist of random oscillations and peaks, which we generalise as continuous and impulsive excitations. In particular, accelerations consist of a base signal between -2 and 4 g, with peaks of 10 g, while contact forces consist of a base signal between 0 and 3 times the static force, and peaks of 3 and 6 depending on front or rear tyre. Based on these experimental observations, we consider continuous and impulsive excitations of different magnitudes.

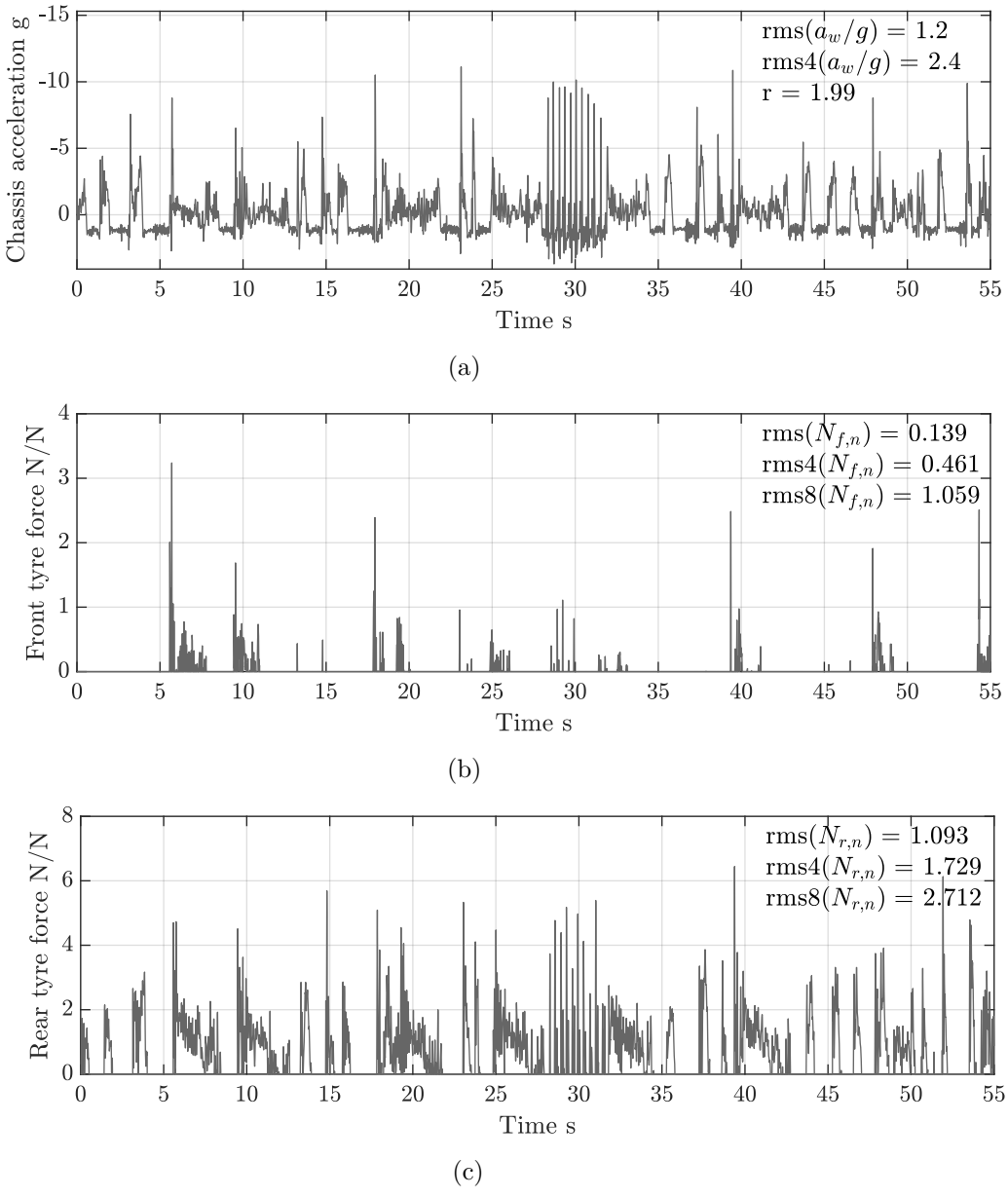

Figure 2.2.3: Accelerations and tyre forces obtained experimentally on a motocross track. The acceleration is measured by an accelerometer, is shown normalised by g, and is positive downwards. The tyre forces are estimated with the procedure described in Chapter 3, are shown normalised by the corresponding static load, and positive in compression. Sign conventions are according to Figure 3.1.1 (a) Chassis vertical accelerations (b) Estimated normal front tyre force (c) Estimated normal rear tyre force.

Table 2.2.4: Classification of roads according to ISO 8608 [1]. Range of values of $G_d(n_0)$ in each class.

	Lower limit m^3	Geometric mean m^3	Upper limit m^3
Class A	–	$2^4\ 10^{-6}$	$2^5\ 10^{-6}$
Class B	$2^5\ 10^{-6}$	$2^6\ 10^{-6}$	$2^7\ 10^{-6}$
Class C	$2^7\ 10^{-6}$	$2^8\ 10^{-6}$	$2^9\ 10^{-6}$
Class D	$2^9\ 10^{-6}$	$2^{10}\ 10^{-6}$	$2^{11}\ 10^{-6}$
Class E	$2^{11}\ 10^{-6}$	$2^{12}\ 10^{-6}$	$2^{13}\ 10^{-6}$
Class F	$2^{13}\ 10^{-6}$	$2^{14}\ 10^{-6}$	$2^{15}\ 10^{-6}$
Class G	$2^{15}\ 10^{-6}$	$2^{16}\ 10^{-6}$	$2^{17}\ 10^{-6}$
Class H	$2^{17}\ 10^{-6}$	$2^{18}\ 10^{-6}$	–

2.2.2.1 Continuous excitation

Continuous excitations, are mainly generated when driving on a road (to distinguish from riding on jumps or whoops). To this end, we consider roads according to ISO 8608 [1], which describes and classifies road profiles according to the power spectral densities, psd, of the vertical displacement of the road. It considers that the road amplitude psd may be fitted by

$$G_d(n) = G_d(n_0)\left(\frac{n}{n_0}\right)^{-K_r}, \tag{2.2.15}$$

where, G_d is the vertical displacement psd in m^3, n is the spatial frequency in cycles/m, n_0 is a reference spatial frequency (= 0.1 cycles/m) and K_r is the exponent of the fitted psd also called waviness. The parameter $G_d(n_0)$ describes the severity of the irregularities of the road and defines road classes according to Table 2.2.4.

We do not have experimental data of road profiles, and as an alternative, we approximate the excitation based on the sensors on the motorcycle. In particular, we search by trial and error, a road class that generates similar accelerations and contact forces, on the three-degree-of-freedom model, as the experimental data.

To generate a weak continuous excitation, representing transit at low speed on a good road, we consider a road class B driven at 10 m/s. By contrast, to generate a strong continuous excitation, representing transit at high speed on a bad road, we consider a road class D, driven at 40 m/s. The procedure for the generation of road profiles in the space domain is detailed in Appendix A.2.

2.2.2.2 Impulsive excitation

Impulsive excitations can be generated by multiple situations, however the fundamental feature is a fast compression, which can be generated by the simulation of a vertical

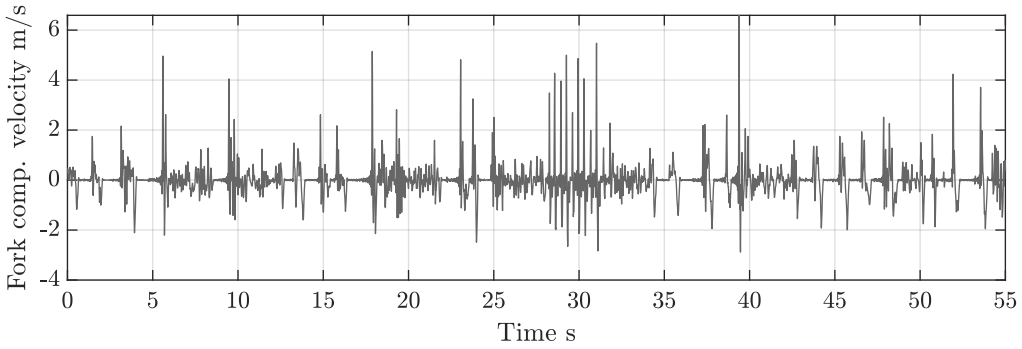

Figure 2.2.5: Experimental fork compression velocities of a motocross motorcycle around a motocross track. Compression is positive.

landing. This is simulated as the response in time to an initial velocity of the three bodies and null initial displacements. To choose representative landing velocities we examine the fork compression velocities of the experimental data available, Figure 2.2.5. By correcting them by the fork angle and neglecting pitch angle, we obtain an estimate of the impulsive velocities of the road over the motorcycle. From this, we generate a weak impulse with a landing at 1 m/s, and a strong impulse with a landing at 4 m/s.

2.2.3 Definition of suspension parameters

The purpose of the indices is to detect the minimums on accelerations and tyre forces, with the variation of suspension stiffness and damping. It is known that the minimum acceleration occurs with no stiffness and damping [2], which is not possible in reality. In practice, the stiffness is fixed on a non-optimal value to support the chassis weight. In this condition, the damping that minimises the accelerations is different from zero, and an expression to calculate it can be found in [2, 19]. Contrarily, for minimum tyre force variation, the optimal stiffness and damping are different from null and an expression for both is known [2]. Following the first procedure, we can assume a constant stiffness fixed on a reference value, and focus on the variation of performance due to damping, while following the second procedure we can focus on the variation due to stiffness and damping. However, to simplify the assessment, we consider variation due to damping only.

To normalise the evaluation we consider the damping ratio

$$\zeta = \frac{c_s}{2\sqrt{k_s(m_c + m_r)}}, \tag{2.2.16}$$

where, the denominator is the critical damping. We consider the critical damping of a single-degree-of-freedom linear system consisting on the chassis and rider mass bouncing on the suspension since it is only for normalisation purposes. In particular, given that with the typical parameters of the front end of a cross motorcycle, detailed in Appendix

A.3, the damping ratio is 0.42, we decide to consider a range around this value, from 0 to 1. Details on expressions of optimal stiffness and damping are discussed on Chapter 5.

2.3 Results and discussion of indices

The equations of motion are integrated in time using the fourth order Runge-Kutta method, implemented in MATLAB [66] as `ode45`. Continuous excitation are integrated over a time span of five seconds, and before evaluating the indices, the first second is discarded to avoid inclusion of the initial transient. Similarly, impulsive excitations are integrated over ten seconds and before evaluating the indices, the final steady-state part of the simulation is removed to avoid distortion in the indices calculation. This is done by trimming the signals at the time at which the chassis amplitude oscillation is smaller than 1 mm.

2.3.1 Continuous excitation

Figure 2.3.1 shows the variation of comfort and handling indices with damping ratio under continuous excitations. Regarding comfort indices, two observations are made. First, the minima are within 0.15 - 0.2 damping ratio, which is lower than expected ($\approx$0.35) according to the literature, see for example [40]. The exception is the Vliet index, which predicts optimal damping considerably higher from the expected values in both cases. Second, with weak and strong excitations, the minima with rms and rms4 coincide. This is expected because the acceleration signal does not have significant peaks, as indicated by the severity ratio r which is mostly under 1.75, not shown here.

Regarding handling indices, three results are of interest. First, a weakness of fly time index is detected. Under a weak excitation, all damping ratios are equally optimal, since the wheel does not lose contact with any of them. Second, with strong excitations, it is possible to see that minimising the force variation with rms4 and rms8 does not imply minimum flying time, even though they are not far off. Third, the minima are around the experimental damping ratio of 0.42 which suggests that the motorcycle is optimised for road handling in continuous excitation.

2.3.2 Impulsive excitation

Figure 2.3.2 shows the variation of comfort and handling indices with damping ratio under impulsive excitations. With respect to comfort indices two results are of interest. First, rms and rms4 predict very similar minimuma. Second, Vliet index for transient conditions, shows better agreement with the rms and rms4 indices, than the one for continuous

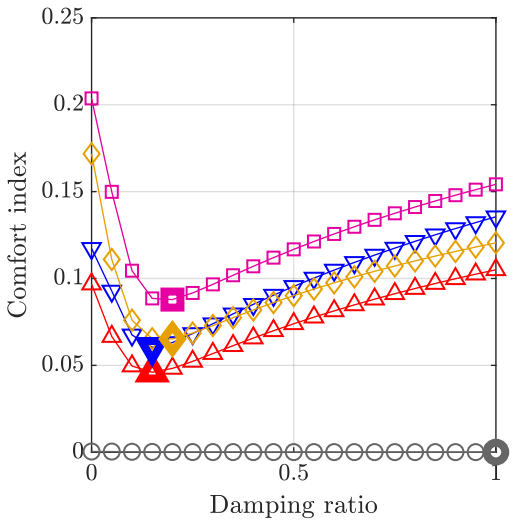

(a) Comfort under weak continuous excitation.

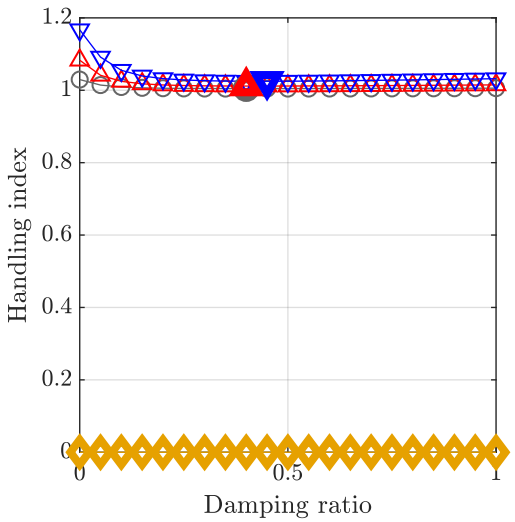

(b) Handling under weak continuous excitation.

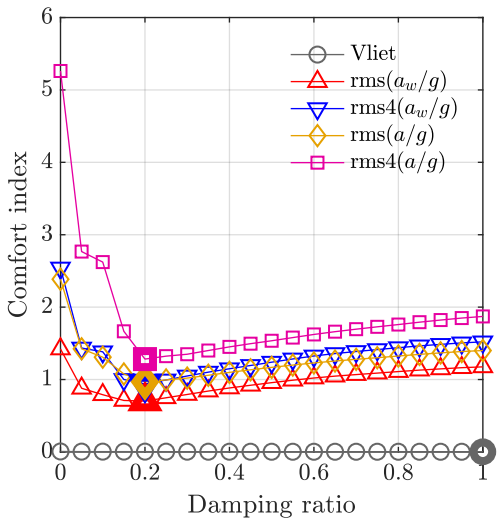

(c) Comfort under strong continuous excitation.

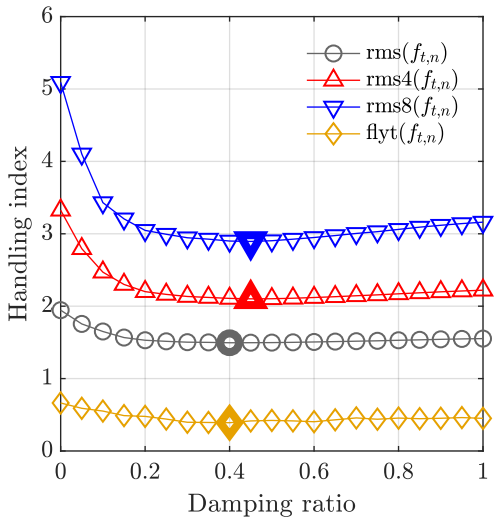

(d) Handling under strong continuous excitation.

Figure 2.3.1: Comfort and handling indices under continuous excitation. High values are undesirable since they represent high accelerations and tyre force variations, respectively. Weak continuous excitation corresponds to driving at 10 m/s on a road class B, and strong continuous excitation, to driving at 40 m/s on a road class D. Thicker markers indicate minimum value.

excitation.

Regarding handling, the effect of mean order is highlighted. Lower order means (rms and rms4) minimises the force variation at very low damping ratio (0.05) while, higher order mean (rms8) tend to minimise the force variation with higher damping ratios. This can be explained by two facts. First, in the low order means, the peak forces tend to make a minor contribution to the mean compared to the rest of the signal because they occur in very short instants of time. But, as the order of the mean increases, the peak forces are amplified more than the rest of the signal, increasing their contribution to the mean, and in the limit when the order is infinite, the mean becomes the maximum value. Moreover it can be proved [67] that for any non-constant signal the magnitude of the mean increases with the order, i.e. rms $<$ rms4 $<$ rms8 $<$ rms∞(=max). Second, as the damping ratio is decreased, there are more force oscillations, the settling time is longer and signal duration is longer. The longer signal tends to reduce the mean, even though the force variation is larger. Consequently, unless the force is amplified with higher order means, the peak forces will tend to be lost as damping is decreased, and the force variation will seem to be reduced, i.e. improved, while the opposite is actually happening. Both facts can be seen in the contact force time histories of Figure 2.3.3. First, in all cases the mean force tends to the maximum force as its order increases. Second, with low damping, rms and rms4 are decreased with respect to higher damping, suggesting a less variable force, while actually, peak forces are larger and more oscillatory. Contrarily high order means indicated that the force variation actually increased. The optimal damping found with rms8 is close to the experimental damping which represent typical values adopted in the industry.

2.3.3 Discussion

The selection of the model and driving situations seems appropriate, since the results are reasonable. For example, under strong continuous excitations, most rms accelerations are below 2 g, and maximum values are about 7-10 g, shown in Figure 2.3.4, as for the experimental data. Regarding forces, under continuous excitations, the rms is about 1.5, while experimentally is 1, and the rms8 is 3, while experimentally is 2.7. Under impulsive excitation, the peak force is 10, while experimentally is 7. To understand this disagreement, it should be considered that the magnitude of the experimental force is not validated, as we will see in Chapter 3, and therefore, it should not be considered as exact.

Regarding the indices, from continuous excitation, Vliet index is discarded since the minimum, which is found on the boundary of the damping ratios evaluated, is not representative of optimal performance. The flying time is also discarded, because it is unable to capture the magnitude of force variations. On the other hand, rms and rms4 of weighted and un-weighted accelerations provide the same results among them in practice. In the same way, rms, rms4 and rms8 of tyre forces are in agreement.

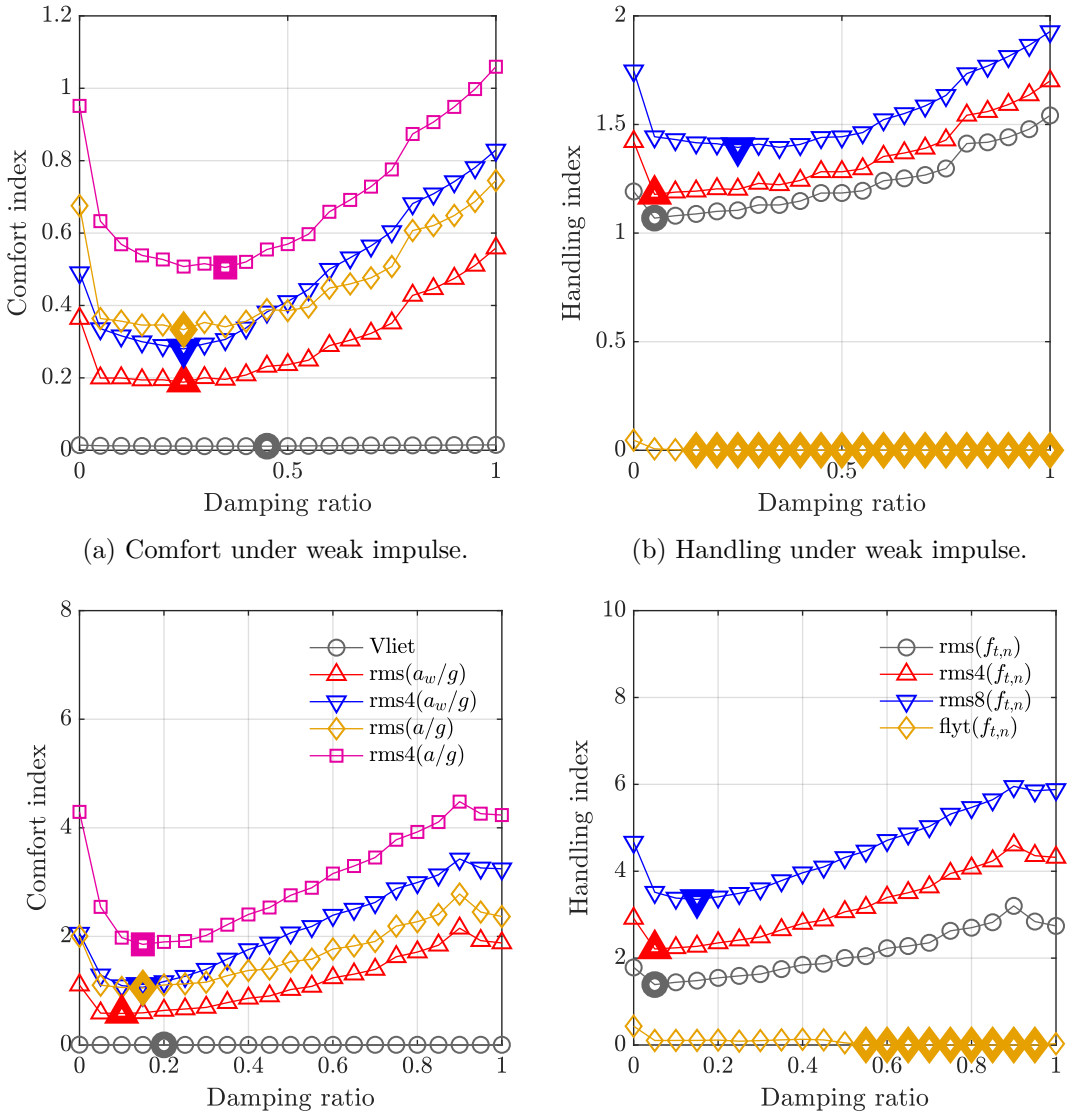

(a) Comfort under weak impulse.

(b) Handling under weak impulse.

(c) Comfort under strong impulse.

(d) Handling under strong impulse.

Figure 2.3.2: Comfort and handling indices under impulsive excitation. High values are undesirable since they represent high accelerations and tyre force variations, respectively. Weak impulse corresponds to landing at a vertical speed of 1 m/s and strong impulse to landing at 4 m/s. Thicker markers indicate minimum value.

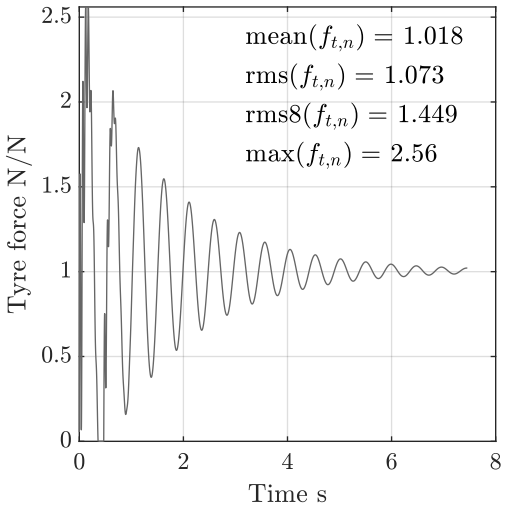

(a) Damping ratio 0.05, weak impulse.

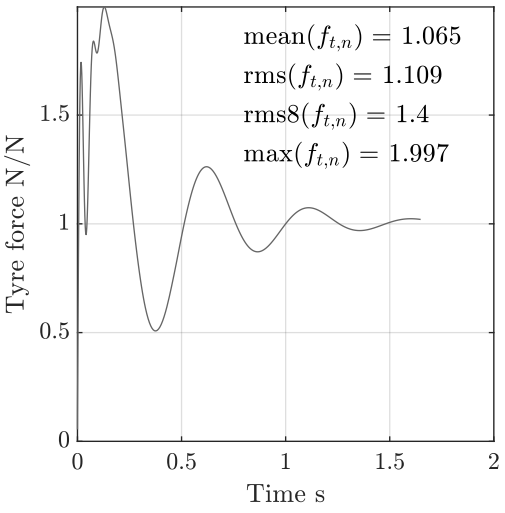

(b) Damping ratio 0.25, weak impulse.

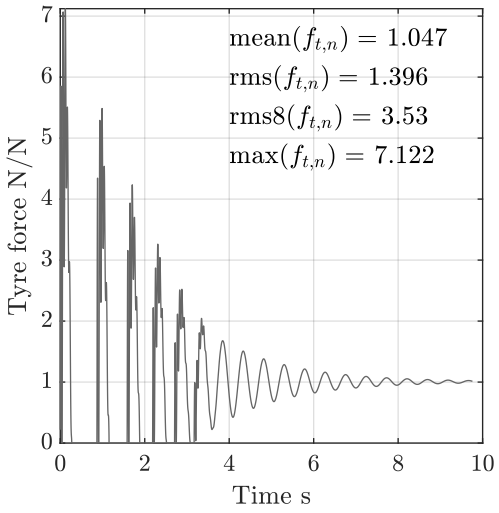

(c) Damping ratio 0.05, strong impulse.

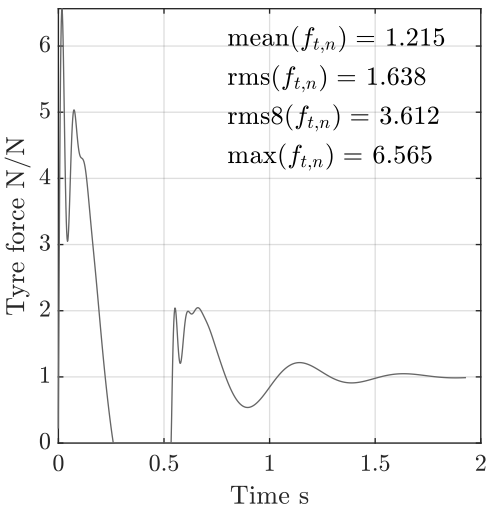

(d) Damping ratio 0.30, strong impulse.

Figure 2.3.3: Contact force over time with selected damping ratios. The damping ratios correspond to the minimum of rms and rms8. The tyre force magnitude is normalised by the static tyre force $f_{t,n}$.

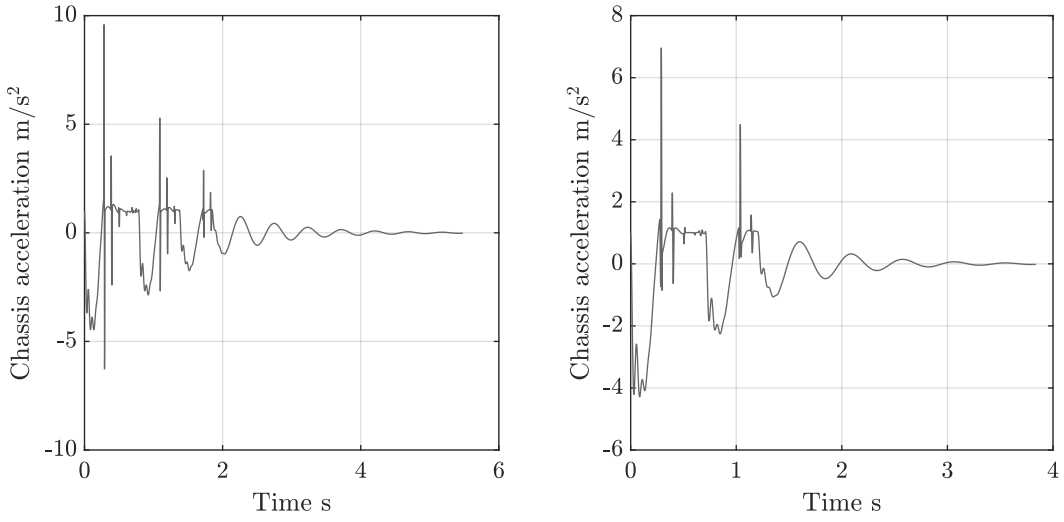

(a) Damping ratio 0.10, strong impulse.

(b) Damping ratio 0.15, strong impulse.

Figure 2.3.4: Chassis acceleration over time with selected damping ratios. The damping ratios correspond to the minimum of rms and rms4 under strong impulse.

From impulsive excitation, considering that the experimental data indicates that the real excitations are intense, ISO 2631 recommends rms4 to assess comfort. Regarding using weighted or unweighted accelerations, under weak and strong impulses, the minimum accelerations are obtained with a difference of 0.1 damping ratio, being the unweighted acceleration with higher damping. Regarding handling, rms and rms4 are discarded because it indicates that the force variation is reduced as damping is reduced, while the opposite is actually happening. On the other hand, rms8 represents force variation correctly under weak and strong impulsive excitations, as well as on continuous excitations, finding optimal values close to the typical values adopted in the industry. It seems to capture the average and peak forces with a good compromise.

It should be highlighted that these results have been obtained with one set of parameters and one particular model. To investigate the sensitivity of the model, we repeated the tests with a significant change in the model, which was the rider attached to the chassis, and the same conclusions were obtained. Therefore, it seems to be a robust conclusion. No parametric tests were carried-out since it is out of scope, however, it can be expected that the conclusions remain valid, at least, with a similar set of parameters, i.e. off-road motorcycles. For a different vehicle parameters, such as a four wheeled-vehicle, the results need to be revised.

2.4 Summary

In this Chapter, we have determined appropriate metrics to assess performance in off-road motorcycles. This has been motivated by the need of meaningful quantities that capture performance, in order to measure it and optimise it.

To select appropriate indices, we compared five comfort indices and four handling indices. For comfort, we considered: Vliet index, two ISO 2631 indices, and the simplified versions of these ISO indices. For handling, we considered rms of tyre forces, and flying time from the literature, and in addition, we proposed rms4, and rms8 based on the nth order average definition. We compared them using a three degree of freedom model under representative continuous and impulsive excitations.

We found out that to assess comfort, rms4(a_w) should be used, however, rms4(a) provides the same or very close results, with the advantage of less computational cost. For handling, we found out that rms8, is the most appropriate, since it provides a representative estimation of force variation in all situations. In this way, we define the performance of an off-road motorcycles by comfort and road holding, the former measured by the fourth-order-mean of the frequency-weighted or un-weighted accelerations, rms4(a_w) or rms4(a), and the latter by the eight-order-mean of the contact force, rms8(f_t).

Measurement of performance in an experimental situation, requires measuring accelerations and contact forces. Since there is no method available to measure forces, in the next Chapter we develop a methodology to obtain them.

CHAPTER 3

Estimation of contact forces for performance measurement

Performance assessment requires measuring accelerations and contact forces as defined in Chapter 2. While measurement of accelerations is straight forward with accelerometers, contact forces are not since direct measurement is complex, expensive and adds weight. On the one hand, wheel force transducers are expensive and heavy with respect to the unsprung mass of the motorcycle. An alternative for the normal force is to measure the radial deformation of the tyre by optical sensing, however this is not feasible either because of the exposure of the lenses to dirt from off-road conditions. On the other hand, building a load cell into the motorcycle parts is complex, since it requires thickness reduction to increase strain and achieve useful sensitivity. However, this approach is invasive, reduces structural resistance of parts, and in off-road, can endanger the driver due to the high loads involved.

As an alternative, we look at contact force estimators for production vehicles and motorcycles which are used as lower-cost alternative for control applications [44]. These estimators are based on inexpensive sensors or on the ones already available on-board. Nonetheless, they are based on assumptions not applicable to off-road motorcycles. Analysing them by force components, first, estimators of the vertical forces, commonly assume flat road or quasi-static state, which leads to neglect the suspension dynamics. In this way, the normal loads can be estimated based solely on the horizontal and lateral accelerations of the chassis. Yet, this assumption is not applicable for off-road motorcycles since the road has large obstacles and a quasi-static state is seldom reached. There are estimators which include the suspension dynamics, however due to the treatment of the pitch angle their representativeness is questionable. For example Acosta [68] in cars and Delvec-

chio [69] in motorcycles, use a quarter car model to calculate the vertical force measuring the acceleration at each end of the suspension with accelerometers and its deflection with a potentiometer. In this model, Delvecchio neglected the pitch angle finding that it did not affect the estimation performance, while Acosta partly accounted for it by considering the displacement of the pitch centre due to longitudinal acceleration. This assumption however, does not seem reasonable in off-road motorcycles, because pitch angle is large, reaching ± 45 degrees, and also this rotation is originated not only by the longitudinal acceleration but also by road slope, such as on the take-off of a jump, and by the riding techniques to overcome certain obstacles, such as wheelies.

Second, estimators of longitudinal forces commonly exploit the wheel dynamics since it is assumed that braking and driving torques are known. In off-road motorcycles however, these torques are not commonly available. A simpler methodology is also used which is based on the longitudinal acceleration measurement. The downside is that only the total longitudinal force can be known. Lastly, estimators of the lateral forces for cars are not applicable because they do not represent the large roll angle of a motorcycle in a turn. For motorcycles, an estimator has been developed by Slimi [46], however it is restricted to on-road since it assumes a flat road and that the characteristics of the road-tyre interaction are known a-priori. Specifically, it is based on a Pacejka tyre model which calculates the normal and lateral forces using the dynamic states of the motorcycle which are estimated using an sliding mode observer. This approach is not representative of off-road since the road is not smooth. Moreover, a-priori knowledge of the road-tyre interaction characteristics is not practical since the road changes recurrently and therefore the estimator would require to consider several road-tyre characterisations. Consequently, the tyre force estimators available in the literature are not suitable for off road motorcycles which are characterised by large pitch rotations and suspension motion.

The aim of this Chapter is to develop a procedure to estimate contact forces suitable for off-road. To this end, first, we derive a the set of equations of the estimator and verify them with a virtual experiment. Subsequently, we test the estimations with experimental data from a motocross track. Lastly, we show the advantages and limitations of the procedure.

3.1 Derivation of the set of equations of the estimator

In this section, we derive the equations of the estimator. First we discuss the dynamical representation of the motorcycle, and derive a set of equations of motion. Next, we derive a set of constraint equations to improve the accuracy of the estimations, and lastly we arrange the set of equations and present the solution method.

We decide to base the estimator on a set of inverse dynamics equations, since we consider that no information is known about the road. This information would allow to calculate

motorcycle motion with a forward dynamic model, from where the tyre forces could be retrieved. However, we consider that knowledge of road elevation is limited in practice. On the one hand, we envisage that it would require a vision based approach, optical or infrared, which would be disturbed by road elements such as water, mud or dust. On the other hand, it needs to measure soil deformation, which in case of sand or mud is of equal or larger magnitude as the tyre deformation. As a consequence, since we can not know the road disturbance, we decide to calculate it from the motion that it produces, i.e inverse dynamics.

Since the motorcycle is composed of multiple interconnected bodies, it is a multibody problem, [47]. These problems can be solved numerically or symbolically. The former strategy, is well suited for final design stages since detailed information is known; while the latter is preferred for early design stages, since it captures the essence of the phenomena [48]. We prefer the second approach since we can additionally manipulate the set of equations to process the experimental data as efficiently as possible. To derive symbolically the equations of motion, we use MBSymba, [48, 49, 70] which is an add-on for Maple [71].

In particular, the mathematical model is derived in three steps. First, we derive the set of inverse equations of motion, from were we get the dynamics of the system. Second, we add a set of constraint equations in order to disregard non-physical solutions that may arise from measurement errors. Third, we manipulate the set of equations to solve them efficiently.

3.1.1 Equations of motion

The equations of motion of the motorcycle are derived under the following four assumptions. First, we consider in plane motion only, since our interest is mainly on manoeuvres such as braking and accelerating. Second, by neglecting structural vibrations, we can represent the motorcycle by four interconnected bodies with five degrees of freedom, which are described by as many coordinates,

$$\mathbf{q} = [x_s, z_s, \mu, z_f, \alpha_r]^T, \tag{3.1.1}$$

where, x_s and z_s are horizontal and vertical displacement of the chassis centre of mass, μ is chassis rotation, z_f is the front suspension compression, and α_r is the rear suspension compression defined as the relative rotation between swingarm and chassis. Third, since the manoeuvres of interest are generally transited in standing position, we consider that the rider interacts with the handlebar and foot pegs only. Fourth, the contact point with the ground is considered to be directly under the wheel centre as seen in nominal condition. This implies that the contact point does not move forward or backwards due to road irregularities, and therefore, normal and tangential components are always aligned

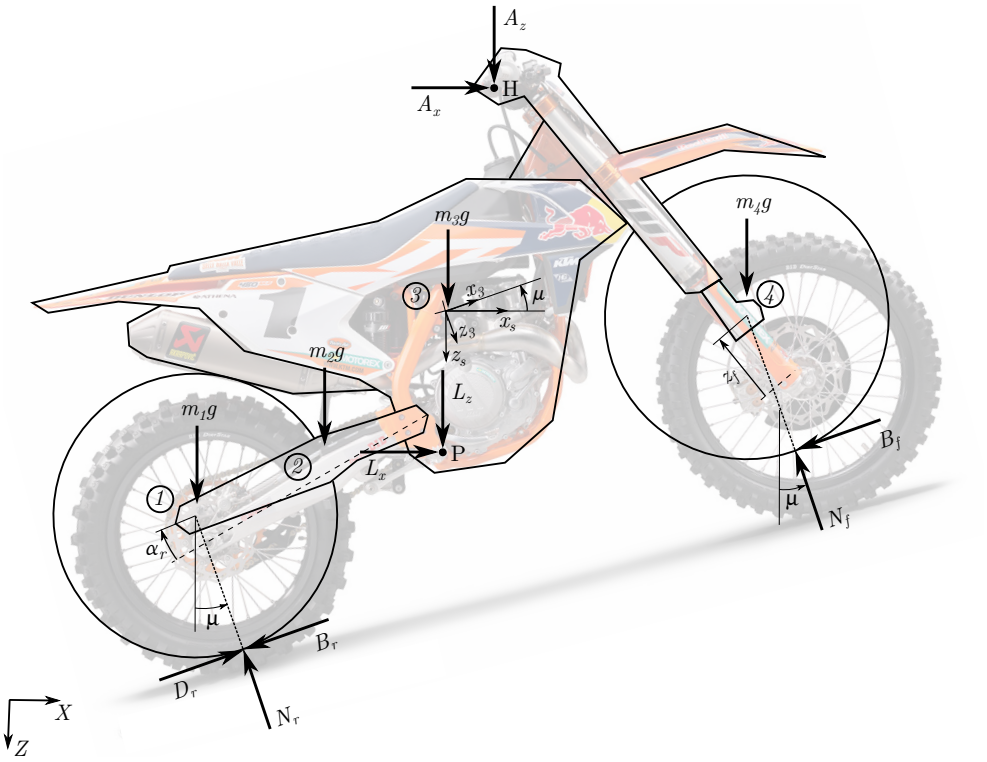

Figure 3.1.1: Motorcycle model. x_s, z_s and μ are horizontal, vertical and angular position of chassis centre of mass; z_f is fork compression, and α_r is swing arm angular compression; A_x, A_z, L_x, L_z are rider's arm and leg forces acting over the handlebar (H) and foot-peg (P); N_r and N_f are normal forces over the tyres assumed to be along the z_3-axis, which is tilted μ from absolute vertical; B_r, B_f are rear and front braking force and D_r is rear driving force which are assumed to be along chassis x_3-axis.

with z_3 and x_3 axis, respectively. This simplification is based on the observation that only when transiting large obstacles, such as *whoops*, Figure 4.3.1, the contact points move significantly from the bottom of the tyres. In this way, the estimation of the contact point position, which is not a trivial task, is avoided and there are only four tyre force components to be determined. Figure 3.1.1, summarises the four assumptions. In-plane motion, four bodies of the motorcycle and five coordinates used to describe their motion, rider forces on foot-peg and handlebar, and contact forces under wheel centre in nominal condition.

We derive five equations of motions, one for each degree of freedom, and collect them as

$$\mathbf{M}\ddot{\mathbf{q}} + \mathbf{m_v} = \mathbf{A_w}g + \mathbf{A_s}\mathbf{f_s} + \mathbf{A_r}\mathbf{f_r} + \mathbf{A_t}\mathbf{f_t}, \tag{3.1.2}$$

where, $\mathbf{M}$ is the mass matrix, $\ddot{\mathbf{q}}$ is the acceleration vector, g is gravity acceleration, $\mathbf{f_s}$, $\mathbf{f_r}$, $\mathbf{f_t}$ are suspension, rider and tyre force vectors respectively and the matrices $\mathbf{A_w}$, $\mathbf{A_s}$, $\mathbf{A_r}$, $\mathbf{A_t}$ project these forces along each of the five coordinates. $\mathbf{m_v}$ is the pseudo-mass vector which contains relative acceleration terms, and also the product of wheels rotational inertia by their angular accelerations. We did not model wheel rotations as coordinates in $\mathbf{q}$ since we

can measure them directly to represent the rotational inertia effect and therefore, we did not need to derive equations of motion for them. See Appendix B, for explicit description of matrices and vectors.

In Equation 3.1.2, masses , rotational inertias, and geometry in $\mathbf{M}, \mathbf{m_v}$ and projection matrices can be measured with no major complication. Accelerations in $\ddot{\mathbf{q}}$, velocities and angular acceleration in $\mathbf{m_v}$, and positions can be measured with accelerometers, potentiometers and tachometers or derived from them; suspension forces $\mathbf{f_s}$ can be estimated from characterisation of the spring and damper; and the rider forces $\mathbf{f_r}$ can be estimated as described in Chapter 4

3.1.2 Constraints on the contact forces

Acknowledging the presence of measurement errors, we derive an overdetermined system to attenuate them. In particular, Equation 3.1.2 consists of five equations to determine four unknown tyre force components. Because of the presence of random errors in the equations, there is no vector $\mathbf{f_t}$ that can satisfy the five equations simultaneously, i.e

$$\mathbf{A_t f_t} - \mathbf{b_1} \neq \mathbf{0}, \quad \forall\ \mathbf{f_t}, \tag{3.1.3}$$

where, $\mathbf{b_1} = \mathbf{M\ddot{q}} + \mathbf{m_v} - \mathbf{A_w}g - \mathbf{A_s f_s} - \mathbf{A_r f_r}$, is the vector of known terms of Equation 3.1.2. Then, the alternative problem is to

$$\begin{aligned} &\text{find } \mathbf{f_t} \text{ that :} \\ &\min_{\mathbf{f_t}} \ \|\mathbf{A_t f_t} - \mathbf{b_1}\| . \end{aligned} \tag{3.1.4}$$

The overdetermined system can not compensate the measurement errors completely and non-physical solutions can be obtained regardless. To reduce these non-physical solutions, we add equality and inequality constraints to the optimisation.

On the one hand, we add inequality constraints to consider that normal forces and front tangential force (braking) can physically exist in one direction only. By defining the rear tangential force as two non-negative forces as well, we add the constraints,

$$\mathbf{f_t} = [N_f\ N_r\ B_f\ B_r\ D_r]^T \geq \mathbf{0}, \tag{3.1.5}$$

where, N_f and N_r are normal forces on front and rear tyres; B_f and B_r are braking forces on front and rear tyre; and D_r is the driving force on the rear tyre. Even though in this way there are five variables to be determined, the problem still has four unknowns, since by definition only D_r or B_r exist at anytime.

On the other hand, we add equality constraints to impose a solution when some terms

are known under four driving conditions. These are: $N_f = B_f = 0$ when front wheel is detached; $N_r = B_r = D_r = 0$ when rear wheel is detached; $B_f = B_r = 0$, when motorcycle is driving (accelerating); and $D_r = 0$ when braking, Table 3.1.2. In order to impose these constraints only under the corresponding conditions, we multiply each element of the constraint equation,

$$\mathbf{f_t} = \mathbf{0}, \tag{3.1.6}$$

by an activation weight, W_{ii}, that is 1 when the condition is satisfied, and 0, otherwise. In this way, we express the constraints as

$$\mathbf{W}\mathbf{f_t} = \mathbf{0}, \tag{3.1.7}$$

where, $\mathbf{W} = \text{diag}(W_{ii})$.

To make $W_{ii} = 1$ under the corresponding driving conditions, we define three auxiliary weights, w_f, w_r and w_d, representing the first three driving conditions: front wheel detached, rear wheel detached, and motorcycle driving, respectively. They take the value of 1 if the corresponding condition is happening, and 0 if not. Since we assume that if the motorcycle is not driving is braking, we can represent braking as $1 - w_d$.

Next, we read Table 3.1.2 horizontally to determine under which conditions the tyre force i is null, and when W_{ii} needs to be 1 to activate the constraint. In particular, since each normal force is null only under one condition, by making the activation weight W_{ii} equal to the corresponding auxiliary weight, it will be 1 only under that condition. Differently, the tangential forces can be null under two conditions. To make the activation weight W_{ii} equal to 1 if any of the two or both conditions are happening, we use the algebraic representation of an *or* logical condition, which is to add the weights and subtract their product. In this way, the activation weights $W_{11}, ..., W_{55}$ are obtained, and shown on Table 3.1.2.

With these constraints, some non-physical combinations are implicitly removed, such as tangential forces combined with no normal forces. Additionally, in this formulation, three driving possibilities have been omitted as well. These are, driving and braking simultaneously, front wheel driving, and no driving nor braking. The first, since it is not expected in normal driving conditions; the second, since front wheel drive motorcycles are very rare; the third, since it is only possible in motionless condition, which is out of interest. When there are no inputs from the rider to drive or brake, which apparently classifies as the third case, actually involves braking because of friction between moving parts.

This imposition of a solution when some terms are known under certain driving conditions could have been done by removing the known terms from the system instead of

Table 3.1.2: Known tyre forces under specific driving conditions. The auxiliary weights w_f, w_r and w_d represent front and rear wheel detachments and motorcycle driving (accelerating), respectively. They are 1 if the condition is happening and 0 otherwise, and are used to calculate the constraint activation weights W_{ii}. The symbol - means that it can be any value.

Tyre force		Magnitude in driving condition				Constraint activation weight
i	$f_{t,i}$	Front detached ($w_f = 1$)	Rear detached ($w_r = 1$)	Driving ($w_d = 1$)	Braking ($w_d = 0$)	W_{ii}
1	N_f	0	-	-	-	w_f
2	N_r	-	0	-	-	w_r
3	B_f	0	-	0	-	$w_d + w_f - w_d w_f$
4	B_r	-	0	0	-	$w_d + w_r - w_d w_r$
5	D_r	-	0	-	0	$(1 - w_d) + w_r - (1 - w_d) w_r$

adding constraints to the system. However this approach requires to reduce the system of Equation 3.1.4, into $\min \|\mathbf{A}'_\mathbf{t}\mathbf{f}'_\mathbf{t} - \mathbf{b}'_\mathbf{1}\|$ for the six driving conditions which are possible: only braking, only driving, driving or braking with front wheel detached, braking with rear wheel detached, and both wheels detached. Even though this option solves a smaller system which would make it faster, we prefer adding the constraints, since numerical implementation is simpler, and the additional calculation time is not significant.

Adding the constraints, the problem is now formulated as

$$\begin{aligned} &\text{find } \mathbf{f_t} \text{ that :} \\ &\qquad \min_{\mathbf{f_t}} \ \|\mathbf{A_t}\mathbf{f_t} - \mathbf{b_1}\|, \\ &\text{subject to:} \quad \mathbf{f_t} \geq \mathbf{0} \\ &\qquad\qquad\quad \mathbf{W}\mathbf{f_t} = \mathbf{0}. \end{aligned} \tag{3.1.8}$$

3.1.3 Formulation of the estimation problem and solution

In order to solve Equation 3.1.8 efficiently, we perform the following transformation. First, we take advantage that the minimisation argument is in least squares form, which enables us to use least squares solvers. These solvers are considerably faster than other optimisation solvers since they exploit the particular formulation. Specifically, to solve an equality constraint least squares problem, as the one in Equation 3.1.8, there are at least four algorithms. Lawson and Hanson [72] describe three: by using a basis of the null space, by direct elimination, and by weighting, while MATLAB uses by default the interior-point-convex algorithm. We chose to solve the problem by weighting, which means appending

the equality constraints $\mathbf{W}\mathbf{f_t} = \mathbf{0}$ to the minimisation argument with a heavy weight, which we do with the diagonal matrix $\mathbf{B_c}$. The main difference with this formulation is that the constraints are not exactly met, which for this situation is beneficial since it helps to compensate for errors in the transitions between active and inactive constraints.

Additionally, in this transformation, we add diagonal matrix $\mathbf{B_d}$ to weight the dynamic equations to take into account possible differences in uncertainties that might exist between equations given that they are obtained from different sensors. In this way, the problem is written as,

$$\begin{aligned} &\text{find } \mathbf{f_t} \text{ that :} \\ &\qquad \min_{\mathbf{f_t}} \left\| \begin{matrix} \mathbf{B_d}(\mathbf{A_t}\mathbf{f_t} - \mathbf{b_1}) \\ \mathbf{B_c}\mathbf{W}\mathbf{f_t} \end{matrix} \right\|, \\ &\text{subject to:} \quad \mathbf{f_t} \geq \mathbf{0}. \end{aligned} \tag{3.1.9}$$

Lastly, we re-write Equation 3.1.9 in compact form as,

$$\begin{aligned} &\text{find } \mathbf{f_t} \text{ that :} \\ &\qquad \min_{\mathbf{f_t}} \left\| \mathbf{B}(\mathbf{A}\mathbf{f_t} - \mathbf{b}) \right\|, \\ &\text{subject to:} \quad \mathbf{f_t} \geq \mathbf{0}, \end{aligned} \tag{3.1.10}$$

where,

$$\mathbf{B} = \begin{bmatrix} \mathbf{B_d} & \mathbf{0} \\ \mathbf{0} & \mathbf{B_c} \end{bmatrix}, \quad \mathbf{A} = \begin{bmatrix} \mathbf{A_t} \\ \mathbf{W} \end{bmatrix}, \quad \text{and} \quad \mathbf{b} = \begin{bmatrix} \mathbf{b_1} \\ \mathbf{0} \end{bmatrix}, \tag{3.1.11}$$

which is a non-negative least squares problem. We solve it using the Lawson-Hanson algorithm for non-negative problems, presented in [72], and implemented in MATLAB [66] as `lsqnonneg`. It is worth remarking that this estimation is for a single instant of time therefore, to estimate along time, it needs to be solved for each sampled time.

The estimator is summarised in Figure 3.1.3. The motorcycle kinematics needed are three displacements, five velocities and seven accelerations, adding up fifteen variables. The suspension and rider forces as well the auxiliary and equation weights need to be provided by the user. These forces can be obtained from direct measurements or from some user defined models. These models can possibly use some of the motorcycle kinematics, such as the suspension models that are commonly based on the displacements and velocities. The auxiliary weights can be obtained from some user defined model or also possibly from the motorcycle kinematics. Lastly, the equation weights need to be defined by the user, and it is reasonable to use constant values, since the relative importance between equations are not expected to change.

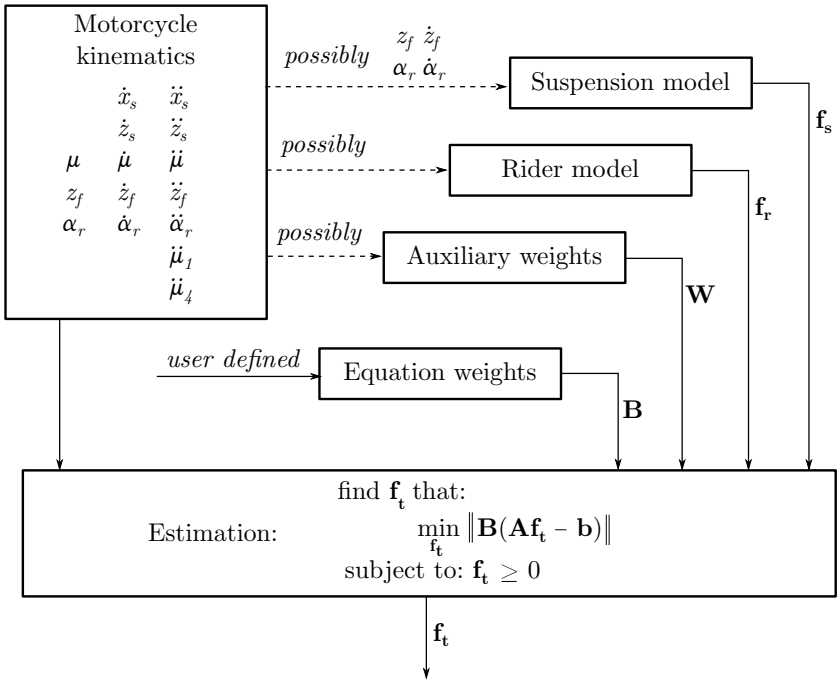

Figure 3.1.3: Estimator layout. The estimator requires fifteen kinematic variables of the motorcycle, together with the suspension and rider forces, and auxiliary and equation weights. The forces and the auxiliary weights can be obtained from direct measurement or from a model possibly based on the motorcycle kinematics. Contrarily, the equation weights need to be defined by the user.

3.2 Verification of estimations with virtual experiments

The estimator is verified using data from a virtual experiment, since measurements are noise free and it is possible to measure the contact forces directly. Four tests are carried out. In each test, a specific manoeuvre is simulated and the motorcycle kinematics is measured. This data is used to estimate the tyre forces with Equation 3.1.10 and are compared to the forces measured directly in the simulation. For the estimator, the suspension forces are linear with displacement and velocities; the rider forces are obtained using the simple rider model of Chapter 4; the auxiliary weights are calculated from the motorcycle kinematics as described in Equation 3.3.6; and the equation weights are defined as 1 for the dynamic equations, since they are noise free, and 100 for the constraint equations, to force the constraints to be met. For the simulation, Working Model 2D [73] is used. The motorcycle is modelled under the same assumptions of the estimator, i.e. in plane motion, four bodies, rider acting over the foot-peg and handlebar, contact point under the wheels in nominal condition as shown in Figure 3.2.1. The suspension forces are defined linear with respect to displacement and velocity. The rider is modelled differently from the estimator. It consists of a point mass, translating in the plane, located nominally over the foot-peg and rearwards of the handlebar, and attached to these points by spring and damper elements. This difference is introduced to investigate the effect of imperfect

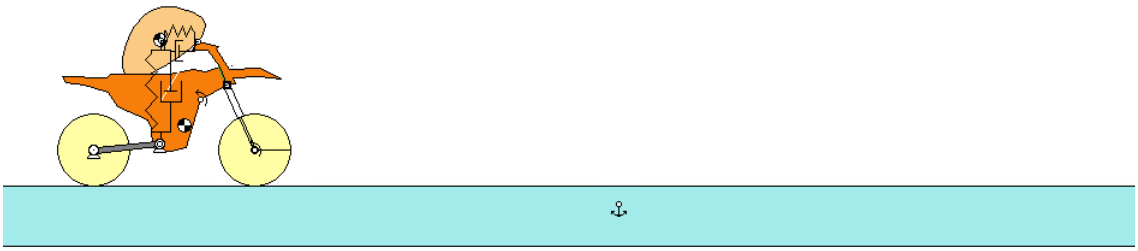

Figure 3.2.1: Virtual experiment in Working Model 2D.

knowledge of these forces by the estimator. The model parameters are listed in Table 3.2.2.

The four tests are as follows. On the first test, 120 Nm of braking torque is applied on the rear wheel and subsequently on the front wheel, to check if the estimator can distinguish the origin of the braking force. On the second test, 60 Nm of braking torque is applied on each wheel simultaneously, to check if the estimator can identify the braking distribution between wheels. On the third test, 120 Nm of driving torque is applied on the rear wheel via shaft drive transmission, to compare with the the fourth test, in which 119.4 Nm of driving torque is applied on the rear wheel via chain transmission, to check the effect of neglecting the chain tension on the estimator. Additionally, in the four tests, the estimation of normal forces is checked. The braking torques and shaft-drive transmission are simulated as external torques acting on the wheel; the front one, reacting on the chassis and the rear one, on the swingarm. The chain transmission is simulated using an engine and a wheel sprocket, together with a dummy gear located above the latter one, due to the impossibility to model an actual chain transmission in WM2D. In particular, an external torque is applied between the chassis and the engine sprocket. The rotation angle of the latter, is mirrored in the opposite direction by the dummy gear, which applies a force on the wheel sprocket on the same point and in the same direction as the chain would do, generating the driving torque on the wheel. Special emphasis has been put in replicating the chain force and its points of action, because it creates a suspension compression which is not modelled in the estimator.

The result for the braking tests are shown in Figure 3.2.3. In test 1, it can be seen that the estimator is able to recognise which wheel is originating the braking force and also provide a close estimate of the magnitude, though front braking is slightly overestimated. In test 2, it can be seen that it recognises that both wheels are braking, but the braking distribution is estimated inconsistently. Specifically, first, it estimates more to the rear, subsequently, more to the front, and then stabilises, with front braking slightly overestimated. The result for the driving tests are shown in Figure 3.2.4. It can be seen that in both tests the magnitude of the driving force is closely estimated, and no significant difference is seen if the motorcycle is shaft- or chain-driven. This implies that neglecting

Table 3.2.2: Motorcycle parameters of virtual experiment.

Parameter	Value	Unit
Chassis mass	81	kg
Rear wheel mass	18	kg
Front wheel mass	12	kg
Rider mass	75	kg
Chassis inertia	21	kg m^2
Rear wheel inertia	0.7	kg m^2
Swing arm inertia	0.8	kg m^2
Front wheel inertia	0.5	kg m^2
Wheelbase	1.35	m
Vertical position of chassis centre of mass (CoM)	0.59	m
Chassis CoM from rear wheel, horizontally	0.77	m
Footpeg from chassis CoM, horizontally	-0.2	m
Footpeg from chassis CoM, vertically	0.14	m
Handlebar from chassis CoM, horizontally	0.10	m
Handlebar from chassis CoM, vertically	-0.70	m
Swingarm CoM from main pin	0.28	m
Swingarm length	0.59	m
Rear wheel radius	0.30	m
Front wheel radius	0.30	m
Caster angle	0.40	rad
Swing arm initial angle	0.25	rad
Front suspension stiffness	9800	N/m
Front suspension damping	533	Ns/m
Rear suspension torsional stiffness	4836	N/rad
Rear suspension torsional damping	236	Ns/rad
Rider arm stiffness	8930	N/m
Rider arm damping	1456	Ns/m
Rider leg stiffness	20180	N/m
Rider leg damping	1833	Ns/m

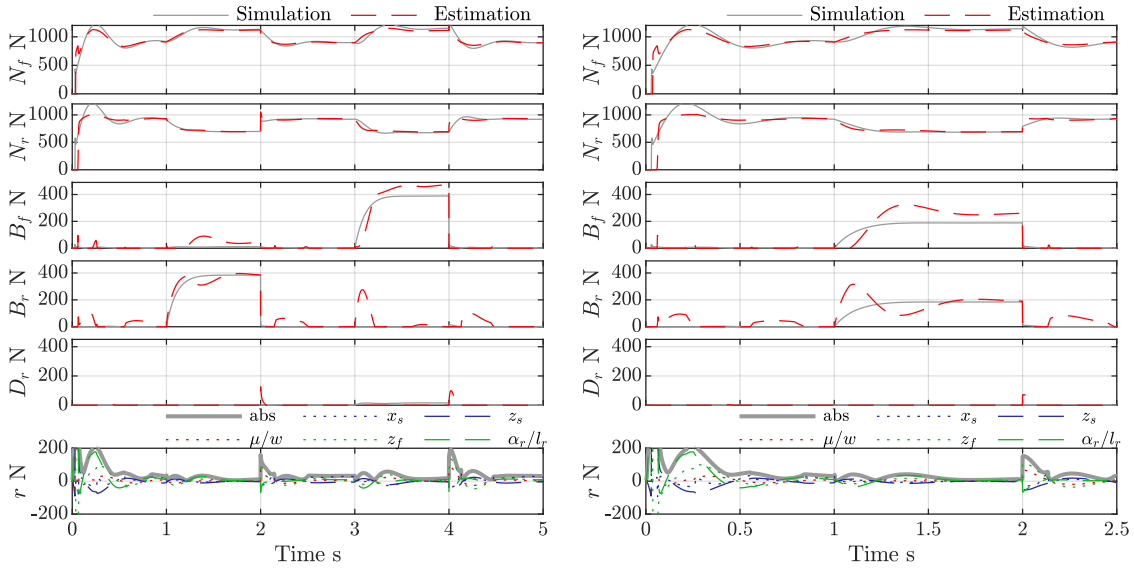

a) Test 1: Single wheel braking

b) Test 2: Dual wheel braking

Figure 3.2.3: Braking tests. On both tests 120 Nm of braking torque are applied. In the first test it is first applied to rear wheel on time interval $t = [1\ 2]$ s and then to front wheel on $t = [3\ 4]$ s, and on the second is split equally between front and rear wheel. r are the residuals of the equations, $\mathbf{r} = \mathbf{B}(\mathbf{A}\mathbf{f_t} - \mathbf{b})$. Absolute value and residuals of the dynamic equations are shown. Residuals of rotational equations have been normalised by a representative length to compare them in the same scale.

chain tension does not add significant error. Normal forces are satisfactorily predicted on the four tests. Load transfer to the front wheel when braking, and to the rear while accelerating are clearly recognized by the estimator. Lastly, it is observed that even though the rider forces are known imperfectly, the tyre forces are closely estimated, which means that the estimator is compensating the error.

The residuals $\mathbf{r} = \mathbf{B}(\mathbf{A}\mathbf{f_t} - \mathbf{b})$ of the estimation are analysed. Each element of $\mathbf{r}$ is the error in the corresponding equation and, on the dynamic equations, they can be interpreted as a force or torque that needs to be subtracted along the corresponding coordinate. For example, the first element indicates a missing force acting over the motorcycle along the x_s coordinate, while the fifth, indicates a missing torque acting on the swingarm along α_r. To compare them in the same scale, the residuals of the rotational equations, μ and α_r, are normalised by the representative lengths w and l_r and are labelled as μ/w and α_r/l_r in the figures. It can be seen that in test 3, when driving torque is being applied, between seconds 1 and 2, the residuals in the five dynamic equations are close to null as expected, since the transmission is the same in the virtual and estimator models. Contrarily, on test 4, the residuals are important since the chain tension is missing in the estimator. Specifically, there is a significant positive residual in the rear suspension compression equation, and also, a negative residual of the pitch equation. The sign of these residuals are consistent with the chain tension absence. This is because by pulling between rear wheel and chassis,

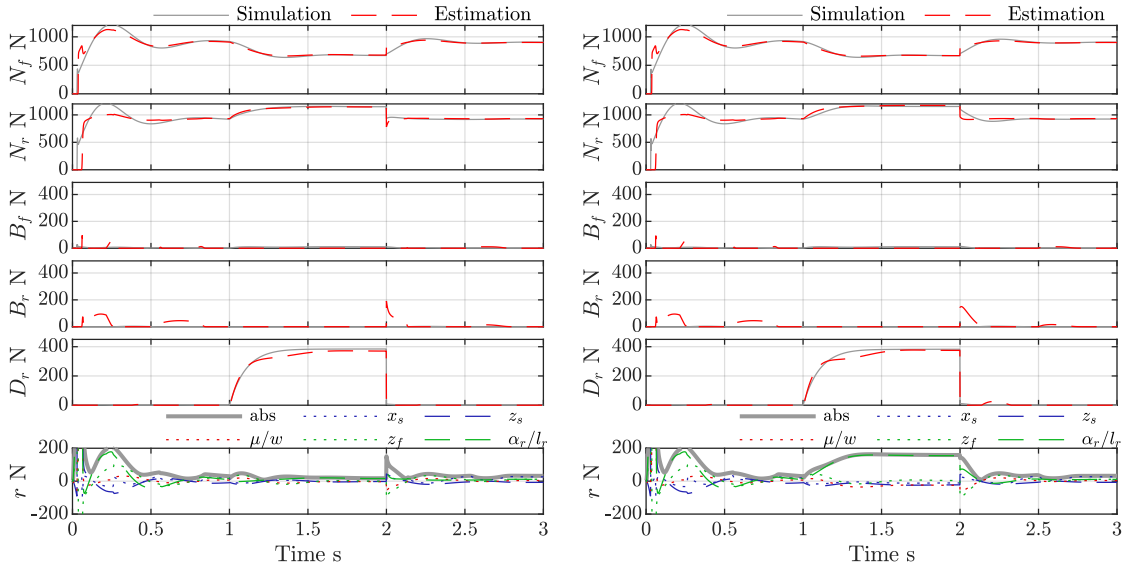

a) Test 3: Shaft drive motorcycle

b) Test 4: Chain drive motorcycle.

Figure 3.2.4: Driving tests. On test 3, 120 Nm are applied directly to the rear wheel via a shaft drive transmission, while on test 4, 119.4 Nm are applied to the rear wheel via chain drive transmission, which is driven by an engine torque of 38 Nm. Chain drive transmission ratio is 3.14. r are the residuals of the equations, $\mathbf{r} = \mathbf{B}(\mathbf{A}\mathbf{f_t} - \mathbf{b})$. Absolute value and residuals of the dynamic equations are shown. Residuals of rotational equations have been normalised by a representative length to compare them in the same scale.

the chain exerts a negative torque over the rear wheel and swing arm, and a positive one over the chassis. Since these two are absent from the equations, if they are added, namely, a positive torque on the pitch equation, and a negative torque on the swing arm equation, it would bring the residuals back to null.

In summary, the equations of the estimator are verified. In the four tests, the estimated forces are in good correspondence with the virtual experiment. The magnitudes and origin of braking forces and driving force are satisfactorily detected, as well as the normal forces. Additionally, it was shown that the omission of the chain tension in the estimator does not affect significantly the prediction of the driving force. Furthermore, the passive rider model used in the virtual experiment served to illustrate that different rider forces over the motorcycle as the one assumed by the estimator does not influence significantly the estimation. Lastly. it should be clarified that in this section we have verified that the equations are free of algebraic errors, however, we do not claim validation of the assumptions of the model, since this requires a real experimental test.

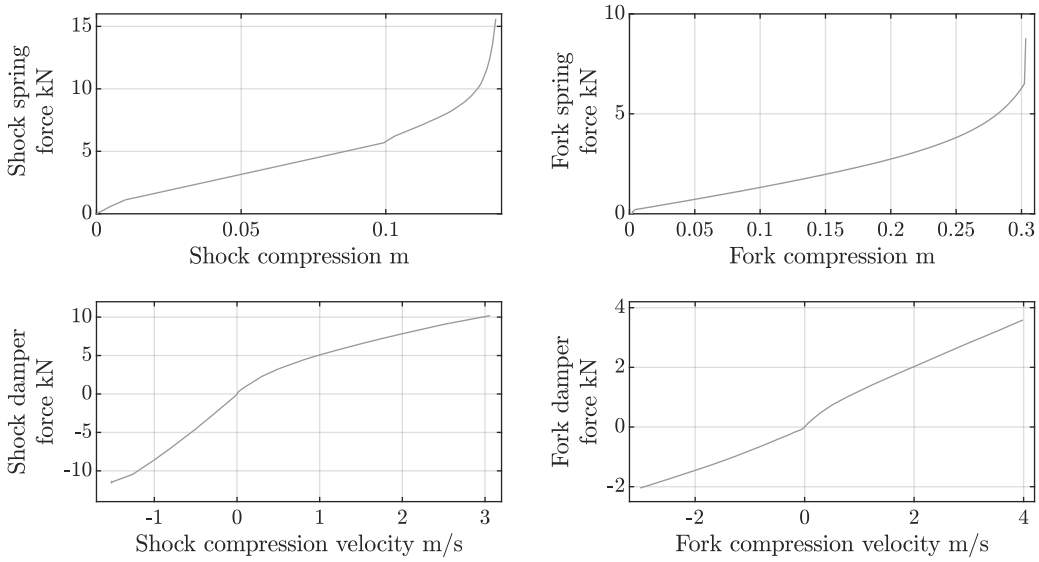

Figure 3.3.1: Shock and fork elastic and damping forces used on the test.

3.3 Application of the estimator to experimental data

In this section, we describe how we use the estimator with experimental data. First, we describe how to obtain the input variables for the dynamic equations as well as the activation weights for the constraints considering two alternative measuring systems. The first one has abundance of sensors and some redundancy of information, but is expensive and cumbersome to use in practice, while the second one uses a minimal set of sensors. Subsequently, we discuss the estimated forces along the motocross track as well as the limitations of the estimator and possible improvements.

3.3.1 Data collection and preprocessing

The test is performed on a motocross scenario. A 2017 motocross motorcycle is used, which has the suspension behaviour depicted in Figure 3.3.1. It is driven by a professional rider on the track shown in Figure 3.3.2. It consists of nine straights and nine turns, abbreviated as S1,...,S9 and T1,...,T9, respectively. S1, S7 and S8 consist of a sequence of jumps while S6 is the *whoops* section, which is a sequence of medium size bumps similar to Figure 4.3.1. Five laps are recorded, each of which is done in approximately 55 s, and lap four is picked randomly for the analysis.

Data is collected with a set of thirteen sensors mounted on the motorcycle as listed in Table 3.3.3. These sensors are chosen since are they commonly available on automotive data acquisition systems. In particular, an inertial unit is located under the seat from which vertical acceleration (a_1) of the chassis, pitch angle (γ_2) and forward velocity (v_3)

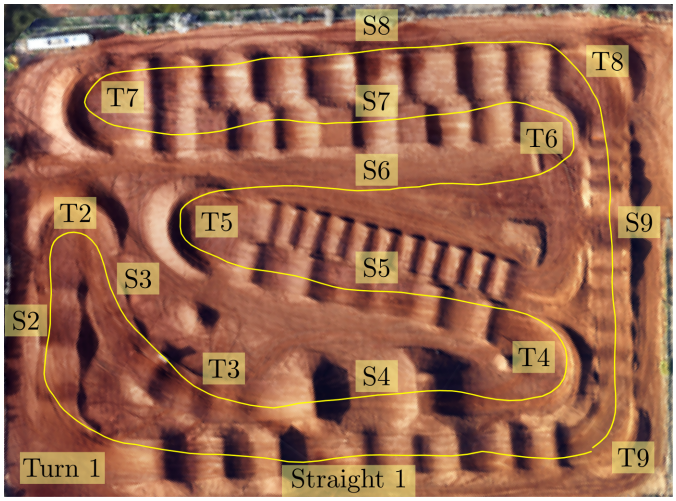

Figure 3.3.2: Trajectory on the track as measured by GPS. There is a discrepancy on straight 6 (S6) because the track was modified between the picture was taken and the test was performed.

are obtained. Additionally, six accelerometers are placed as follows: one at each end of the fork (a_7, a_8), one at each end of the shock (a_{10}, a_{11}) and two aligned with z_3 axis: one on steering head (a_4) and the another on tail (a_5). Also, potentiometers are placed along the fork (l_6) and shock (l_9), and angular speed of each wheel (ω_{12}, ω_{13}) is measured by Hall sensors.

This set of thirteen sensors provide eight out of the fifteen kinematic variables required by the estimator and the remaining seven can be obtained by numerical differentiation or integration of the measured ones. It is a redundant set of sensors in the sense that double differentiation or integration of a measured variable yields another measured variable. For example, double differentiation of the front suspension compression (l_6) yields the suspension acceleration ($a_7 - a_8$). This redundancy of information makes it possible to compensate the error introduced by numerical differentiation and integration. Given that an integrated or differentiated variable is only an approximation to the desired variable, we keep the origin of the variable in the notation. For example $\frac{dv_{x_s}}{dt}$ is not substituted by a_{x_s}.

The downside of a redundant implementation is that the relatively large number of sensors restricts the practical use of the estimator, therefore, we also consider a minimal set of sensors. In principle, seven measurements are required (one measurement per coordinate) since the rest can be obtained by differentiation or integration of the available one. However, if we neglect slippage of the wheels assuming pure rolling, we can calculate the wheel angular acceleration from the forward speed, reducing the set to five measurements. From the three variables that we can measure on each coordinate, we choose the accelerations, since accelerometers are the simplest and cheapest sensors. An exception is made on the forward displacement, in which we prefer the GPS speed since is also a commonly

Table 3.3.3: Description of sensors on the motorcycle. Vertical and lateral and longitudinal are with respect to the body in which they are mounted. The redundant set of sensors is redundant in the sense that double differentiation or integration of a measured variable yields another measured variable. The minimal set has the minimum number of sensor required for a satisfactory estimation of forces.

Sensor	Magnitude	Direction	Location	Redundant set	Minimal set
a_1	Acceleration	Vertical	Under seat	✓	
γ_2	Angle	Lateral	Under seat	✓	✓
v_3	GPS Speed	Forward	Under seat	✓	✓
a_4	Acceleration	Vertical	Steering head	✓	
a_5	Acceleration	Vertical	Rear seat	✓	
l_6	Length	Along fork	Fork	✓	
a_7	Acceleration	Along fork	Steering head	✓	✓
a_8	Acceleration	Along fork	Front wheel	✓	✓
l_9	Length	Along shock	Shock	✓	
a_{10}	Acceleration	Along shock	Shock upper mount	✓	✓
a_{11}	Acceleration	Along shock	Shock lower mount	✓	✓
ω_{12}	Angular speed	Wheel axis	Front wheel	✓	
ω_{13}	Angular speed	Wheel axis	Rear wheel	✓	

available measurement. In addition to these sensors, we consider the pitch angle measurement, since without it the estimation of the tyre forces, particularly the rear forces, are not satisfactory. This is because the estimation of the angle by double integration of the acceleration is deficient. It is worth remarking that this minimal set of sensors is not unique since other combinations can be chosen.

The preprocessing with each set of sensors consist in the following steps. First, measurements are filtered by a lowpass FIR filter with passband and stopband frequencies of 20Hz and 40Hz respectively. Second, algebraic operations are made as specified for each layout. Third, differentiations and integrations are performed. The former by a FIR differentiator with the same frequency limits as the lowpass filter and the latter by the transfer functions $H_1(z)$ for single integrations and $H_2(z)$ for double, which are

$$H_1(z) = \frac{1}{1 + az^{-1}} \tag{3.3.1}$$

$$H_2(z) = \left(\frac{1}{1 + az^{-1}}\right)^2 \tag{3.3.2}$$

where $z = e^{j\omega t}$ and $a = -0.99$. Lastly, the average values are corrected. All accelerations and velocities are corrected to have an average value of zero in one lap, since it is assumed that the previous and following lap are driven in a very close way. Otherwise the following lap is started at a different velocity and position, respectively. Additionally on the min-

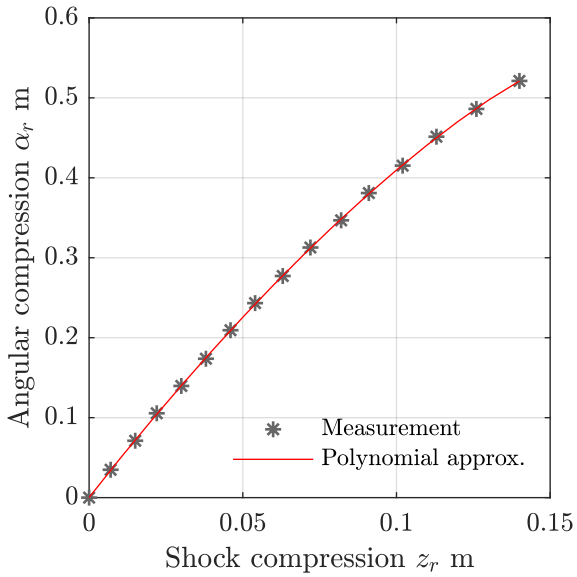

Figure 3.3.4: Relative angle between chassis and swing arm (angular compression) as a function of shock position.

imal set, the average value of each suspension compression is considered to be its static compression, which is corroborated by the potentiometer measurement of the redundant set. Furthermore, negative displacements are made zero, since it is known that they are due to integration error and not to a physical phenomenon.

The preprocessing for the redundant set, is as follows and summarised on Table 3.3.5. Four variables are obtained directly from sensors: horizontal velocity, vertical acceleration , pitch angle, and front suspension compression. Four more variables are obtained from algebraic operations on the measured signals. The front suspension acceleration is measured from the difference between the accelerometers on steering head and front wheel, $a_7 - a_8$. The rear suspension compression angle and acceleration are calculated from the shock potentiometer l_9 and the difference between accelerometers $a_{10} - a_{11}$, using the procedure described in Cossalter [40],

$$\alpha_r = \alpha_r(z_r), \tag{3.3.3}$$

$$\ddot{\alpha}_r = \frac{d^2\alpha_r}{dz_r^2}\dot{z}_r^2 + \frac{d\alpha_r}{dz_r}\ddot{z}_r, \tag{3.3.4}$$

where, $z_r = l_9$, $\ddot{z}_r = a_{10} - a_{11}$ and shock compression velocity $\dot{z}_r$ is estimated as $\frac{dl_9}{dt}$. The relationship between shock position and relative angle between chassis and swing arm $\alpha_r(z_r)$, is shown in Figure 3.3.4. In particular, we fit a polynomial function to the data, since it is simpler to obtain the derivatives for the acceleration calculation. The pitch angle acceleration is measured from the difference between acceleration on steering head a_4 and rear seat a_5 divided by the distance between them l_{st}. Next, five variables

Table 3.3.5: Calculation of variables with the redundant set. It consists of thirteen sensors with which eight variables are obtained. The remaining seven are obtained by differentiation and integration. Measured magnitudes have a numbered subindex according to Table C.0.1.

Coordinate		Position	Velocity	Acceleration
Chassis horizontal displ.	x_s		$v_{x_s} = v_3$	$a_{x_s} \approx \frac{dv_{x_s}}{dt}$
Chassis vertical displ.	z_s		$v_{z_s} \approx \int a_{z_s} dt$	$a_{z_s} = a_1$
Chassis pitch angle	μ	$\mu = \gamma_2$	$v_\mu \approx \int a_\mu dt$	$a_\mu = \frac{a_4 - a_5}{l_{st}}$
Front suspension compr.	z_f	$z_f = l_6$	$v_{z_f} \approx \frac{dz_f}{dt}$	$a_{z_f} = a_7 - a_8$
Rear suspension compr.	α_r	$\alpha_r = f(l_9)$	$v_{\alpha_r} \approx \frac{d\alpha_r}{dt}$	$a_{\alpha_r} = g(a_{10} - a_{11})$
Front wheel rotation	μ_4			$a_{\mu_4} \approx \frac{d\omega_{12}}{dt}$
Rear wheel rotation	μ_1			$a_{\mu_1} \approx \frac{d\omega_{13}}{dt}$

are obtained by differentiation: chassis horizontal acceleration, suspension compression velocities and wheel angular accelerations. Lastly, two variables are obtained by single integration: chassis vertical velocity and pitch rate.

The preprocessing of the minimal set, is summarised on Table 3.3.6. The difference from the redundant set are the following. The vertical acceleration measurement is replaced by the average of the on-board mounted suspension accelerometers corrected by their angles with respect to the vertical axis. Similarly, the pitch angle acceleration is obtained from the difference of these measurements. Additionally, the suspension displacements are replaced by double integration of the corresponding accelerations. As a consequence, the suspension rates are obtained from integration rather than differentiation. The suspension accelerations considered are the wheel acceleration instead of the relative. This is because we found it to yield better estimation of the displacement after the double integration. We believe that is because of the degradation that the double integration introduces mainly in the low frequencies of the signals. According to their frequency spectra (not shown here), this directly affects the chassis acceleration since their main components are below 10 Hz, while wheel accelerations get less distorted since they also have important components in the $10 - 20$ Hz range. Lastly, wheel angular acceleration are obtained by differentiation of forward velocity instead of the corresponding angular velocity.

Figure 3.3.7 shows a comparison of some signals resulting from both sets. Forward velocities and pitch angle are coincident since they have the same origin. Vertical accelerations and front suspension compression are closely estimated with the minimal set, but peaks are smaller. Contrarily, rear suspension velocity is modestly estimated. It is possible to improve the estimation by selecting the filter constant a by comparing the desired signal against the measured one (from the redundant set). However, given that this is not possible in a practical application of the minimal set, we disregard this option. Instead, we use the same filter constant for every integration, and accept the disparity of

Table 3.3.6: Calculation of variables with the minimal set. It consist of six sensors with which six variables are obtained. The remaining nine are obtained by differentiation and integration. Measured magnitudes have a numbered subindex according to Table C.0.1. ρ is the angle between shock axis and z_3.

Coordinate		Position	Velocity	Acceleration
Chassis horizontal displ.	x_s		$v_{x_s} = v_3$	$a_{x_s} \approx \frac{dv_{x_s}}{dt}$
Chassis vertical displ.	z_s		$v_{z_s} \approx \int a_{z_s} dt$	$a_{z_s} = \frac{a_7 c_\epsilon + a_{10} c_\rho}{2}$
Chassis pitch angle	μ	$\mu = \gamma_2$	$v_\mu \approx \int a_\mu dt$	$a_\mu = \frac{a_7 c_\epsilon - a_{10} c_\rho}{l_{st}}$
Front suspension compr.	z_f	$z_f \approx \iint a_{z_f} dtdt$	$v_{z_f} \approx \int a_{z_f} dt$	$a_{z_f} = -a_8$
Rear suspension compr.	α_r	$\alpha_r \approx \iint a_{\alpha_r} dtdt$	$v_{\alpha_r} \approx \int a_{\alpha_r} dt$	$a_{\alpha_r} = g(-a_{11})$
Front wheel rotation	μ_4			$a_{\mu_4} \approx \frac{dv_3/R_f}{dt}$
Rear wheel rotation	μ_1			$a_{\mu_1} \approx \frac{dv_3/R_r}{dt}$

estimation.

The next step is to detect the three driving conditions in which part of the solution is known, using the available variables. On the one hand, driving (accelerating) is detected directly by the horizontal acceleration of the chassis. On the other hand, wheel detachment cannot be detected directly with the available sensors, and it is approximated by the suspension strokes, since full extension is reached when the wheel is in the air. The limitations of this approximation are the instants right after detachment and right after contact recovery. The former, since it takes some time for the suspension to reach full extension due to damping, while the latter, since a minimum force is required to begin compression due to stiction.

Two rules are defined to determine if the condition is happening. On the one hand, the motorcycle is driving if the horizontal acceleration is positive. On the other hand, the wheel has detached from the ground if the corresponding suspension compression is reduced below a threshold. Since the three signals used for the detection are not just 0 and 1, their magnitudes are mapped onto the interval [0 1], using the saturation function defined in Appendix A.1,

$$\mathrm{sat}(y, y_0) = \frac{1 + \sin(\mathrm{atan}(y/y_0))}{2}, \tag{3.3.5}$$

In this way, the three auxiliary weights, w_f, w_r and w_d are calculated as:

$$\begin{aligned} w_d &= \mathrm{sat}(\ddot{x}_s,\ \ddot{x}_{s,sat}), && 1,\ \text{if motorcycle is driving;} \\ w_f &= \mathrm{sat}(-z_f + z_{f,min},\ z_{f,sat}), && 1,\ \text{if front wheel lost contact;} \\ w_r &= \mathrm{sat}(-\alpha_r + \alpha_{r,min},\ \alpha_{r,sat}), && 1,\ \text{if rear wheel lost contact.} \end{aligned} \tag{3.3.6}$$

where, $z_{f,min}$ and $\alpha_{r,min}$ are the threshold values to detect detachment and $\ddot{x}_{s,sat}$, $z_{f,sat}$

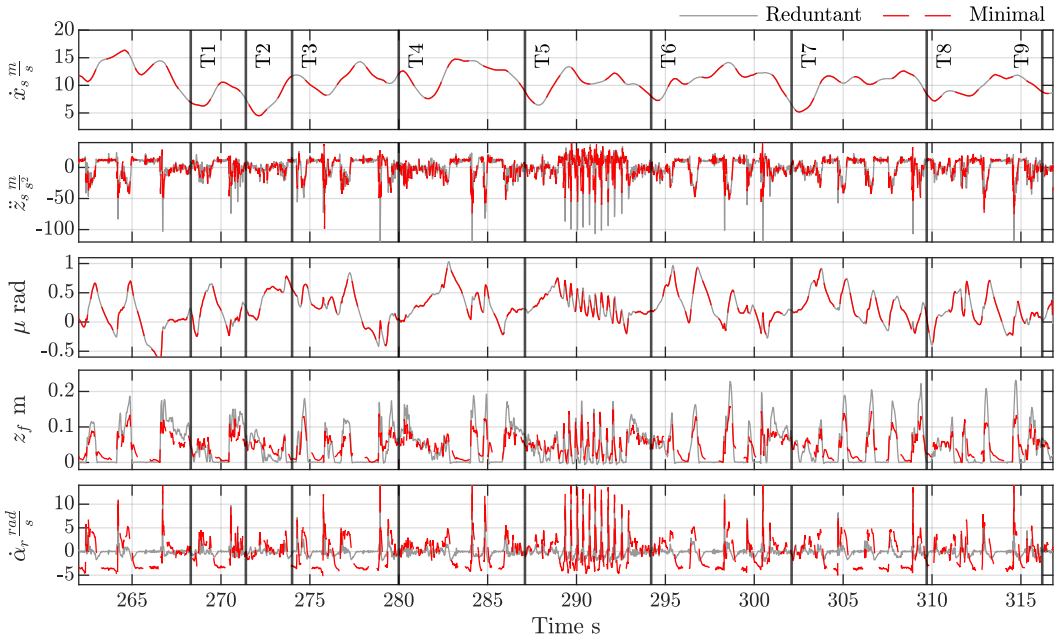

Figure 3.3.7: Five signals after preprocessing. Forward velocity and pitch angle are the same since they have the same origin. Vertical accelerations and front suspension compression are closely estimated with the minimal set, but peaks are smaller. Rear suspension velocity is modestly estimated due to integration errors.

and $\alpha_{r,sat}$ are parameters that control the transition from 0 to 1, of each signal. Figure 3.3.8, illustrates the three signals used to detect the driving conditions, $\ddot{x}_s$, z_f and α_r, and their mapping onto the auxiliary weights w_d, $w_f = W_{11}$ and $w_r = W_{22}$ according to the rules defined in Equation 3.3.6. Additionally, W_{33}, W_{44} and W_{55} are shown, which are obtained according to Table 3.1.2.

Lastly, the equation weights in $\mathbf{B_d}$ are set to 1 as the default value, and $\mathbf{B_c}$ are set to 100, to force the constraints to be met.

3.4 Analysis of contact forces

Using the estimator proposed in Section 3.1 together with kinematic measurements treated according to Section 3.3.1, we are able to provide, an estimation of the contact forces generated by an off-road motorcycles in real driving conditions, which are shown in Figure 3.4.1.

The forces estimated with both sets of sensors vary consistently with the obstacles of the track. Zones of jumps, braking and acceleration can be clearly recognised from the forces. For example, a zone of three jumps can be identified on S1. There are three absences

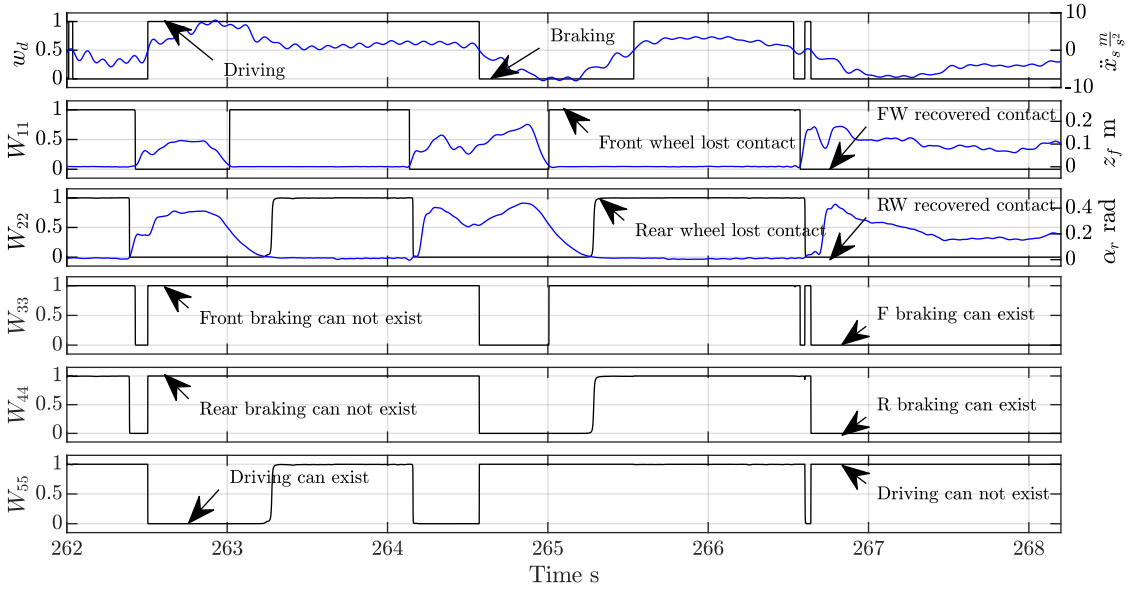

Figure 3.3.8: Auxiliary weights w_d, $w_f = W_{11}$ and $w_r = W_{22}$ record the occurrence of driving, front, and rear wheel detachments, based on horizontal acceleration, front, and rear suspension compression, respectively. Weights W_{11} to W_{55} are obtained according to Table 3.1.2.

of force, showing the instants when the motorcycle is flying. In between them, normal and driving forces show that as soon as it lands, it throttles to the next jump. After the third jump, braking forces can be seen in both wheels, which shows that the brakes are applied just after landing. After the braking zone, the driving force to exit the turn is also depicted. A similar pattern can be recognised on S7 and S8. On S6, the transit over *whoops* can be clearly identified by the impulsive shape of the normal forces. On S4 and S5, large jumps can be identified as relatively long absence of forces.

Furthermore, taking a closer look into the normal forces, Figure 3.4.2, it is possible to distinguish short detachments, for example in the rear wheel while braking before T6. This is of interest for performance assessment, since if these detachments are reduced a harder braking could be possible.

In Figure 3.4.2 it is also possible to observe a rear braking force in the middle of the *whoops* section. In this section, the bumps get between the front and rear wheels, creating a normal force tilted backwards, and not aligned with z_3 axis as assumed by the estimator. The horizontal component of this force reduces the speed of the motorcycle and is detected as a braking force. Nonetheless, the detection of this braking is also of interest for performance assessment, since it creates unwanted braking.

When comparing these forces with preceding and subsequent laps on the test (not shown here), the same pattern of forces is seen. Small variations such as the number of detachments in braking or magnitude of peaks in landings, show that variations in driving

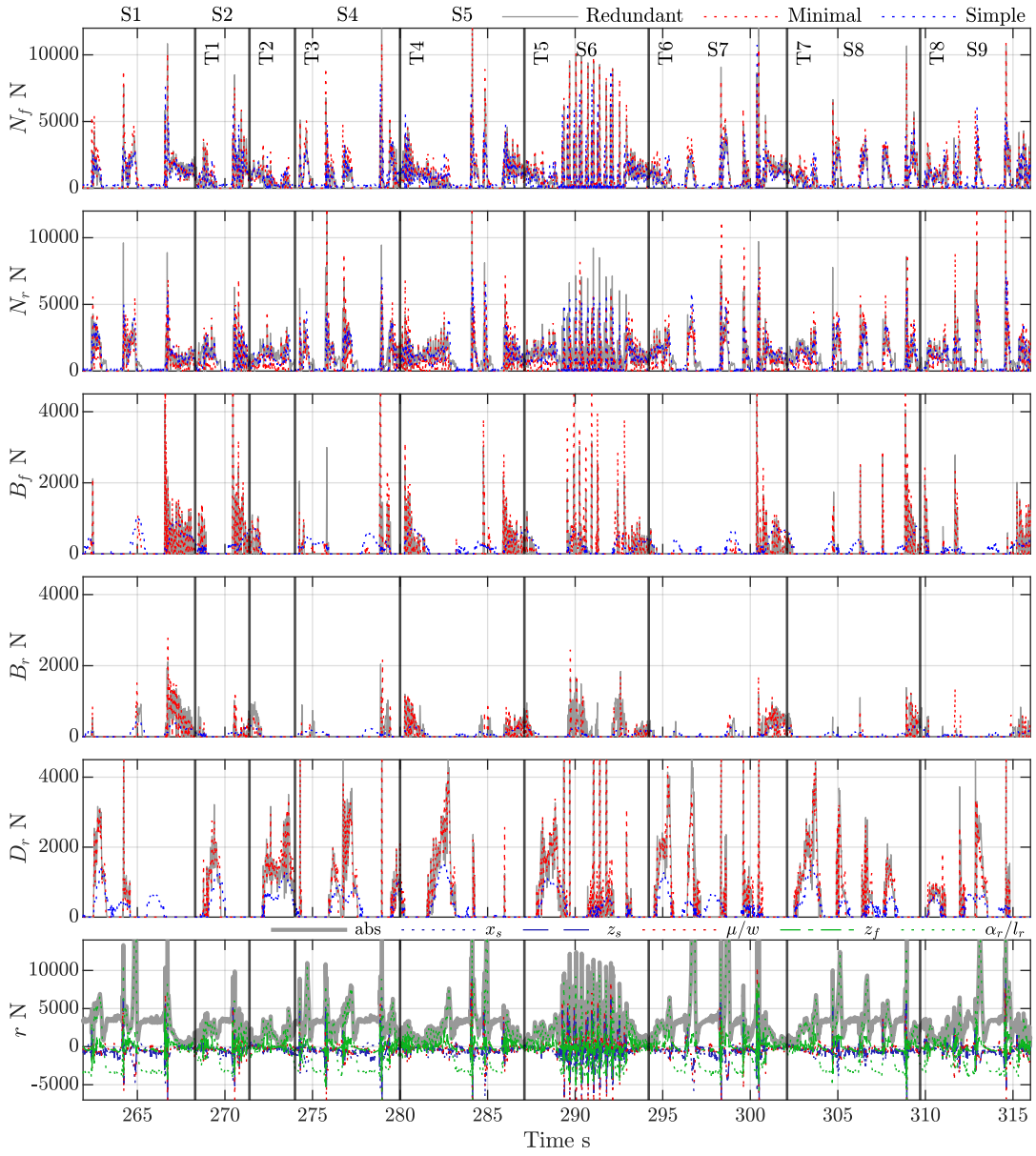

Figure 3.4.1: Contact forces on a motocross track estimated considering a redundant and minimal set of sensors. Zones of jumps, braking, accelerations can be recognized. Residuals of the minimal set (absolute value and dynamic equations) are shown. Estimation of contact forces with a simpler methodology is in good agreement on the normal force but not on the horizontal ones.

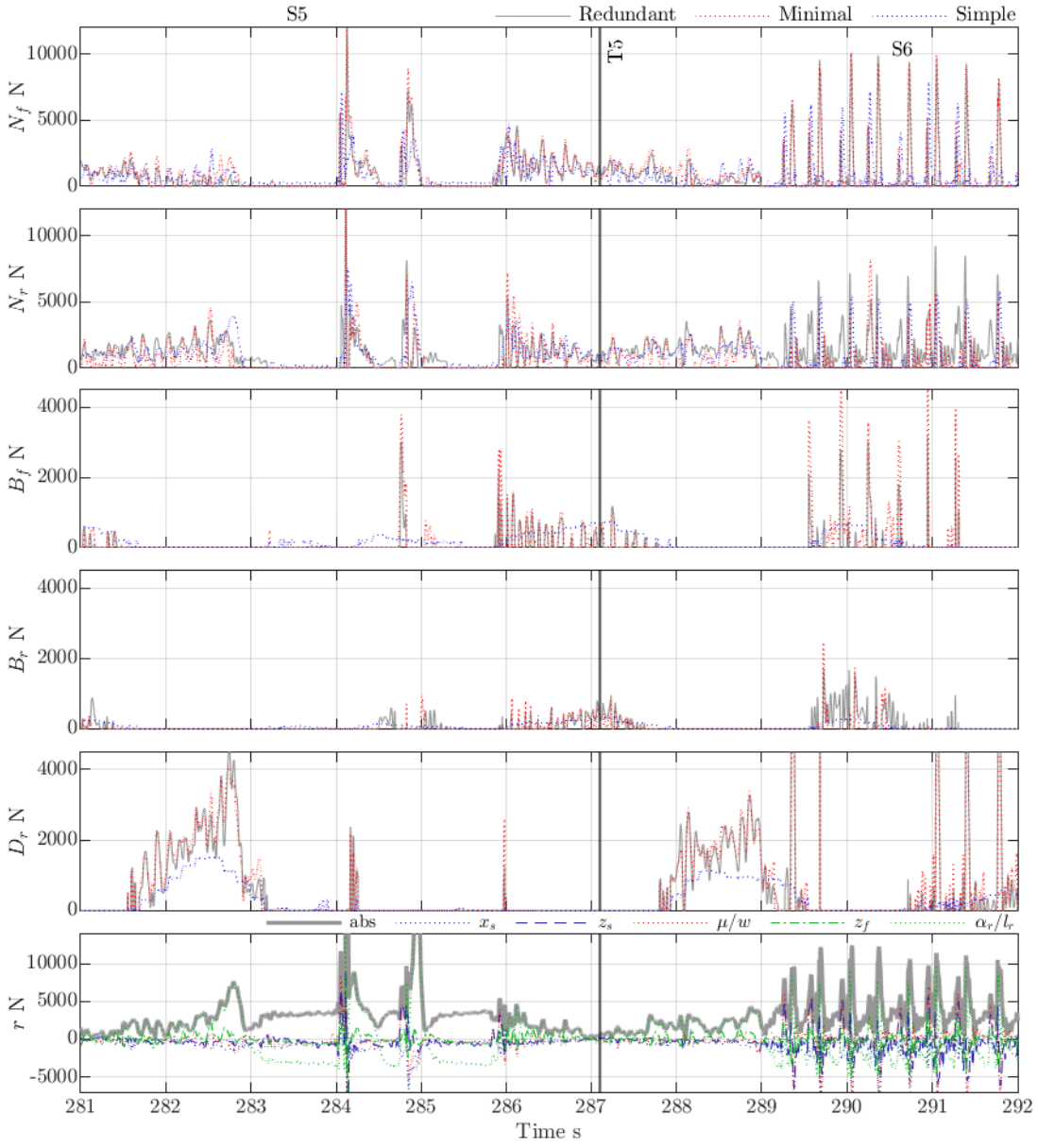

Figure 3.4.2: Close up of turn 6. Peaks in normal forces show the *whoops* of S6; absences of rear normal force between $t = 293$ and 294, show detachments of the rear wheel on the braking phase; and rear braking force around $t = 290$ s shows the braking effect of the *whoops* due to the horizontal component of the normal force. Residuals of the minimal set (absolute value and dynamic equations) are shown. Estimation of contact forces with a simpler methodology is in good agreement on the normal force but not on the horizontal ones. Larger residuals on the impact zones and smaller on the turn, shows that the estimator's assumption are in better agreement with reality in the latter.

along tests can also be distinguished.

Comparing the estimations with both sets, it is possible to see that there is a significant correlation between them. The obstacles on the track as well as the driver inputs can be identified with both. Moreover the magnitudes are very close among them as well. On a closer look of Figure 3.4.2 it is possible to distinguish some differences, such as some absences of peak around $t = 290$ s in the rear normal force. Nonetheless, a satisfactory estimation is possible with less than half of the sensors used in the redundant set.

The residuals of the estimation with the minimal set are depicted in Figures 3.4.1 and 3.4.2. Peaks around landings and high impacts zones show that in these parts the estimator's assumptions diverge from reality. From the four assumptions of the dynamic equations and the simplifications of the rider model, the most feasible cause is the assumption of constant vertical force of the rider since it is unlikely that the rider can absorb impacts perfectly. Contrarily, around turns, as seen in Figure 3.4.2, the residuals are significantly lower than on straights, indicating that the estimator assumptions are in better agreement with reality. The main contribution to the residuals, comes from the rear suspension equation, α_r. This residual is correlated to the estimation of the rear suspension velocity, as shown in Figure 3.3.7, from where we can deduce that it is its origin. Also, this can be corroborated by the residuals obtained with the redundant set, not shown here, which do not show the important contribution from the α_r equation, since the rear suspension velocity is estimated in a better way. Given that this discrepancy affects directly the rear wheel, it can explain the differences found on the rear wheel forces.

The estimator is compared against simple methodologies of calculation. On the one hand, the normal forces are calculated using a quarter car assumption as Delvecchio [69] (although he used it in a Kalman filter architecture) considering only the vertical forces on the wheels,

$$N_f = S_f \cos(\epsilon) + m_4 \ddot{z}_4 \tag{3.4.1}$$

$$N_r = \frac{TS_r}{l_r} + m_1 \ddot{z}_1 \tag{3.4.2}$$

where, S_f is front suspension force and TS_r is rear suspension torque, while $\ddot{z}_1$ and $\ddot{z}_4$ are vertical accelerations of front and rear wheels. On the other hand, the horizontal forces are calculated assuming a quasi-static condition with which only the horizontal acceleration is required. Since it is not possible to estimate the braking distribution with this methodology, it is assumed to be 70% on the front.

$$B_f = 0.7m\ddot{x}_s, \quad \ddot{x}_s < 0 \tag{3.4.3}$$

$$B_r = 0.3m\ddot{x}_s, \quad \ddot{x}_s < 0 \tag{3.4.4}$$

$$D_r = m\ddot{x}_s, \qquad \ddot{x}_s \geq 0 \tag{3.4.5}$$

where $m = m_1 + m_2 + m_3 + m_4 + m_r$ is the total mass of the system, and in the case of $\ddot{x}_s < 0$, $D_r = 0$ and if $\ddot{x}_s \geq 0$, $B_f = B_r = 0$. Results show a modest correspondence on the normal forces. This implies that the contribution of the perpendicular force over the fork and the force along the swingarm acting on its main pin are moderate relative to the normal forces. On the other hand, results for horizontal forces are not in good agreement with our estimator. For example in Figure 3.4.2, around $t = 287$ s the braking forces are less oscillatory and of lower magnitudes, which is the result of assuming a quasi-static condition. Also, there are horizontal forces in absence of normal forces as predicted for example at $t = 283.5$ s, which is the result of not combining the information on the horizontal and vertical directions. This shows that the wheel dynamics can not be neglected in off-road motorcycles. Moreover, in a broader sense, this analysis shows that estimators found in the literature are not representative of these motorcycles.

These results show that the estimated forces vary consistently with the obstacles of the track. Moreover, it is shown that it can provide additional valuable information for optimisations such as detachments, *whoops braking* and variations in driving along tests. Furthermore, since this information is derived from objective measurements, it is free from rider's bias and is reproducible. Furthermore, it has been shown that a satisfactory estimation is possible with a minimal set of sensors which increases the practical applicability of this method.

A limitation of this estimator is that its precision was not determined, since it was not feasible, in practice, to measure the contact forces with the envisaged methodology. Consequently, the magnitude of estimated forces should not be taken as exact, and instead only as a reference. The estimator has thirty nine inputs: twenty parameters to describe the motorcycle, fifteen kinematic variables and four external forces. The twenty parameters are geometrical and inertial, thus, they can be measured with a relatively high accuracy and fourteen of them do not vary over time. The exceptions are tyre radius, that is reduced due to compressions, and chassis mass and inertia that is reduced due to fuel consumption, which also affects the location of centre of mass. The former can decrease up to 25% and it affects the calculation of moments of tangential forces B_f, B_r and D_r around the chassis centre of mass, and around the swingarm main pin. Since, three equations are not affected, the compensation effect of the overdetermined system is expected to attenuate this variation significantly. Due to fuel consumption, chassis mass can decrease by around 10%, and inertia and centre of mass location, less than 2%, because the fuel tank is close to the centre of mass. Since it affects all the equations of motion, the compensation effect might not be important, and should be considered if performance is analysed over an entire gasoline tank. For analysis over a few laps, the effect is expected to be imperceptible. Regarding the fifteen kinematic variables, they can be measured directly or calculated from the measured ones. Errors in measurements are expected to be attenuated by the compensation effect of the overdetermined system and the constraint equations. The

calculated signals do not incorporate new information to the system, thus, they can not compensate errors, reducing the accuracy of the estimator. Regarding the influence of external forces, it is shown in Chapter 4, that the estimated forces have a low sensitivity to them, mainly due to the compensation effect. A detailed sensitivity analysis is out of the aim of this Chapter however, given that the inputs are available with a relatively high accuracy, the precision of the estimations should be reasonably good.

Lastly, considering that, in the preprocessing, the lowpass filter, integrations and differentiations can be performed almost on real time (there is a delay due to the filter), and that the step of average correction could be modified to be performed on real time, this estimator has the potential to be exploited as the basis for a controller of a semi-active suspension system, and if lateral dynamic is added, it could also be used for stability control in off-road riding.

3.5 Summary

In this Chapter we have developed an estimator of contact forces for off-road motorcycles. It was developed to solve the need for a procedure to assess performance experimentally.

It is based on kinematic measurements and inverse dynamics to overcome the difficulty of direct sensing. Measurement errors are attenuated by an overdetermined set of equations, and non-physical solutions are reduced with a set of constraints that limits the existence of tensile force on tyres, and of tangential force without a normal one. Verification against a virtual experiment shows that the estimation is in good agreement despite chain tension omission and considering a different set of rider forces.

Experimental tests showed that the estimated forces vary consistently with the obstacles of the track and details, such as wheel detachments and *whoops braking*, can be distinguished. Furthermore, we have shown that a satisfactory estimation is possible with a minimal set of sensors. Therefore, we consider that it is reasonable to use it as an objective methodology to assess performance. Although the estimator has been developed to assess performance, it can be used as a basis to develop an on board control system to improve riding safety.

In the next Chapter, we discuss a rider model to be used in this estimator.

CHAPTER 4

Rider model for inverse dynamics calculations

In Chapter 3, we derived an estimator of the contact forces considering the rider as external forces acting on the motorcycle. The magnitudes of these rider forces can be obtained by any method, since no assumption was made on their characteristics, except that they act on the foot peg and handlebar. An option is to measure them directly by load cells on these points, however this approach is invasive, complicates the data acquisition system and would be reasonable to use only to validate models. An alternative is to estimate them from other measurements, which is the method we choose, since it is less invasive and simpler to implement.

In this chapter, we investigate a suitable description for the rider forces to be used in the estimator. First, we develop a rider model based on the assumption of passive behaviour, which is the predominant method in the literature. Since there is no evidence on the validity of this assumption, we develop a second model, which is simpler and based on a different set of assumptions. We compare them using experimental data collected on a motocross track and select the best suited for off-road driving.

4.1 Review of rider models

The rider is an important component of the overall motorcycle dynamics. His/her mass contribution to the motorcycle-rider system is non-negligible [51]. Additionally, in off-road, the rider drives mainly in the standing position, where arms and legs provide significant vibration isolation [50].

A comprehensive description of forces at hands and feet is complex and laborious. This is because the human body is a structure with heterogeneous mass distribution and multiple degrees of freedom. Moreover, it is controlled by conscious and unconscious decisions through a combination of passive and active actions of muscles and tissues. Considering the motion of large joints only and neglecting deformation of parts, the human-body can be reduced to a collection of interconnected rigid bodies.

Motorcycle models have been developed considering the rider in the seated position since they were developed with focus on control strategies in on-road driving [52] [53], (see [51] for a review). The dynamics of a seated and standing rider are significantly different, consequently these models are not valid for off-road.

Rider models in standing positions are found in similar activities. For example, in off-road bicycles, the rider also drives in standing position and is exposed to off-road excitations. These models were developed by Wilczynski [54] and Wang [50] to estimate frame loads in these bicycles. In particular, the rider was reduced to five rigid bodies: torso, upper and lower legs and arms, connected by six joints: wrist, elbow, shoulder, hip, knee and ankle. Only passive action of muscles is considered. Specifically, elastic and damping elements, connecting hip to ankle and shoulder to wrist, representing muscular action of legs and arms, respectively. Wilczynski's model was compared against experimental measurements showing good agreement, while Wang identified stiffness and damping of arms and legs for this model. Another interesting example are horse riders. For example, Cocq et al, [55], had studied rider model requirements for different riding techniques, such as sitting trot, rising trot and modern jockey technique. They modelled the rider with a single mass with a vertical degree of freedom, connected to the horse by spring and damper elements. They confirm the hypothesis that in standing position, the leg spring stiffness and damping are low.

In summary, the description of rider forces is not simple since there are several bodies involved and joints are actuated by passive and active elements. On the one hand, considering fewer bodies is a reasonable simplification in off-road bicycles and horse riding, and have been validated experimentally in both activities. Likewise, it is a reasonable simplification in off-road motorcycles, since the relative motion between the heavier parts of the body (head, torso and upper legs) is small even under large motions of legs and arms.

On the other hand, neglecting the active action as in both examples can be put in doubt in off-road motorcycles, because due to the larger amplitude of excitations, the active actions might be required to control the larger motions. This doubt can be supported by an observation made by Garret [74] on human landings, which are similar to impulsive excitations received while riding standing-up. He explains that only during the first 50 to 80 milliseconds immediately after the impact, the reaction is passive, afterwards is

active as well. In the absence of conclusive evidence to neglect the active action in our application, we decide to test it, by comparing a passive rider to a rider model with the basic dynamics. To this end, in the following, we develop both models.

4.2 Derivation of a passive rider model: Rider A

The passive rider model is derived considering a single body since it suffices to test if the active action of arms and legs can be neglected. In particular, the following four considerations are made for this simplification. First, head, upper and lower torso masses are considered on the torso since they show small relative motion among them. Second, the motion of arms and legs masses is neglected, because the masses are small compared to the torso. Third, upper arm and leg masses are added to the torso, since their motion is similar. Fourth, lower arm, lower legs, hand and foot, are considered as point masses on the handlebar and foot peg, since their motions with respect to the chassis are small or negligible.

The muscular action of arms and legs is passive only and consists of linear springs and dampers, as considered in the literature. They act between shoulder and hands and hip and feet, respectively. Together, these forces provide two constraints on the torso.

Because the torso has three degrees of freedom, a third constraint has to be added. In the cyclist models, the horizontal translation of the rider has been constrained. However, we opt to constrain the torso rotation because we have observed that in off-road motorcycle driving, head and torso are kept predominantly at about a constant angle, while the relative distance between rider and chassis changes constantly to overcome different obstacles. This behaviour is also observed in horse racing riders.

We implement this, by an external torque in the torso which cancels-out any resultant torque between arms and legs. In reality, this torque is produced at hip and shoulder. However, to simplify modelling, shoulder torque is neglected because it is expected to be much smaller compared to the hip counterpart. The reason for this assumption is that the muscles responsible for hip rotation (glutes, psoas and illacus) are larger and more powerful than the muscles responsible for shoulder rotation (pectoralis major, latissimus dorsi and teres major). This is because, the former muscles are responsible for keeping the torso vertical, which involves around half of body weight, while the latter are for arm motions which are around 5% of body weight each.

Summing up the assumptions, the rider is reduced to one body connected to the motorcycle by two linear spring-damper elements, and keeps the torso angle constant thanks to an internal torque at the hip, as shown on Figure 4.2.1.

The generalised coordinates used to describe the motion of the rider are: displacement

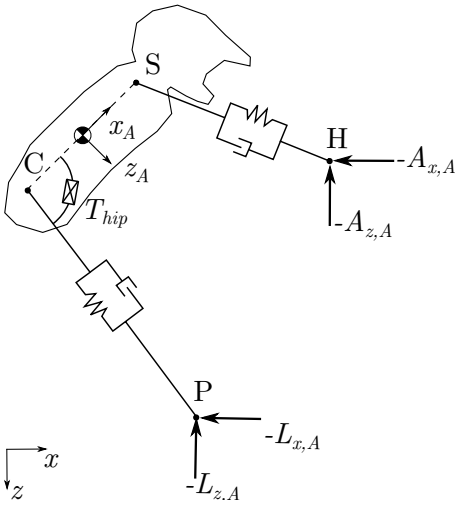

Figure 4.2.1: Rider A model. Rider A consists of one body connected to the motorcycle by arm and legs, assumed to act passively, and a torque on the hip, T_{hip}, that keeps the torso angle constant. The motion of handlebar (H) and foot-peg (P) excite the rider, and from the spring and dampers models of arms and legs, the forces are retrieved.

along the hip-shoulder direction, x_A, and perpendicular to it pointing to the motorcycle, z_A. They are collected in

$$\mathbf{q_A} = [x_A, z_A]^T. \tag{4.2.1}$$

The selection of these coordinates is because eventually, they can be related directly to an inertial sensor attached to the rider's torso, as done equivalently on the motorcycle. The rider is excited by the motion of the chassis, which is assumed to be known from measurements. This motion is the input to rider and is described by

$$\mathbf{u} = [x_s, z_s, \mu, \dot{x}_s, \dot{z}_s, \dot{\mu}]^T. \tag{4.2.2}$$

4.2.1 Leg and arm forces

Rider forces are defined in an absolute reference frame as,

$$\mathbf{f_{r,A}} = [L_{x,A}\ L_{z,A}\ A_{x,A}\ A_{z,A}]^T = [L_x\ L_z\ A_x\ A_z]^T, \tag{4.2.3}$$

where, L and A are leg and arm forces, subindices x and z indicate forward and downward components, and subindex A refers to rider A. The latter index is dropped in this section to simplify notation. We express them as functions of the generalised coordinates $\mathbf{q_A}$ and the inputs $\mathbf{u}$, to remove them from the equations of motions, as follows.

By definition, since no torque is applied on the shoulder or wrist, the arm force is

composed of a single force inline with it,

$$\begin{aligned}\mathbf{A} &= [A_x\ A_z]^T,\\ &= \mathbf{f_a},\\ &= f_a\hat{\mathbf{u}}_{\mathbf{S,H}},\end{aligned} \tag{4.2.4}$$

where, f_a is its magnitude and $\hat{\mathbf{u}}_{\mathbf{S,H}}$ the unit vector along the arm, defined positive from shoulder (S) to handlebar (H).

Differently, on the leg, due to the hip torque, the leg force is composed of an inline plus a perpendicular force,

$$\begin{aligned}\mathbf{L} &= [L_x\ L_z]^T,\\ &= \mathbf{f_l} + \mathbf{f_{l,t}},\\ &= f_l\hat{\mathbf{u}}_{\mathbf{C,P}} + f_{l,t}\hat{\mathbf{u}}_{\mathbf{l,t}},\end{aligned} \tag{4.2.5}$$

where, f_l and $f_{l,t}$ are inline an perpendicular force at the foot-peg respectively, while, $\hat{\mathbf{u}}_{\mathbf{C,P}}$, is the unit vector along the leg, positive from hip (C, from Spanish, cadera) to foot-peg (P) and $\hat{\mathbf{u}}_{\mathbf{l,t}}$ the unit vector perpendicular to the leg, obtained by $\pi/2$ rotation of the previous one.

The unit vectors are obtained from the distance vectors,

$$\hat{\mathbf{u}}_{\mathbf{S,H}} = \frac{\mathbf{r}_{\mathbf{S,H}}}{\|\mathbf{r}_{\mathbf{S,H}}\|}, \tag{4.2.6}$$

$$\hat{\mathbf{u}}_{\mathbf{C,P}} = \frac{\mathbf{r}_{\mathbf{C,P}}}{\|\mathbf{r}_{\mathbf{C,P}}\|}, \tag{4.2.7}$$

$$\hat{\mathbf{u}}_{\mathbf{l,t}} = \begin{bmatrix}0 & -1\\ 1 & 0\end{bmatrix}\hat{\mathbf{u}}_{\mathbf{C,P}}, \tag{4.2.8}$$

where,

$$\mathbf{r}_{\mathbf{S,H}} = \mathbf{x}_{\mathbf{H}}(\mathbf{u}) - \mathbf{x}_{\mathbf{S}}(\mathbf{q}_{\mathbf{A}}), \tag{4.2.9}$$

$$\mathbf{r}_{\mathbf{C,P}} = \mathbf{x}_{\mathbf{P}}(\mathbf{u}) - \mathbf{x}_{\mathbf{C}}(\mathbf{q}_{\mathbf{A}}), \tag{4.2.10}$$

where, $\mathbf{x}$ refers to the position of a point. In this way, all unit vectors are described in terms of rider $\mathbf{q_A}$ and the motorcycle $\mathbf{u}$ positions only.

The magnitude of the forces inline with leg and arm are due to springs and dampers. They are considered linear with their length l and rate of change $\dot{l}$, as on [54] and [50],

$$f_l = k_l(l_{l0} - l_l) + c_l\dot{l}_l, \tag{4.2.11}$$

$$f_a = k_a(l_{a0} - l_a) + c_a\dot{l}_a, \tag{4.2.12}$$

where, k and c are stiffness and damping coefficients, l_{l0} and l_{a0} are initial lengths of leg and arm. These lengths and rate of change are described by

$$l_l = \|\mathbf{r_{C,P}}\| = \left(\mathbf{r_{C,P}} \cdot \mathbf{r_{C,P}}^T\right)^{0.5}, \tag{4.2.13}$$

$$l_a = \|\mathbf{r_{S,H}}\| = \left(\mathbf{r_{S,H}} \cdot \mathbf{r_{S,H}}^T\right)^{0.5}, \tag{4.2.14}$$

$$\dot{l}_l = \frac{dl_l}{dt}, \tag{4.2.15}$$

$$\dot{l}_a = \frac{dl_a}{dt}, \tag{4.2.16}$$

In this way, f_l and f_a are also described in terms of rider $\mathbf{q_A}$ and the motorcycle $\mathbf{u}$ positions only.

Lastly, an expression for $f_{l,t}$, is derived using Euler's equation on the rider,

$$0 = \mathbf{r_{A,P}} \times (\mathbf{f_l} + \mathbf{f_{l,t}}) + \mathbf{r_{A,H}} \times \mathbf{f_a}, \tag{4.2.17}$$

where,

$$\mathbf{r_{A,P}} = \mathbf{r_{A,C}} + \mathbf{r_{C,P}}, \tag{4.2.18}$$

$$\mathbf{r_{A,H}} = \mathbf{r_{A,S}} + \mathbf{r_{S,H}}, \tag{4.2.19}$$

are the distances from centre of rider A, to foot peg and handlebar respectively. Expanding terms of Equation 4.2.17,

$$0 = (\mathbf{r_{A,C}} + \mathbf{r_{C,P}}) \times (\mathbf{f_l} + \mathbf{f_{l,t}}) + (\mathbf{r_{A,S}} + \mathbf{r_{S,H}}) \times \mathbf{f_a}, \tag{4.2.20}$$

we find that some cross products can be solved directly as,

$$\begin{aligned} \mathbf{r_{C,P}} \times \mathbf{f_l} &= \mathbf{r_{C,P}} \times f_l \ \hat{\mathbf{u}}_{\mathbf{C,P}} \\ &= f_l(\mathbf{r_{C,P}} \times \hat{\mathbf{u}}_{\mathbf{C,P}}) \\ &= f_l(l_l \cdot 1 \cdot \sin(0)) = 0, \end{aligned} \tag{4.2.21}$$

$$\begin{aligned} \mathbf{r_{C,P}} \times \mathbf{f_{l,t}} &= \mathbf{r_{C,P}} \times f_{l,t} \ \hat{\mathbf{u}}_{\mathbf{l,t}} \\ &= f_{l,t}(\mathbf{r_{C,P}} \times \hat{\mathbf{u}}_{\mathbf{l,t}}) \\ &= f_{l,t}(l_l \cdot 1 \cdot \sin(\pi/2)) = f_{l,t} l_l, \end{aligned} \tag{4.2.22}$$

$$\begin{aligned} \mathbf{r_{S,H}} \times \mathbf{f_a} &= \mathbf{r_{S,H}} \times f_a \ \hat{\mathbf{u}}_{\mathbf{a}} \\ &= f_a(\mathbf{r_{s,H}} \times \hat{\mathbf{u}}_{\mathbf{a}}) \\ &= f_a(l_a \cdot 1 \cdot \sin(0)) = 0, \end{aligned} \tag{4.2.23}$$

reducing Equation 4.2.20 to

$$0 = \mathbf{r_{A,C}} \times \mathbf{f_l} + \mathbf{r_{A,C}} \times \mathbf{f_{l,t}} + f_{l,t} l_l + \mathbf{r_{A,S}} \times \mathbf{f_a}. \tag{4.2.24}$$

This is an implicit expression for $f_{l,t}$. It is a function of $\mathbf{f_l}$, $\mathbf{f_a}$ and l_l only, which in turn, are expressed as a function of $\mathbf{q_A}$ and $\mathbf{u}$ in Equations 4.2.4 to 4.2.16. The internal distances of the torso, $\mathbf{r_{A,C}}$ and $\mathbf{r_{A,S}}$, are constant terms, since the torso neither rotates nor deforms.

Additionally, we can find an expression for the hip torque as a function of $\mathbf{q_A}$ and $\mathbf{u}$ using Euler's equation on the leg,

$$0 = -T_{hip} + \mathbf{r_{C,P}} \times (\mathbf{f_l} + \mathbf{f_{l,t}}), \tag{4.2.25}$$

which, by considering Equations 4.2.21 and 4.2.22, can be reduced to the trivial result that hip torque is,

$$0 = -T_{hip} + f_{l,t} l_l, \tag{4.2.26}$$

where, $f_{l,t}$ and l_l had already been defined in terms rider and motorcycle positions.

In this way, it is shown that in order to estimate the rider forces $f_{r,A}$ it is necessary to know its motion $\mathbf{q_A}$ as well as the motorcycle motion $\mathbf{u}$. It is assumed that the latter is available from measurements for the estimator, since that is the purpose of this model. However, the former is not measured for the estimator and there are two option to obtain them, measure or calculate. For measuring, acceleration can be obtained from accelerometers, while positions can be obtained by a vision based approach described by Cheli et al. [75]. By combination of integral and derivative of the previous measurements, the velocities can be obtained. However, this measurement requires cumbersome experimental implementation, and would be more reasonable to spend this effort in load cells at handlebar and foot-peg to measure the rider forces directly, or use this measurements in an inverse dynamics model of the rider. Since the first aim of this model is to prove the hypothesis of passive forces with a simple model, we decide to calculate them. To this end, we write the equations of motion of the rider, and integrate them to obtain $\mathbf{q_A}$.

4.2.2 Equation of motion and solution

Using a Newton approach, two equations of motion are derived in matrix form,

$$\mathbf{M_A}\ddot{\mathbf{q}}_\mathbf{A} + \mathbf{m_A}' = \mathbf{B_w} g + \mathbf{B_m}\ \mathbf{f_{r,A}}, \tag{4.2.27}$$

where, $\mathbf{M_A}$ is the rider mass matrix,; $\mathbf{m_A}'$ is a pseudo-mass vector containing products of velocities; $\mathbf{B_w}$, $\mathbf{B_m}$, are matrices that project the weight g and rider force $\mathbf{f_{r,A}}$, into the generalised coordinates. All of these terms, except g, are dependent on the rider position $\mathbf{q}_A$, while $\mathbf{f_r}$, is also dependent on the motorcycle motion $\mathbf{u}$. The system is non linear because the geometry changes significantly, therefore it can only be solved by numerical integration for which a Runge-Kutta integrator suffices. This integrator requires to reduce

the system to a first order differential equation,

$$\dot{\mathbf{v}}_\mathbf{A} = {\mathbf{M}_\mathbf{A}}^{-1}(\mathbf{B}_\mathbf{w} g + \mathbf{B}_\mathbf{m}\, \mathbf{f}_{\mathbf{r},\mathbf{A}} - {\mathbf{m}_\mathbf{A}}'), \tag{4.2.28}$$

$$\dot{\mathbf{q}}_\mathbf{A} = \mathbf{v}_\mathbf{A}, \tag{4.2.29}$$

from where the rider $\mathbf{q_A}$ motion will be obtained, and by using the equations derived in Sub-Section 4.2.1, the rider forces are obtained,

$$\mathbf{f}_{\mathbf{r},\mathbf{A}} = \mathbf{f}_{\mathbf{r},\mathbf{A}}(\mathbf{q}_\mathbf{A}, \mathbf{u}). \tag{4.2.30}$$

The codes for the derivation of the equations of rider can be found in Appendix D.

It should be highlighted that this procedure requires the integration of equations of motion. This process is expensive computationally, so it would require a relatively powerful processor to be able to calculate rider forces in real time. Considering that this model might be improved in a second stage by adding degrees of freedom and/or bodies and joints, it would yield an even more expensive calculation. Nonetheless, after the rider motion is known, the rider forces are calculated in an economical way, since it only requires algebraic operations.

4.3 Derivation of a simple rider model: Rider B

The simple rider model is derived with the aim of calculating the fundamental dynamics of the rider. The motion of the rider is complex, involves several parts, and is unknown. Partly, the latter characteristic is the reason for the equations of motions of Rider A. However on certain situations, it is reasonable to assume a simplified motion from where the elementary nature of the forces can be implied.

First, observation of the rider driving on irregular roads Figure 4.3.1, shows that the centre of gravity, which is approximately in the hip, is almost on a constant vertical position, i.e.

$$\Delta z_B \approx 0, \tag{4.3.1}$$

where, z_B is the absolute vertical position of the rider. Consequently, velocity and acceleration are small,

$$\dot{z}_B \approx 0, \tag{4.3.2}$$

$$\ddot{z}_B \approx 0. \tag{4.3.3}$$

Then, from a vertical equation of motion, it can be shown that vertical forces of arm

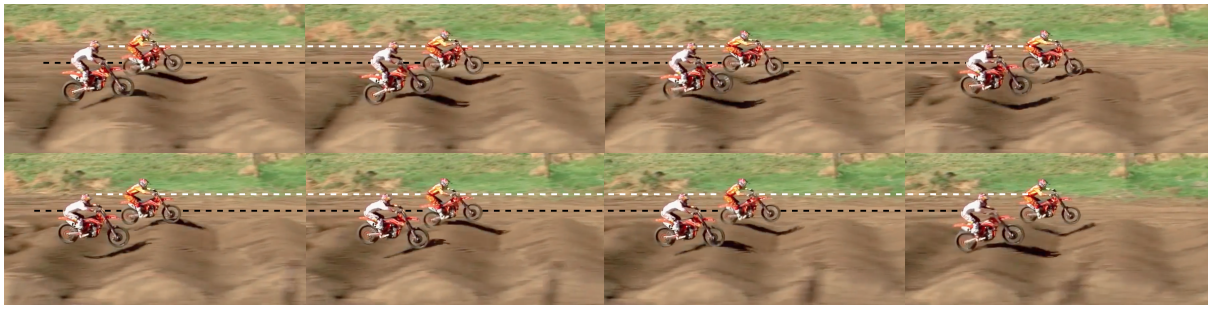

Figure 4.3.1: Two motorcycles riding through *whoops* section. It shows that although the riders moves broadly, the vertical position of their hips shown in white and black dashed lines, remains roughly at the same height [76].

and leg are close to equilibrium with the rider's weight, and consequently, are close to constant:

$$m_r \ddot{z}_B = -L_z - A_z + m_r g, \tag{4.3.4}$$

$$0 \approx -L_z - A_z + m_r g, \tag{4.3.5}$$

$$L_z + A_z \approx m_r g \rightarrow \text{const.} \tag{4.3.6}$$

Second, from observation of the rider in braking and acceleration, it can be seen that his/her centre of mass barely moves horizontally with respect to the chassis, which implies that their horizontal positions, and hence accelerations, should be similar

$$x_B \approx x_s, \tag{4.3.7}$$

$$\ddot{x}_B \approx \ddot{x}_s, \tag{4.3.8}$$

where, x_B and x_s are absolute horizontal positions of rider and motorcycle chassis. From an horizontal equation of motion, it can be shown that the horizontal forces counteract the inertial force only.

$$m_r \ddot{x}_B = -L_x - A_x, \tag{4.3.9}$$

$$m_r \ddot{x}_s \approx -L_x - A_x, \tag{4.3.10}$$

To further simplify the representation, we assume that the vertical force is completely exerted through the legs ($A_z = 0$) and the horizontal, by the arms ($L_x = 0$), as shown in Figure 4.3.2, resulting in,

$$\mathbf{f_{r,B}} = [L_x \; L_z \; A_x \; A_z]^T = [0 \; m_r g \; -m_r \ddot{x}_s \; 0]^T. \tag{4.3.11}$$

Additionally, we consider that all components are zero if contact is lost in front and rear wheels simultaneously.

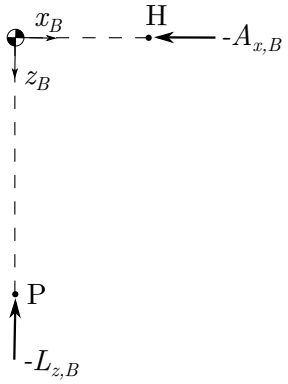

Figure 4.3.2: Rider B model. Rider B consist on two forces explicitly defined on terms of chassis motion ($\ddot{x}_s$).

An interpretation of the resulting model in vibration terms, is that the rider is perfectly isolated from the motorcycle in the vertical direction, and rigidly attached in the horizontal direction. Another interpretation of the resulting model is that the rider mass is suspended vertically by a zero stiffness spring (with an infinite preload) and attached horizontally, by an infinite stiffness spring. The zero stiffness spring appears to be the limiting case of a rider, since Cocq [55], detected that horse racing riders, can be modelled with a very low vertical stiffness.

The underlying difference between both models are the assumptions. On Rider A, they are made on the equations of motion that calculate the kinematics, while on Rider B, they are made directly on the kinematics. The consequence of this is that Rider A can potentially represent accurately the kinematics, but it can also diverge significantly from reality if any significant phenomenon is being omitted from the equations. Conversely, on Rider B a simplified version of the real motion is assumed. Taking into account that the forces depend on the motion, Rider A might provide a very close as well as very far estimation of rider-motorcycle forces, while Rider B, although not exact, is known to be similar to the real interaction.

4.4 Comparison of rider models using experimental data

The performance of both rider models are compared for three driving conditions using data collected with a motocross motorcycle. First, we compare arm and leg forces of both rider models. The rider mass is 75 kg, and stiffness and damping of arm and leg of rider A are: $k_a = 23100$ N/m, $c_a = 515$ Ns/m, $k_a = 74000$ N/m, $c_l = 1350$ Ns/m as suggested by [54]. Then, we use these forces as inputs for the estimator described in Chapter 3, to compare

the estimated tyre forces. Data is collected and processed according to Sub-Section 3.3.1.

Three diverse driving conditions are selected to analyse the performance of the models. The first situation consists of two consecutive jumps of ≈ 0.8 s flying time; the second situation consist of ten bumps, usually referred as *whoops*; and the third situation is a cornering manoeuvre which includes braking and exit acceleration phases.

The forces of the riders on each situation are shown in Figure 4.4.1. It shows that Rider A forces are significantly larger and more oscillatory than Rider B forces. For example, on landings of jumps ($t = 1$ and $t = 2.8$ s), L_z and A_x are about 4 and 6 times larger; and on cornering, A_x oscillates seven times more. These forces are unlikely to be representative of reality, in the first instance because forces of more than 3000N, (1500 N on each limb) can hardly be resisted by hands or feet, and second, if they would, it would imply large motions of the rider, which is not observed in reality.

The unrealistic motion of Rider A explains the unrealistic forces and implies that a significant phenomenon has been omitted from the equations. A mistake in the algebra of the equations of motion was discarded by comparing it against a model with the same assumptions developed in Working Model 2D, showing identical outputs. A mistake in the parameters was also discarded, since several combinations were tested with similar results. For example, increasing damping, reduces the number of oscillations but increases the magnitude of forces. The reduced number of bodies or degrees of freedom is unlikely to be responsible, since the amplitude and number of oscillations depend on the total mass, stiffness and damping. Because of this, we presume that the missing phenomena is the active action of muscles, since it would stop the motion after an event and absorb the impacts using very low forces. In this way, the assumption of passive representation of the rider, appears to be invalid for off-road motorcycles.

On the other hand, Rider B does not yield unreasonable forces. However, it misses the larger vertical forces expected on take-off before jumps and on landings, and the variable force expected on whoops. Nonetheless, considering its simplicity, it is a valuable model.

The result of using both riders in the tyre forces estimator of Chapter 3, are shown in Figure 4.4.2. In broad terms, it can be seen that the estimations are similar and in most of the disagreements, forces with Rider A are larger. In jumps, normal forces, and the driving force before them, are similarly estimated with both riders, though with Rider A, N_f and D_r are about two times larger. In *whoops*, peaks in normal forces and the sequence braking-driving-braking are detected with both riders. Disagreements are seen in B_r and D_r which are higher with Rider A, and in N_f, where there are extra peaks estimated with Rider A. In cornering, braking and driving forces, as well as load transfers due to these forces, are in good agreement with both rider models. The major discrepancies are seen on D_r and B_r which are more oscillatory with Rider A. Considering that the rider forces are linear in the equations of motion of the estimator, it is expected to obtain larger and

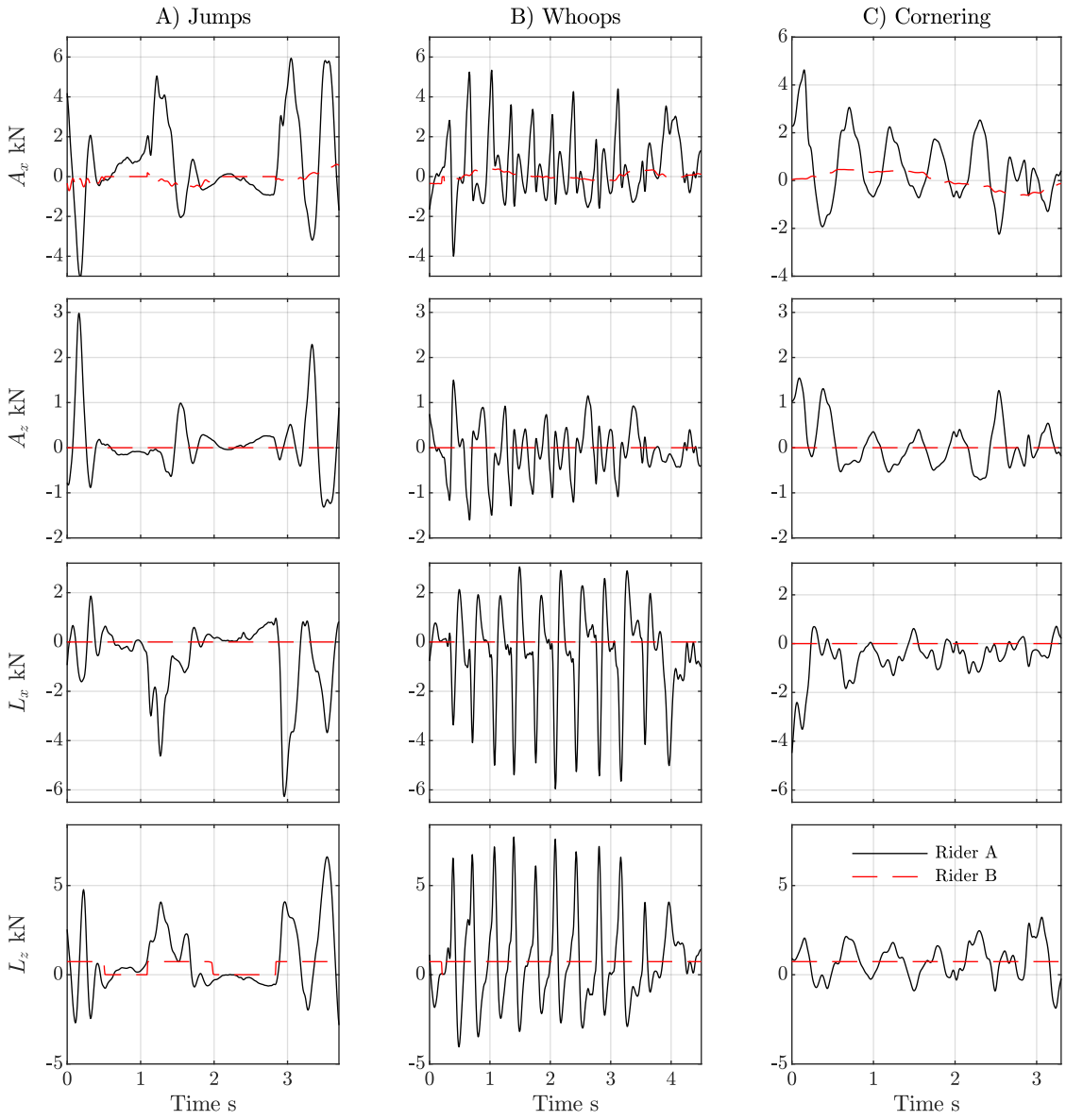

Figure 4.4.1: Rider forces estimated with both models with data collected at a motocross track. Rider A dynamics are modelled with passive elements and requires simultaneous integration of two equations of motion, Rider B dynamics are proportional to motorcycle measurements.

more oscillatory forces with Rider A. However, since the equations of motion are solved in the least squares sense, these larger forces are compensated to fit the remaining data of the equations.

The compensation effect of the estimator, made that two significantly different rider forces, yield similar contact forces. This implies that if Rider B is significantly different from reality, the contact forces will not be significantly affected. Consequently, Rider B, is an adequate representation for the estimation of the rider forces.

4.5 Summary

In summary, in this Chapter we have investigated a suitable description for the rider forces to be used in the estimator. After discarding direct measurement because it add complexity, and chose to estimate them. Validated methodologies for estimation on similar activities, such as off-road cycling and horse riding, are based on passive behaviour of the rider, neglecting the active action. However, there is no evidence that this assumption is valid in off-road motorcycles.

To test this assumption, we have compared, using experimental data, a passive rider model (Rider A) to an elementary rider model (Rider B) which represents the fundamental underlying dynamics of the rider. Both models were derived for this purpose, the former by simplifying and adapting the available ones, and the latter, as a novel approximation.

We found out that Rider A is less representative of reality than Rider B, because the force are more oscillatory and of larger magnitude. Since with an active element it would be possible to reduce the oscillations and magnitude, we consider that this is evidence that the assumption of passive behaviour is not valid for off-road motorcycle.

Parallel to this, we have found that the fundamental dynamics yielded by Rider B is a reasonable representation of the rider forces to be used in the estimator. This is because one one hand, Rider B, is not considerably far from the real forces and on the other hand, we found that the estimator is able to compensate significantly different rider forces (Rider A and Rider B) due to its least squares formulation.

In this way, we have provided evidence that passiveness is not a valid assumption for an off-road rider representation, and additionally we have provided an alternative methodology to estimate these forces.

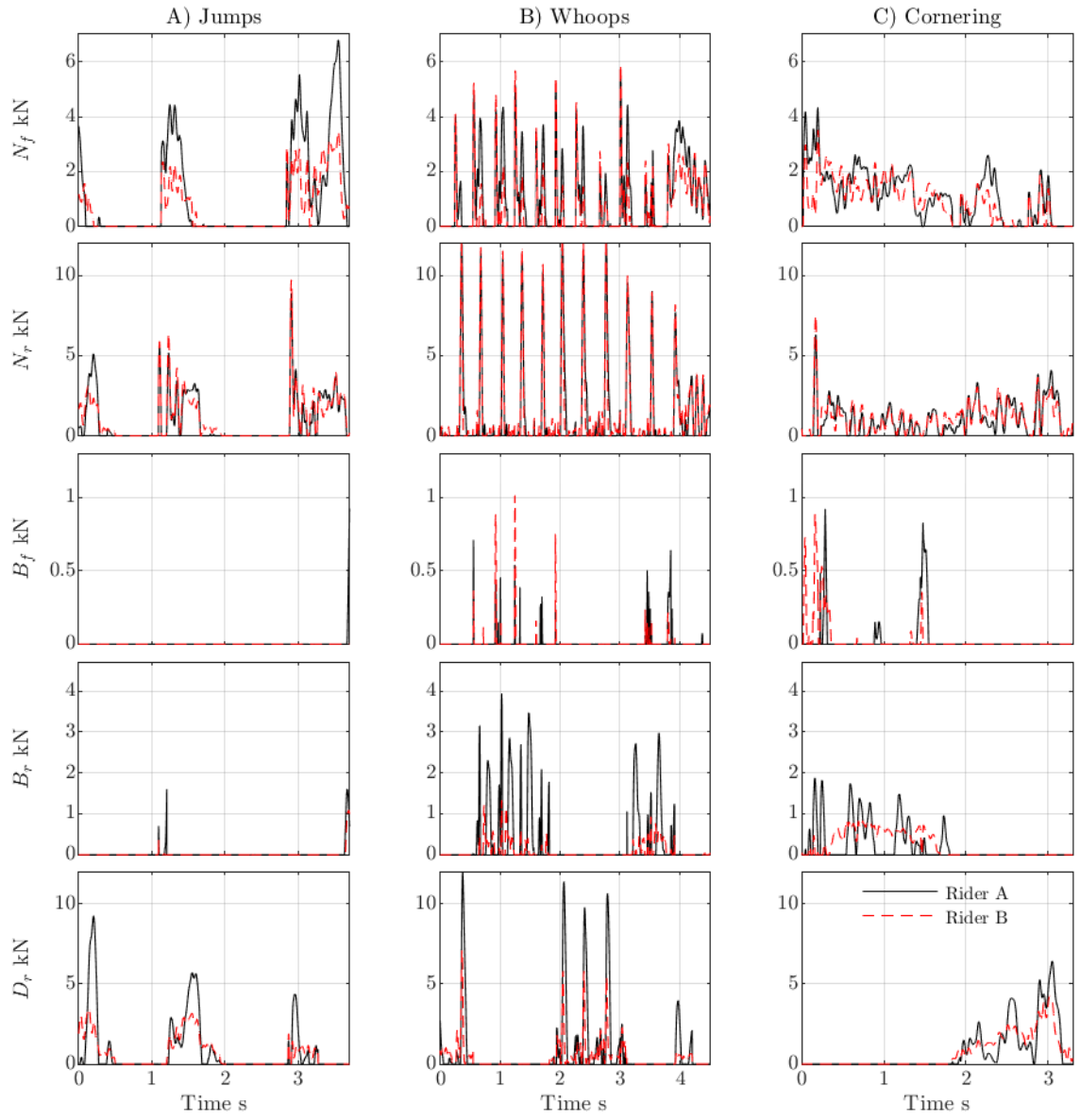

Figure 4.4.2: Contact forces estimated with both rider models. In general similar, but Rider A shows larger and more oscillatory forces than Rider B.

CHAPTER 5

Optimisation of performance and design recommendations

In Chapter 2, we defined performance metrics for an off-road motorcycle, and in Chapters 3 and 4 we developed a procedure to estimate contact forces and a rider model to assess performance experimentally. In this Chapter, the aim is to calculate an optimal suspension for an off-road motorcycle to understand its characteristics. To this end, first, we investigate the main methods used to calculate optimal suspensions to select a suitable one. Subsequently, we apply it to a particular class of motorcycle, where we formulate the optimisation problem by describing the numerical model of the system, the design variables, objectives and solution method. Then, we analyse optimal damping curves, Pareto-fronts and relations between variables and objectives, and finish with a summary of the main characteristics of optimal suspensions.

5.1 Review of optimisation methods in vehicle dynamics

As discussed in Chapter 2, the objectives of the suspension system are to maximise comfort, road holding and working space in the broad range of conditions in which the vehicle is expected to be driven. These objectives are assessed by chassis accelerations, tyre forces, and suspension stroke, respectively. These variables are calculated using models with different levels of simplifications of reality, from where optimal suspension values are calculated. In the following, we examine the main models used for optimisations and their optimal values. First, we describe road modelling, then we explain simple vehicle models used for analytical optimisations, and we finish with a revision of numerical methods used to optimise realistic models.

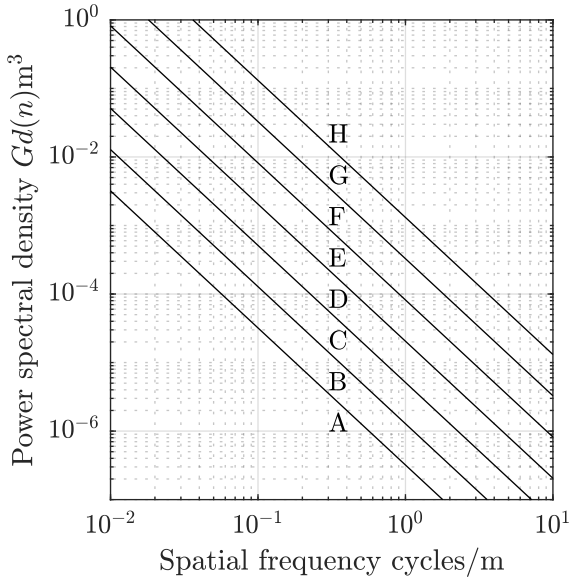

Figure 5.1.1: Road classes bands defined by ISO 8608 [1]. Lower and upper limits of road classes A and H, respectively, are open.

5.1.1 Road surface description

The road inputs to the vehicle models described in the following sections are generally road profiles. These profiles are modelled mainly by two approach which are described next.

Initially, in the 1950s, the road profile was considered sinusoidal [77], but measurements of aircraft runaways [78] and subsequently on vehicle roads, indicated that road roughness contains a broad frequency spectra. Specifically, the power spectral density of the road vertical displacement G_d, can be approximated as a power function

$$G_d(n) = cn^{-w} \tag{5.1.1}$$

where, n is the spatial frequency, w the waviness, and c a constant. This approach is widely used and currently recommended by standard ISO 8608 [1], using $c = \frac{G_d(n_0)}{n_0^{-w}}$, which is used to classify roads, as shown in Figure 5.1.1 and detailed in Chapter 2.

The second approach, uses a double slope psd, for improved matching to experimental data at low frequency. It is implemented for example, as

$$G_d(s) = \frac{A}{1 + \tau s}, \tag{5.1.2}$$

by Thompson [34], using the values $\tau = 1/10\pi$ and A from 0.2 to 1.0. This approach is not used as frequently as the first one, but it can be found, for instance, in [34–37].

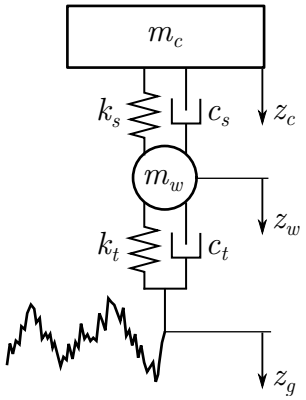

Figure 5.1.2: Single-wheel-station model. m, c, k, and z refer to mass, damping, stiffness and downward displacement, respectively, and subindices c, s, w, t, and g specify chassis, suspension, wheel, tyre and ground, respectively.

5.1.2 Single-wheel-station model

One of the main models used for optimisations is the single-wheel-station model [2], since it is simple enough to perform analytical optimisations. It is the most elementary model able to capture chassis accelerations, tyre forces, and suspension stroke. It represents the vertical motion of a quarter-car or half-motorcycle by two masses (chassis and wheel) connected to the ground and between them by springs and dampers, Figure 5.1.2.

In linear models, the system is represented by transfer functions $H(s)$ in the Laplace domain s. These transfer functions are written to represent the three objectives, i.e., between road vertical displacement z_g [29, 37] or road vertical velocity $\dot{z}_g$ [2, 19], and chassis acceleration, suspension deflection or tyre deflection, such as in [2]

$$H_A(s) = \frac{\ddot{z}_c(s)}{\dot{z}_g(s)}, \tag{5.1.3}$$

$$H_{SD}(s) = \frac{z_c(s) - z_w(s)}{\dot{z}_g(s)}, \tag{5.1.4}$$

$$H_{TD}(s) = \frac{z_w(s) - z_g(s)}{\dot{z}_g(s)} \tag{5.1.5}$$

where, H_A, H_{SD} and H_{TD} are acceleration, suspension deflection and tyre deflection transfer functions, respectively. Explicit description of these functions are obtained using different methods, such as graphic [29] or control theory [2, 19]. With knowledge of the system (H) and the road input $G(s)$, the variance of the output $Y(s)$ is calculated as

$$\sigma_y = \frac{1}{2\pi j} \int_{-j\infty}^{j\infty} H(s)H(-s)G(s)ds, \tag{5.1.6}$$

and minimised to find optimal stiffness and damping values, as done for example, by Gobbi et al. [37] and Thompson [29].

An alternative approach is followed by Limebeer and Massaro [2] and Shiebe et al. [19]. In particular, they calculate the expected rms of the output $\mathbf{y} = Hw$ for a unit variance white-noise w input, utilising the finite-horizon 2-norm of the system H, which is defined as

$$||H||^2_{2,[0,t_f]} = \varepsilon\left(\frac{1}{t_f}\int_0^{t_f} \mathbf{y}^T(t)\mathbf{y}(t)dt\right) \tag{5.1.7}$$

where, $\varepsilon(\cdot)$ is the expectation operator. If the integral is bounded for $t_f \to \infty$, it becomes an infinite-horizon 2-norm, and by writing H as constant state-space matrices $\mathbf{A}, \mathbf{B}, \mathbf{C}$, the norm is calculated as

$$||H||_2^2 = \text{trace}(\mathbf{CLC}^T), \tag{5.1.8}$$

where, $\mathbf{AL} + \mathbf{LA}^T + \mathbf{BB}^T = \mathbf{0}$. In particular, Limebeer and Massaro [2], derive a general expression that directly relate suspension parameters to vehicle performance by minimising the single objective function

$$J = ||H_A||_2^2 + q_1||H_{SD}||_2^2 + q_2||H_{TD}||_2^2, \tag{5.1.9}$$

where, q_1 and q_2 are weighting factors, and q associated to H_A has been dropped without loss of generality. By differentiating J with respect to the suspension parameters, they derive expressions for optimal stiffness and damping,

$$k_s^{opt} = \frac{q_2 k_t m_c m_w}{k_t^2 + q_2(m_c + m_w)^2} \tag{5.1.10}$$

$$c_s^{opt} = \sqrt{\frac{k_t^2(m_c + m_w)(k_s^2 + q_1 m_c^2) + q_2 k_s^2(m_c + m_w)^3 + q_2 k_t m_w m_c(k_t m_c - 2k_s(m_c + m_w))}{k_t(k_t^2 + q_2(m_c + m_w)^2)}}. \tag{5.1.11}$$

where, tyre damping c_t has been dropped since it is small compared to suspension damping. For an insight into the general characteristics of optimal suspension, we show three cases of this solution:

Optimal comfort. Setting $q_1 = 0$ and $q_2 = 0$ yields,

$$k_s^{opt,com} = 0, \tag{5.1.12}$$

$$c_s^{opt,com} = 0, \tag{5.1.13}$$

which tells that a perfect suspension should not transmit any force to the chassis. In practice, this is not possible because at least a spring force is needed to support the chassis weight. For a realisable suspension, a non-optimal stiffness has to be accepted,

$k_s > 0$, for which the optimal damping is

$$c_s^{opt,com,2} = \sqrt{\frac{m_w + m_c}{k_t}} k_s. \tag{5.1.14}$$

Optimal road holding. Setting $q_1 = 0$, $q_2 \to \infty$, and using l'Hôpital's rule,

$$k_s^{opt,rh} = \frac{k_t m_c m_w}{(m_c + m_w)^2}, \tag{5.1.15}$$

$$c_s^{opt,rh} = \sqrt{\frac{k_s^2(m_c + m_w)^3 + k_t m_w m_c(k_t m_c - 2k_s(m_c + m_w))}{k_t(m_c + m_w)^2}}. \tag{5.1.16}$$

Optimal working space. Setting $q_1 \to \infty$ and $q_2 = 0$ yields,

$$k_s^{opt} = 0, \tag{5.1.17}$$

$$c_s^{opt} = 0, \tag{5.1.18}$$

which, as explained for optimal comfort, is not realisable. Accepting a non-optimal stiffness, the optimal damping is

$$c_s^{opt,2} = \infty, \tag{5.1.19}$$

which is not realisable either.

As a numerical example, consider $m_w = 12$ kg, $m_c = 81$ kg, $k_t = 150$ kN/m and $k_s = 15961$ N/m, obtained from Table A.3.1 assuming the rider to be rigidly attached to the chassis, then the optimal suspension for comfort and road holding are

$$c_s^{opt,com,2} = 397 \text{ Ns/m}, \tag{5.1.20}$$

$$k_s^{opt,rh} = 16857 \text{ N/m}, \tag{5.1.21}$$

$$c_s^{opt,rh} = 1091 \text{ Ns/m}. \tag{5.1.22}$$

From these solutions, three general characteristics of optimal suspensions can be extracted:

1. It is not possible to optimise the three objectives simultaneously. A trade-off must be made, in this case, by defining q_1 and q_2. The conflict between comfort and road holding has been mentioned by several authors, such as in [4, 24, 38], and between comfort and working space as well, see for example [31, 39].

2. For a given k_s, optimal damping for comfort is smaller than for road holding, which agrees with Thompson [34] and Guiggiani [4].

3. Optimal working space is not realisable.

The model examined here has two basic limitations. First, any interaction between front and rear ends of the vehicle is ignored. The relevance of this simplification can be quantified by the coupling mass, which is explained in Sub-section 5.1.3.

The second limitation is that the three force elements (k_s, k_t and c_s) are assumed linear. On the one hand, this assumption is valid for the spring and tyre only for small oscillations, such that suspension and tyre ends are not reached nor tyre detaches from the ground. This is likely to occur on smooth roads, but not on poor roads.

On the other hand, "linear viscous damping" is far from reality [20], since real dampers present some purpose-built non-linearities. One of these, is the asymmetric behaviour, i.e. different compression and extension damping coefficients, as illustrated in Figure 5.1.3a. Dixon [38] indicates that typical values of asymmetry ratio,

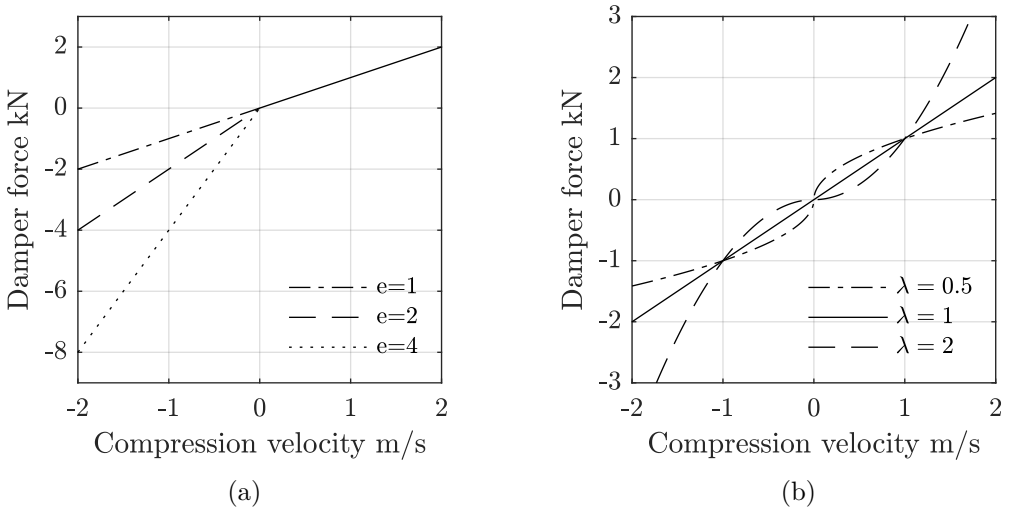

Figure 5.1.3: Damping non-linearities. a) Asymmetry, illustrating Equation 5.1.23 with fixed compression damping coefficient and variable extension damping coefficient, $e = 1$ is the symmetric case. b) Progressivity, described according to Equation 5.1.24, where $\lambda = 0.5$ is referred as digressive, $\lambda = 2$ as progressive, and $\lambda = 1$ is the linear case.

$$e = \frac{c_{s,extension}}{c_{s,compression}} \tag{5.1.23}$$

for passenger cars are between 1 to 4 and for motorcycles between 4 to 19, while Cossalter [40], indicates that asymmetry ratios for motorcycles are larger than 2. The ratio has been optimised for particular excitations using numerical simulations. For example, Thompson [34] found that for steps up and down of 25 mm and 60 mm, which are upward or downward abrupt changes in road elevation, the acceleration was minimised with asymmetry ratios between 1 and 3, while for rough roads, with values between 1 and 4.

Another of these non-linearities is the progressivity factor λ [38], illustrated in Figure 5.1.3b, by which the damping force is described by

$$f = c_s \dot{z}_s |\dot{z}_s^{\lambda-1}|. \tag{5.1.24}$$

On the one hand, progressive behaviour, $\lambda > 1$, can be desirable for comfort, because at low damping speeds the damping coefficient is low, thus it approaches to the optimal comfort damping ($c = 0$) [39]. On the other, digressive behaviour, $\lambda < 1$, can be desirable because for a given maximum force, it dissipates more energy [40]. Nonetheless, Metwalli [39] argues that among $\lambda = [0.5,\ 1,\ 2]$, the best progressivity factor is $\lambda = 1$, i.e. linear damping, because $\lambda < 1$ degrades comfort for small amplitude inputs, and $\lambda > 1$ causes longer settling times.

Analytical optimisations of suspensions in which non-linearities are included, are laboriously derived, and hence no general conclusions are found. Under certain assumptions, solutions can be found, but they are hardly applicable. For example, for strictly harmonic excitation, Genta [20] shows that damping asymmetry causes no effect on comfort nor on handling, evaluated with the maximum acceleration and tyre force respectively. However, harmonic road excitation is hardly representative of a real excitation, and thus this result is limited in practice.

5.1.3 In-plane vehicle model

A more realistic model, is the in-plane vehicle model [2]. This model consist of the chassis connected to the front and rear wheels by suspension systems, and the wheels to the ground by a spring and possibly a damper, as displayed in Figure 5.1.4. It considers chassis and wheels vertical motions, as well as chassis pitch motion. Even though no analytical optimisation of the suspension is found with this model, it is relevant for the analysis of the simplifications done on the single-wheel-station model. In the following, we examine the interactions between front and rear wheel-stations, as well as between pitch and bounce modes.

Regarding interactions between front and rear wheel-stations, [2] shows that if the coupling mass is null, front and rear stations become uncoupled and can be treated as two separate systems. This mass is,

$$m_{cp} = m_c \left(1 - \frac{I_{c,y}}{abm_c}\right) = 0, \tag{5.1.25}$$

where, the variables are described in Figure 5.1.4. Other authors [4, 5] use the equivalent criterion of the dynamic index equal to unity $\rho = \frac{I_{c,y}}{abm_c} = 1$, to define front and rear uncoupling. Thompson [29] showed that for a rather high coupling between front and rear ends ($\rho = 0.6$), the contribution of the rear wheel excitation to the front tyre deflection

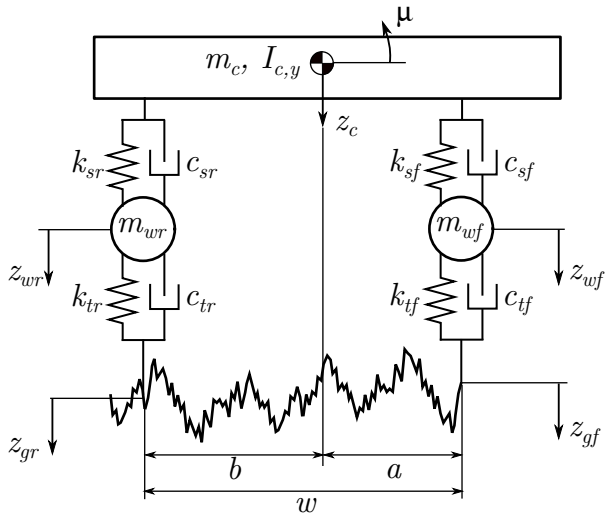

Figure 5.1.4: In-plane vehicle model. m, c, k, z and μ refer to mass, damping, stiffness downward displacement, and pitch rotation, respectively, and subindices c, s, w, t, and g specify chassis, suspension, wheel, tyre and ground, respectively. The appended subindices r and f indicate rear and front ends respectively. $I_{c,y}$ is rotational inertia around y-axis, perpendicular to the plane of the vehicle. a and b are horizontal distances from sprung centre of mass to front and rear ends, respectively, and $w = a + b$ is the wheelbase.

is small compared to the deflection due to front wheel excitation, and vice versa. He adds, that as the dynamic index increases to more realistic values, the contribution is even less important. Therefore, he concludes that the use of single-wheel-station model to optimise tyre deflections is an appropriate approximation. Considering that typical dynamic index for passenger vehicles are 0.95 according to [4] and 0.7-0.9 according to [29], using the single-wheel-station model to calculate optimal suspensions, is a reasonable approximation. However, in motorcycles this index is not as high as in cars. Considering typical values, such as $m = 240$ kg, $I = 50$ kgm^2, $a = 0.8$ m and $b = 0.9$ m as example 6.4 of [2], the index is $\rho = 0.37$. This indicates that front and rear suspensions interact significantly in a motorcycle and therefore they should be optimised simultaneously. A design recommendation aids in reducing the number of variables to optimise. According to [4] it is desirable to design the suspensions considering proportional viscous damping, which in a vehicle with no inerters means $\mathbf{C} = \beta\mathbf{K}$ and implies

$$\beta = \frac{c_{sf}}{k_{sf}} = \frac{c_{sr}}{k_{sr}}. \tag{5.1.26}$$

where $\mathbf{C}$ and $\mathbf{K}$ are the dynamic matrices of the in-plane model of Figure 5.1.4. The argument in favour of proportional damping is that bounce and pitch motions get synchronised, and that the nodes of each mode are fixed, which does not occur with non-proportional damping.

Regarding interactions between pitch and bounce motions, Guiggiani [4] shows that if

the relative stiffness ratio is one,

$$\eta = \frac{k_{sf}a}{k_{sr}b} = 1, \tag{5.1.27}$$

these motions are uncoupled. Given that it depends on the suspension stiffness, it can be modified and considered a design parameter, which can aid in the optimisation as well. Guiggiani argues that $\eta \approx 0.95$ is a reasonable value, since with the typical parameters of a vehicle, the pitch centre gets located close to front seat, reducing the pitch on the rider which is more annoying than bounce.

It should be noted that it is possible to satisfy both conditions, i.e uncouple front and rear with $\rho = 1$ and uncouple bounce and pitch with $\eta = 1$. However, in this situation, there are infinite mode shapes and nodes are located randomly, therefore is a condition that needs to be avoided [4].

Analytical solutions of optimal suspensions are not found in the literature, probably because the equations become cumbersome to deal with analytically [4]. Furthermore, as noted with the single-wheel-station model, adding non-linearities in the real vehicle, limits the applicability of conclusions derived from linear models. This is why, the common approach to optimise suspensions of realistic models is by numerical optimisations.

5.1.4 Numerical optimisations

Numerical optimisations are used in models in which analytical solutions are excessively laborious or do not exist. Next, we review two formulations of optimisations, followed by the main solution algorithms.

A common optimisation formulation is to merge the multiple objectives into a single-objective. The procedure is to define a vehicle model and solve it in the time domain over one or more road excitations. Next, accelerations and tyre deflections (or contact forces) are measured and combined them into a single objective function. Then, an optimisation algorithm minimises this function by iteratively modifying the design variables and at the end of the process, the optimal values are reported. For example, in [22], a linear in-plane vehicle is simulated over a bump of 0.1 m at a speed of 60 km/h. The objective function

$$J = w_1 J_1 + w_2 J_2 + w_3 J_3 + w_4 J_4, \tag{5.1.28}$$

is calculated, where $w_i = 0.25$ and

$$J_1 = \max(\ddot{z}_c), \tag{5.1.29}$$

$$J_2 = \max(\ddot{\mu}), \tag{5.1.30}$$

$$J_3 = \mathrm{rms}(z_{tf}), \tag{5.1.31}$$

$$J_4 = \text{rms}(z_{tr}), \tag{5.1.32}$$

and minimised with a genetic algorithm modifying front and rear stiffness and damping.

The representativeness of the system can be improved incorporating non-linearities such as bump stops, detachments, and non-linear damping by directly changing the description of the force equations and choosing appropriate design variables, but with no changes in the procedure. For example, Georgiou et al. [16] describes damping force as bilinear; while Ozcan et al. [14] describes the damping force as $f_d(\dot{z}_s) = Ae^{-k\dot{z}_s} + Be^{q\dot{z}_s}$, where A, B, k, q are parameters determined empirically; and Catania et al. [41] uses a B-spline description $f_d(\dot{z}_s) = \sum_{k=1}^{r} N_k^n b_k$, for road motorcycle dampers, where N_k^n are the spline coefficients and b_k are parameters obtained by fitting experimental data.

The benefit of formulating the optimisation with a single-objective is that it yields a solution with relatively low computational cost, but the shortcoming is that it is difficult to select the relative importance between objectives [42], and no insight between design variable and objectives nor between objectives is obtained [30].

This leads to the second approach, which is to formulate the optimisation as multi-objective as,

$$\min_{x \in \mathbb{R}^n} \mathbf{f}(\mathbf{x}) \tag{5.1.33}$$

$$\mathbf{h}(\mathbf{x}) = \mathbf{0} \tag{5.1.34}$$

$$\mathbf{g}(\mathbf{x}) \leq \mathbf{0} \tag{5.1.35}$$

$$\mathbf{x} \in \mathbf{X} \tag{5.1.36}$$

where, $\mathbf{x}$ are the design variables, $\mathbf{f}(\mathbf{x})$ is the vector of objective functions, $\mathbf{h}(\mathbf{x})$ and $\mathbf{g}(\mathbf{x})$ are equality and inequality constraints, and $\mathbf{X}$ is the variable space, which can be continuous and/or discrete [30]. The solutions are the Pareto-optimal set, also called Pareto front, in which each solution improves at least one objective function and worsen at least one of the others. In this way, all the possible and optimal design solutions from which a solution can be selected, are known. The advantage of this formulation is that the chassis design problem can be addressed comprehensively, optimising several variables (~ 40) for multiple manoeuvres (~ 40) simultaneously, as found, for example, in works of Gobbi et al. [24, 25] and Tey et al. [42]. The main disadvantage of this formulation is that calculating the Pareto-front is computationally expensive [30].

Regarding the algorithms used to solve these optimisations (single- and multi-objectives), a basic classification is into iterative or heuristic methods. The former begin at an initial point, search a direction of movement towards the minimum considering the gradient of the objective function, and possibly second order derivatives (Hessian), determine a step size and move into that direction and step size. Examples are BFGS Quasi-Newton Algo-

rithm, which approximates the Hessian matrix, and Pattern Search, which approximates the gradient and the Hessian matrix using the objective function. The main limitation of these algorithms is that they could get trapped in local minima [12]. They are suited for problems with simple to medium complexity objective functions.

Heuristic methods use diverse strategies to approximate to the global minima with a certain probability. In vehicle dynamics, genetic algorithms are commonly used [16,21,22, 24,42,43]. It consists of a population being reproduced iteratively, allowing the best fitted individuals to reproduce to the next generation, leading towards the optimal solution. *A population* refers to a set of *individuals* or genome, each of which is a point $\mathbf{x_i}$ on the variable space and the *fitness* of each individual is the value of the objectives functions $\mathbf{f}(\mathbf{x_i})$ in that point. The advantage of these methods is that they approach the global minima of complex problems efficiently, but as a downside, it requires a large computational effort, convergence to the minimum is not guaranteed and progress after approaching the global minima is not efficient.

5.1.5 Summary

In summary, we have examined the main methods used to design suspensions. We have shown that for the single-wheel-station model, there are expressions for the calculation of optimal suspensions, which are limited to linear stiffness and damping. Also it is shown that including non-linear elements can improve performance, however, equations become cumbersome and analytical solutions are not available. Also, we analysed the in-plane model to show that the single-wheel-station model is a reasonable approximation to perform optimisations, and also explained that calculation of optimal suspensions analytically with this model, is cumbersome.

Because of this, realistic vehicle models, are optimised numerically. The optimisations are formulated as a single-objective by merging the objective into one, or as multi-objectives by considering them simultaneously. The former is less computationally expensive, but it gives no insight into the solution, which is done by the latter. The algorithms used to solve them are iterative or heuristic. The former are gradient-based, therefore they can get trapped in local minima, while the latter are non-gradient-based and avoid this problem, however, they are not efficient in finding the actual minima, and are computationally expensive.

Considering that in an off-road motorcycle non linearities, such as detachments, are recurrent, and non-linear damping is found on every suspension, a realistic optimisation of the suspension parameters needs to be done numerically. Specifically, in order to have a range of optimal solutions that allows a better understanding of the problem and to avoid arbitrary decisions of weights, multi-objective optimisation seems to be the logical

approach. As a solution method, the genetic algorithm is chosen, since its efficacy in vehicle dynamics has been widely proven.

5.2 Formulation of the optimisation problem

In this section, we apply the selected method to calculate the optimal suspension of a cross motorcycle. The optimisation goal, is to improve performance by modifying stiffness and damping parameters, and determine relations between design variables and performance. In this type of off-road driving, three conditions are considered to be critical for performance: braking, accelerating out of the turn, and transit through whoops. We consider a modern motorcycle (KTM-450 SXF, 2017), which possesses state-of-art suspension system, and data from the motocross track described in Chapter 3 as the reference for the optimisation. Next, we build a numerical model able to simulate the forward dynamics of the three conditions, which is verified with the experimental data. This model is utilised to calculate accelerations and contact forces, which are used to calculate the objective functions. The optimisation is formulated as multi-objective and solved with a genetic algorithm. The optimal solutions are analysed as well as relations between variables and performance. In the following, we describe the numerical model of the system, the design variables, the performance indices, and the solution method for the optimisation.

5.2.1 Numerical model of the motorcycle

The virtual representation of the motorcycle is based on a software developed at the University of Padova called FastBike, a multibody code implemented in Simulink, and validated experimentally [79–82]. It is chosen as the starting point, essentially because it includes the lateral dynamics which was not considered in the model developed in Chapter 3. Its inclusion would have been time consuming since at least three degrees of freedom are needed to be included (yaw, roll and steering angles), and it would have needed at least a virtual verification, whereas FastBike is readily available and moreover is validated experimentally. FastBike consists of a main block which contains the equations of motion; it accepts as inputs steering torque, front and rear wheel torques, and general forces and torques on its centre of mass; and the outputs are the position and velocities of its bodies. We implemented it with a linear tyre force description since the lateral forces are small and non-linear suspension forces which include the variable relation between shock compression and wheel displacement. The rider controls roll angle and speed by applying steering torque and front and rear wheel torques, by means of two PID controllers [52]. Additionally, the simple rider model of Chapter 4 is added to represent the forces, i.e. the rider is considered driving in standing position exerting a constant force in the vertical direction and inertial forces in the longitudinal and lateral directions [83]. Details of

implementation in Simulink are found in Appendix E.

The three critical situations are implemented in the Simulink code by setting appropriately three inputs: road profile, target speed and roll angle. These values are determined from the experimental data, as explained next.

5.2.1.1 Braking and accelerating out of the turn

The procedure to find the inputs for braking and accelerating out of the turn, consists of two steps. First, we make sure that simulation is possible with the measured data on a smooth road. Second, given that the road profile was not measured, we search for a profile that produces similar suspension velocities to the recorded data.

Simulation of braking using the measured GPS velocity as the target speed input, does not present major difficulties. Contrarily, simulation of acceleration out of the turn is more restrictive since a fall to the inner side of the turn, a low-side [40], might occur if excessive throttle is applied while leaning. However, with the measured data as inputs, the simulation is completed successfully.

Specifically, the target speed and roll angle imposed are: decelerate in straight line from 10 to 4 m/s in 2 s (-3 m/s^2) for braking manoeuvre, and accelerate in 1 s from 7.2 to 11.1 m/s while simultaneously rolling up from 0.7 to 0 rad of roll, for acceleration manoeuvre.

The road profile is determined by trial and error, finding that with a road class D for braking, and C for accelerating, the suspension velocities are in agreement with the experimental ones, as shown in Figure 5.2.1. The high frequency of the experimental signals had been low-pass filtered at 20 Hz, since higher frequencies are out of interest. Therefore, disagreement on this range is irrelevant. Low frequencies are not expected to be replicated either since the experimental one contains the effect of large wavelength obstacles such as purpose-built ramps, which are not present in a regular rough road. The road is built according to ISO-8608 [1] in the space domain, as detailed in Appendix A.2. The amplitude considered on each road is the geometric mean of the corresponding class.

5.2.1.2 Whoops

The inputs for whoops are approximately known, but simulation is challenging. GPS velocity is variable. It begins at 13.4 m/s, decreases to 10.2 m/s and increases back to 12.2 m/s, while the roll angle is null. The road profile is approximated as a sinusoid of $\approx$ 3.6 m wavelength and $\approx$ 0.3 m amplitude. However, simulations with these inputs is unsuccessful.

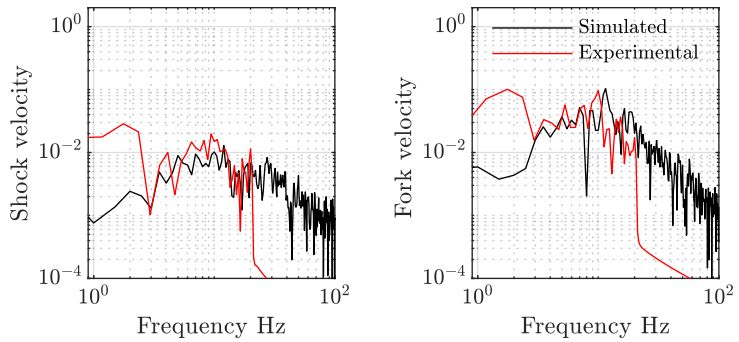

(a) Braking - Shock (b) Braking - Fork

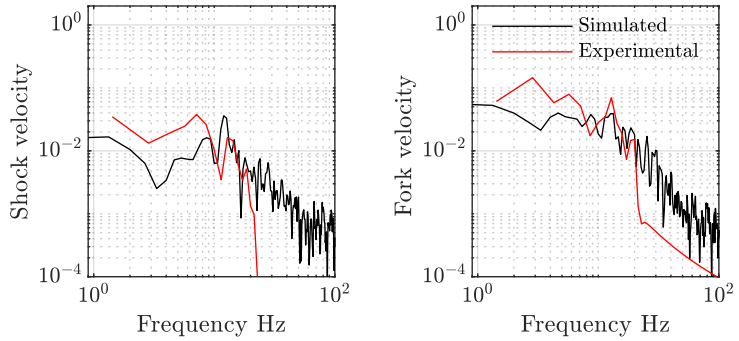

(c) Accelerating - Shock (d) Accelerating - Fork

Figure 5.2.1: Comparison of experimental and simulated suspension velocities spectra. Experimental signals are filtered at 20 Hz as explained in Chapter 2.

In real-life, the motorcycle makes contact only on the crests of the sinusoids, which is possible because the rider exerts a significant control over the motorcycle, Figure 4.3.1. It involves shifting frontwards and backwards his/her position relative to the motorcycle and partial throttling when the rear wheel is in contact. If the sets of inputs are not met, failure such as frontward or backward flip happens. The mechanism of both failures, is the generation of a considerable backwards or frontward force under the centre of mass of the motorcycle. In particular, frontward flip is the most likely to arise, since it occurs if the positive slope of a bump is hit by either the wheel while flying, creating a considerable backward normal force. Conversely, backward flip is less likely to arise since it occurs if excessive throttle is applied while in the positive slope of the bump. To overcome the simulation problem, we carried out simulations in three increasing size of whoops, 0.1, 0.2 and 0.3 m of amplitude, and applied extra controls through the rider if needed.

On whoops of 0.1 m amplitude, it is hardly possible to transit at 12 m/s, Figure 5.2.2. It can be seen that the suspension velocities are not replicated properly. Some bumps are skipped, magnitudes are between 10% to 50% lower, and contact is made not only at the crests of the whoops but also in between.

On whoops of 0.2 m amplitude, after numerous unsuccessful attempts, we are able to

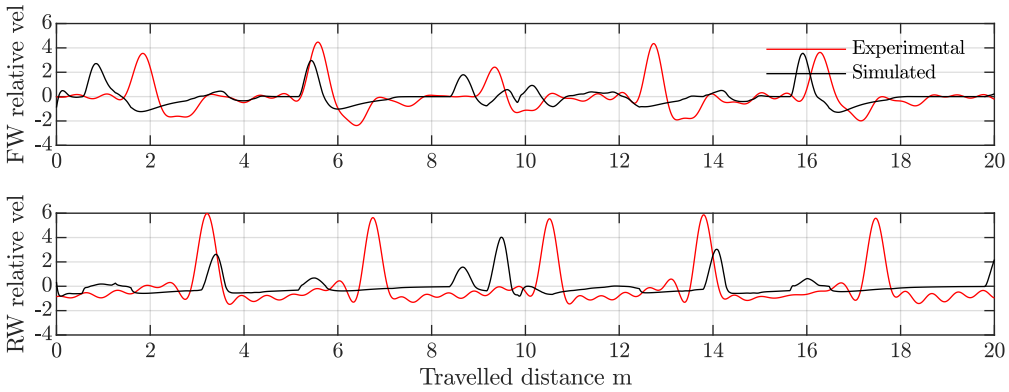

Figure 5.2.2: Experimental vs simulated velocities on 0.1 m amplitude whoops.

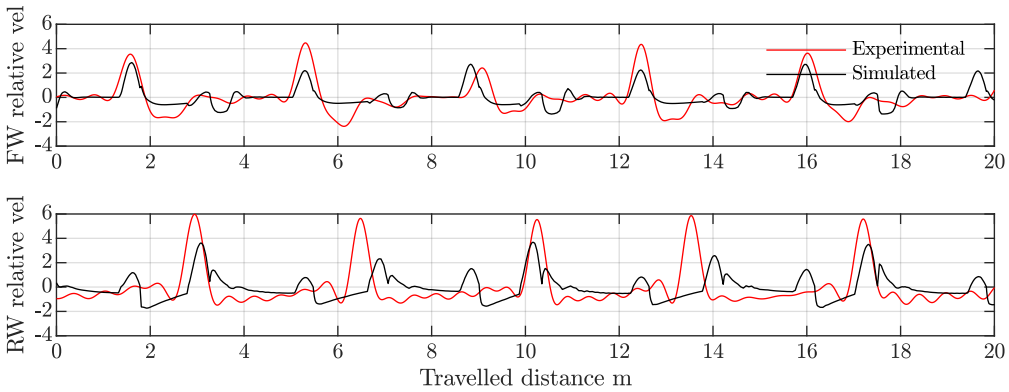

Figure 5.2.3: Experimental vs simulated velocities on 0.2 m amplitude whoops.

simulate transit at 12 m/s only with a pitch controller, Figure 5.2.3. This controller consist on an external torque applied on the chassis, replicating coarsely the control exerted by the rider. It is proportional to the pitch and pitch rate, it is applied only when the motorcycle is flying so it does not interfere with suspension compressions and it is saturated to ± 5000 Nm. In particular, stiffness and damping are selected such that pitch undamped natural frequency is 1 Hz and a damping ratio of 0.5, both found by trial and error. In this case, transit is more consistent. Compressions occur synchronised with the experimental ones and no bumps are skipped. However, the magnitudes are up to 50% lower on front wheel and up to 70% less on rear wheel. Double compressions are seen on the rear wheel, which occur because after rear wheel loses contact, pitch controller rotates the motorcycle backwards, making the rear wheel recover contact again. If the pitch controller is let to act while contact is happening, larger compression speeds are possible and no double compression occurs.

On whoops of 0.3 m amplitude, it is possible to transit at 12 m/s with the previous pitch controller, but the motorcycle skips whoops. For a regular transit, a slight vertical control is added, Figure 5.2.4. It consist on a vertical force applied on the motorcycle centre of mass, proportional to the position and vertical velocity, only when there is no

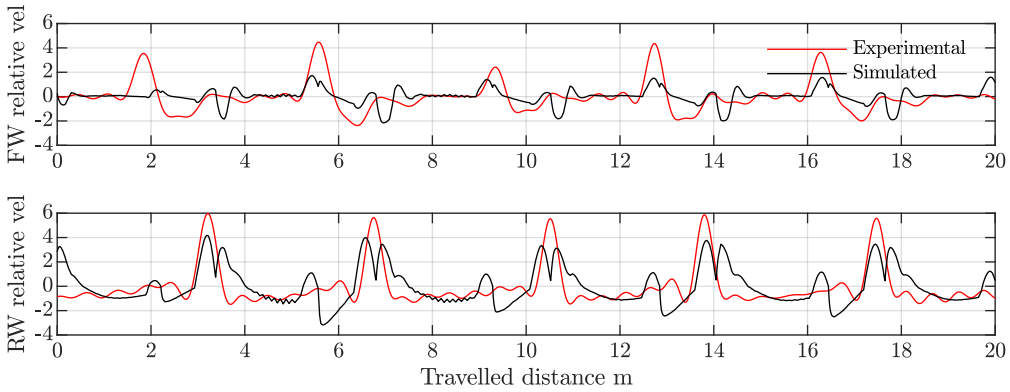

Figure 5.2.4: Experimental vs simulated velocities on 0.3 m amplitude whoops.

contact. The force is saturated to 30 % of the weight of the rider to replicate coarsely a possible impulse from the rider and does not becomes extremely unrealistic. Stiffness and damping are selected in a similar way as for the pitch controller: 1 Hz vertical undamped natural frequency and 0.3 damping ratio, both found by trial and error. In this situation, the replication is also consistent and synchronised with the experimental data. The magnitudes at the rear wheel are about 30% lower that the experimental ones, and on the front, they are about 60% lower. Double compressions are produced due to limiting the pitch controller to act only when there are no tyre forces, as in 0.2 m whoops.

Summarising, we are able to simulate a motorcycle transiting through real size whoops with the aid of a pitch and vertical position controls, obtaining a reasonably good representation of suspension velocities. Using pitch aid only, it is possible to simulate transit on up to 0.2 m whoops, in which case, the suspension velocities are matched with moderate differences. Lastly, with no aid, it is possible to simulate only up to 0.1 m whoops, in which case, the suspension velocities are matched poorly. We acknowledge that by using pitch and vertical control on 0.3 m whoops, we are intervening excessively, however if no aid is used, the representation is poor. We consider that simulation with a pitch aid only on 0.2 m whoops is a reasonable trade-off between intervention and representativeness, therefore is the one used for optimisations. Better matching of the experimental velocities requires a more realistic rider model. Possibly enhance the passive nature of the controller with an active control and/or with a predictive strategy (act before an obstacle) such that the motorcycle is positioned in a specific way before hitting each bump.

5.2.2 Design variables

We consider the elastic and damping non-linear forces as design variables. An accurate description of these forces require several parameters, which in a multi-objective algorithm is computationally expensive. Since, a detailed optimisation is out of our aim, we describe the forces with a moderate number of parameters. First, we describe the parametrisation

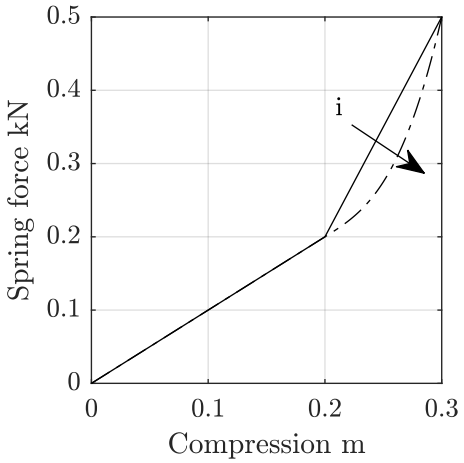

Figure 5.2.5: Parametrisation of non-linear spring according to Equation 5.2.1. Parameters used are $k = 1$ kN/m, $F_M = 0.5$, kN, $z_{sM} = 0.3$ m, $z_{s,i} = 0.2$ m, —— $i = 1$, and — - $i = 3$.

of the forces, then, a reduction of the number of design parameters, and lastly the design space.

The parametrisation of the elastic force requires to describe the linear force of the spring plus the exponential increase due to gas compression and bump-stop, such as

$$f_e = kz_s + (F_M - kz_{sM}) \left(\frac{z_s - z_{s,i}}{z_{sM} - z_{s,i}} \right)^i, \tag{5.2.1}$$

presented in [25] and reproduced in Figure 5.2.5. The first term in this equation, is the spring force, and the second, a power function representing the spring plus bump stop effects. z_{sM} and F_M are the maximum suspension stroke and force at that point, respectively, and $z_{s,i}$ is the stroke at which the exponential function begins to act. Design variables in this description are spring stiffness k, engaging position of bump-stop $z_{s,i}$, end exponent of the power function i. A simpler option is to apply a gain to the measured force, representing if the overall elastic force needs to be increased or decreased, Figure 5.2.6. Since our main interest is to illustrate the procedure, we consider the second description, which is applied on each suspension as

$$f_e = kf(x), \tag{5.2.2}$$

where, k is the gain, and $f(x)$ is the corresponding measured elastic force, as detailed in Figure 5.2.6.

Parametrisation of the damping force can be done by different methods, such as exponential and B-spline mentioned in subsection 5.1.4, or multi linear (bi-, tri-, quadri-linear, etc). For the reference dampers Figure 5.2.7, we consider that a quadri-linear function is

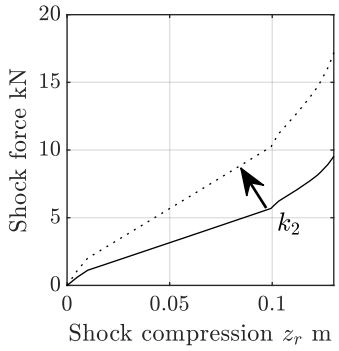

(a) Shock

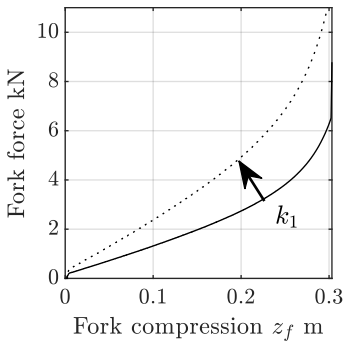

(b) Fork

Figure 5.2.6: Springs parametrisation. The elastic force is composed of the spring on the first ≈2/3 of the stroke, to which, gas compression and bump stop are added on the last ≈1/3 of the stroke. The parameters for the optimisation are k_1 and k_2 representing amplification of the elastic force in all the working range as displayed.

a reasonable description for these curves. The front and rear forces are described as,

$$f_{d,f} = \begin{cases} C_4\dot{z}_f & \dot{z}_f \leq v_2 \\ C_3\dot{z}_f & v_2 < \dot{z}_f \leq 0 \\ C_1\dot{z}_f & 0 < \dot{z}_f \leq v_1 \\ C_2\dot{z}_f & v_1 < \dot{z}_f \end{cases} \tag{5.2.3}$$

$$f_{d,r} = \begin{cases} C_8\dot{z}_r & \dot{z}_r \leq v_4 \\ C_7\dot{z}_r & v_4 < \dot{z}_r \leq 0 \\ C_5\dot{z}_r & 0 < \dot{z}_r \leq v_3 \\ C_6\dot{z}_r & v_3 < \dot{z}_r \end{cases} \tag{5.2.4}$$

where, C_i are damping coefficients and v_i are speeds at which the slope changes (knee velocity). In particular, the optimisation variables are defined as gains with respect to the reference values as with the elastic force and collected in $\mathbf{c} = [c_1,\ c_2,\ c_3,\ c_4,\ c_5,\ c_6,\ c_7,\ c_8]$ and $\mathbf{v} = [v_1,\ v_2,\ v_3,\ v_4]$.

A reduction in the number of parameters is made to reduce the complexity of the optimisation. In particular, we decide to fix the knee velocities based on the experimental measurement of suspension velocities reducing the optimisation variables to eight. The criterion used is as follows.

We consider the cumulative distribution function (cdf) [84, 85] of the velocities, which indicates the probability of occurrence of a velocity smaller than a specific real value a and is defined as,

$$F(a) = \int_{-\infty}^{a} f(\dot{z})d\dot{z}, \tag{5.2.5}$$

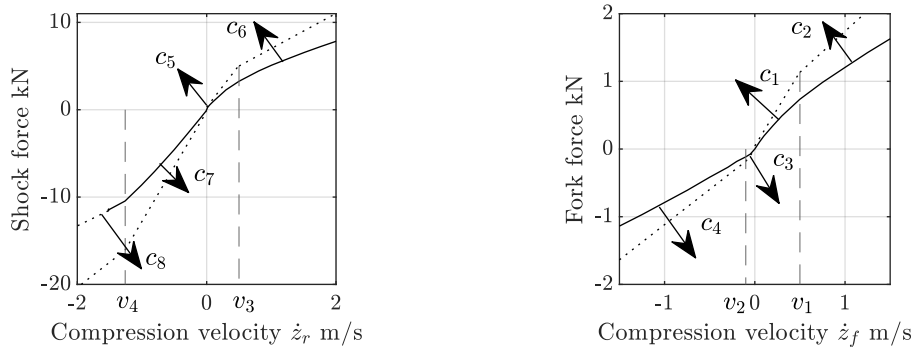

(a) Shock (b) Fork

Figure 5.2.7: Dampers parametrisations. Damping forces are parametrised as quadrilinear, Equations 5.2.3- 5.2.4 and the optimisation parameters are $c_1, ..., c_8$ representing amplification of damping coefficients. The reference damping coefficients are $\mathbf{C}_{ref} = [C_1,\ C_2,\ C_3,\ C_4,\ C_5,\ C_6,\ C_7,\ C_8] = [1460,\ 808,\ 1155,\ 693,\ 6393,\ 2677,\ 8388,\ 3866]$ Ns/m, and its knee velocities, which are the points at which the slopes changes, are $\mathbf{v} = [v_1,\ v_2,\ v_3,\ v_4] = [0.5,\ -0.1,\ 0.6,\ -1.3]$ m/s, respectively.

where, $f(\dot{z})$ is the probability distribution function (pdf) of the suspension velocity $\dot{z}$. For discrete random variables, it can be shown [84], that

$$F(a) = \sum_i p_i, \tag{5.2.6}$$

where, p_i is the probability that the random variable $\dot{z}$ assumes the value $\dot{z}_i$, with $\dot{z}_i \leq \dot{z}_{i+1}$. Each probability can be estimated from the experimental data as the number of occurrences of velocities n_{vi} in the interval i of the velocity range, divided by the width of the interval w_i and the number of elements of the sample n,

$$p_i = \frac{n_{vi}}{n w_i} \tag{5.2.7}$$

which, can be plotted as an histogram. As the number of samples n increases, the resolution of the measurement increases, and width is reduced, the cdf becomes smoother as in Figure 5.2.8.

A cumulative distribution of 0.5 divides the suspension velocities into two ranges which are equally probable to occur. In particular, as the sample size increases, the suspension velocity at which cdf is 0.5, tends to zero, which means that positive and negative velocities are equally probable to occur, Figure 5.2.8. In the same way, by considering also the velocities at which cdf is 0.25 and 0.75, the velocities are divided into four ranges which are equally likely to occur.

Considering that each damping coefficient influences the vehicle dynamics only in a specific range of damper velocities, by setting knee velocities where cdf is 0.25 and 0.75, the four damping coefficients will have the same probability to have an influence on the

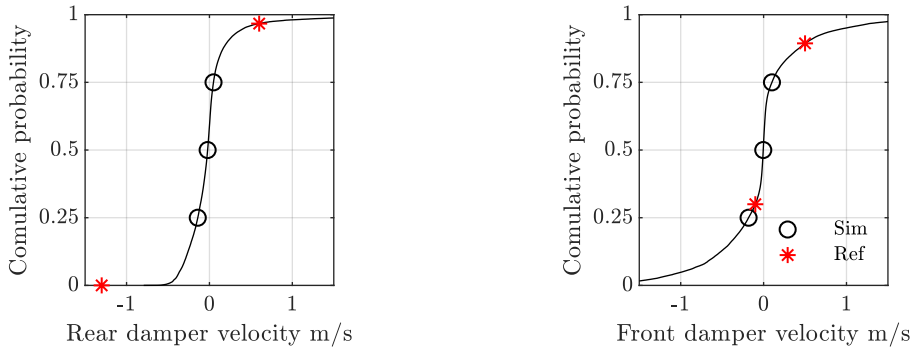

(a) Shock (b) Fork

Figure 5.2.8: Cumulative distribution of suspension speeds. * knee velocities of reference suspension, O knee velocities at which cdf is 0.25 and 0.75 which are used for simulations. These velocities are $\mathbf{v}_{ks} = [0.1 \ -0.18 \ 0.05 \ -0.14]$.

dynamics. This optimises the damper to operate on the four damping coefficients in equal amounts, but this does not necessarily imply that the dynamics of the motorcycle is optimised. Nonetheless, it sets a way to define and assess the knee velocities. For example, in Figure 5.2.8 the knee velocities of the reference suspension are shown. It can be seen that on the shock, these velocities occur on the extremes of cdf, which imply that the damper operates mostly as a bilinear and thus, the effort of building four slopes into the damping curve is not being rewarded.

The space of these variables is continuous since each damping coefficient can be amplified or reduced continuously. For simplicity, it is set to $\pm 20\%$ of the reference suspension for the dampers, which are achievable values in practice, and to $\pm 10\%$ for the springs, since simulations on whoops becomes troublesome with softer or harder springs. Discrete variables could be considered if the variable represent parts that are available only in specific configurations, such as springs.

5.2.3 Performance indices

According to the conclusion of Chapter 2, comfort should be assessed by rms4 of chassis frequency-weighted accelerations and road holding by rms8 of contact force. Two considerations are made for the optimisation. First, taking into account that the cost function is evaluated thousands of times in a genetic algorithm, that the frequency weighting process is slightly costly computationally, and that the optimal damping found with weighted and un-weighted accelerations is the same or very close, we decide to evaluate comfort by rms4 of chassis un-weighted accelerations. Second, since there are two contact forces, the selection for evaluating road holding is not unique, since they could be considered in separate or in a single index. Given that our aim is to describe the procedure, we consider a single index, specifically, as the sum of the contact forces.

The performance indices for the optimisation are defined as comfort and road holding indices normalised with respect to the indices obtained with the reference suspension,

$$J_1 = \frac{\text{rms4}(\ddot{z}_s)}{\text{rms4}(\ddot{z}_s)_{ref}}, \tag{5.2.8}$$

$$J_2 = \frac{\text{rms8}(N_r + N_f)}{\text{rms8}(N_f + N_r)_{ref}}. \tag{5.2.9}$$

In this way, $J_1 < 1$ and $J_2 < 1$ represent improvements with respect to the reference suspension, since it implies less acceleration and force variations and consequently improvement in comfort and road holding. The reference suspension is calculated on each of the three conditions, before each optimisation.

5.2.4 Optimisation problem and solution

Explicitly, the optimisation is formulated as,

$$\min_{x \in \mathbb{R}^n} \mathbf{f}(\mathbf{x}) \tag{5.2.10}$$

$$\mathbf{x} \in \mathbf{X} \tag{5.2.11}$$

where,

$$\mathbf{f}(\mathbf{x}) = [J_1 \ J_2], \tag{5.2.12}$$

$$\mathbf{x} = [k_1 \ k_2 \ c_1 \ c_2 \ c_3 \ c_4 \ c_5 \ c_6 \ c_7 \ c_8], \tag{5.2.13}$$

$$\mathbf{X} : 0.9x_i < x_i < 1.1x_i, \quad i = 1, 2 \tag{5.2.14}$$

$$\mathbf{X} : 0.8x_i < x_i < 1.2x_i, \quad i = 3, ..., 10 \tag{5.2.15}$$

which is solved for each of the three driving conditions. The algorithm used to find the Pareto-front is the multiobjective Genetic Algorithm, implemented in MATLAB in the `gamultiobj` function [86].

An overview of the optimisation process for each driving condition is shown in Figure 5.2.9. First, the genetic algorithm generates a random set of possible solutions x within the search space X and evaluates the performance indices of each of them. For this, each configuration of spring and damper, x is plugged into FastBike and transit on the road profile with the target motion determined for the corresponding driving condition are simulated. In this simulation, the rider model used is the simple model from Chapter 4. The resulting chassis acceleration and tyre contact forces are evaluated with Equations 5.2.8 and 5.2.9. Next, the algorithm executes operations on the performance of each solution, creates a temporary Pareto front and a new set of solutions. subsequently, it evaluates if any of the stopping criteria are met, if so, the last Pareto front is given,

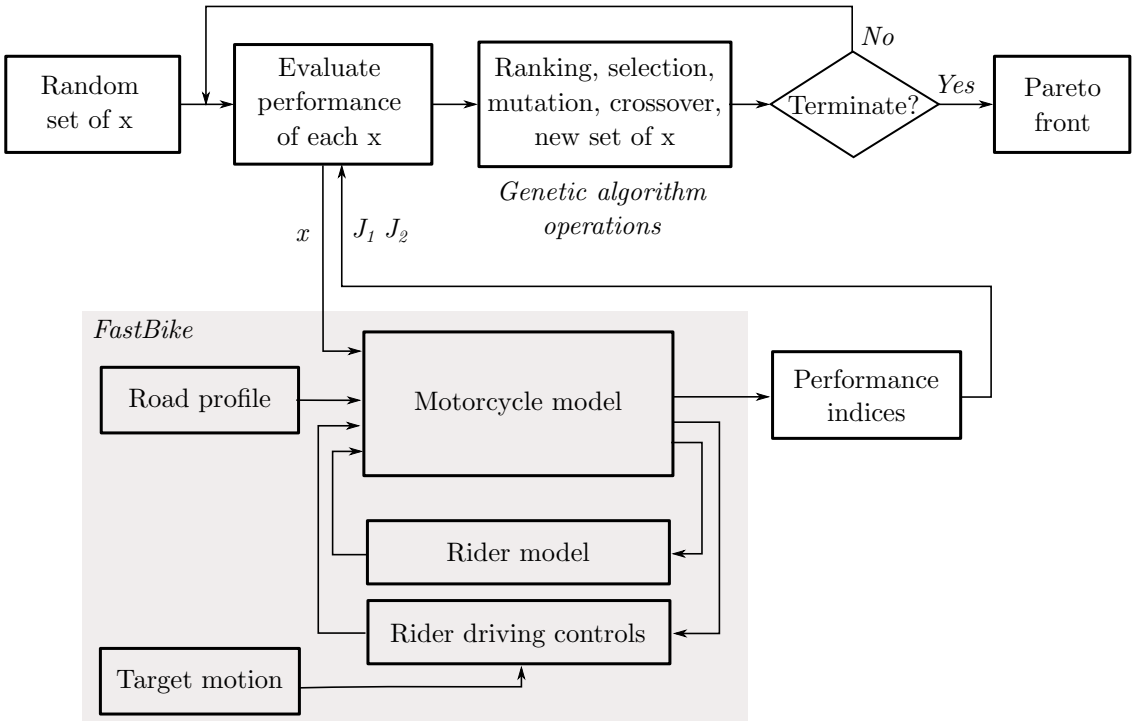

Figure 5.2.9: Optimisation process. Genetic Algorithm begins with a random set of solutions. Next, each solution is simulated on FastBike with the road profile and target motion set for each driving condition, from where the performance indices are calculated. Solutions are treated according to genetic algorithm rules. If any of the stopping criteria is met, the best ranked solutions are the Pareto front, otherwise, a modified population is re-evaluated.

otherwise, simulations with the new set of solutions are performed until any stopping criteria are met.

5.3 Results

For each condition, the optimisation problem is solved, obtaining the optimal elastic and damping curves shown in Figures 5.3.1 - 5.3.3. It can be seen that there are no values on the limits of the space variable, which indicates that the solutions are actual minima and not values limited by the boundaries. Also, the dispersion of results is low, since the maximum standard deviation of any variable across the set, is lower than 0.1, equivalent to 10% gain. Regarding the elastic gains, the average are between 1 and 1.03, which indicates that the reference suspension is very close, or it is, the optimal solution and that the three conditions require very similar stiffness. Regarding the optimal damping curves, in the shock are lower (softer) than the reference in the three situations, while in the fork, they are mostly coincident.

The optimal solutions mapped into the objective space, the Pareto front, are shown in

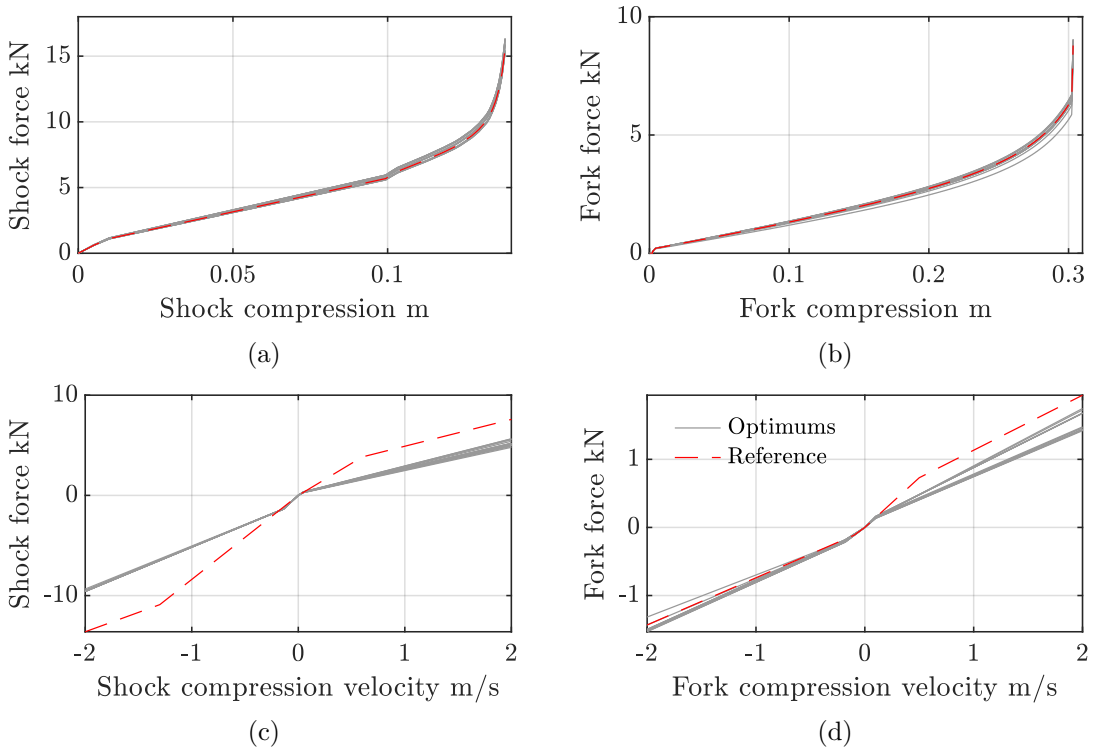

Figure 5.3.1: Optimal stiffness gains and dampings for whoops. Solutions are close to reference, except damping on rear and on front compression. Overlapping of solution makes difficult individual distinction. $\bar{x} = [1.00,\ 1.01,\ 1.02,\ 0.90,\ 0.94,\ 1.03,\ 1.02,\ 0.93,\ 1.17,\ 1.14]$, $\sigma_x = [0.030,\ 0.026,\ 0.069,\ 0.078,\ 0.067,\ 0.038,\ 0.087,\ 0.046,\ 0.007,\ 0.008]$.

Figure 5.3.4 for the three situations. It can be seen that improvements of up to 7% are achievable in comfort, and 4% in road holding. In whoops, the improvement is mainly possible in comfort, while in braking and acceleration, both objectives can improve. The result of larger improvement in comfort than road holding has been obtained by Georgiou et al. [16] in a numerical optimisation of passive and semi-active suspensions.

To understand the characteristics of optimal suspensions, we analyse how variables and objectives change in the Pareto front. To this end, we analyse the correlations between design variables and/or objective values in Figures 5.3.5-5.3.7.

Each matrix of plots, illustrate the correlation matrix $\mathbf{R}$, which is calculated considering matrix $\mathbf{A} = [\mathbf{x}\ \mathbf{f}(\mathbf{x})]$ consisting of the design variables concatenated with objective values. The elements in $\mathbf{R}$ have the following meaning:

- Elements in the diagonal matrix $\mathbf{R}_d = \{R(i,j) :\ i = j\}$, show the correlation of a variable or an objective against itself, which is always one. To occupy that space more fruitfully in the matrix of plots, the histogram is shown instead.
- Elements in sub-matrix $\mathbf{R}_v = \{R(i,j) : i \leq 10,\ j \leq 10,\ i \neq j\}$, show the correlation between design variables. If the correlation between two variables is high, it means

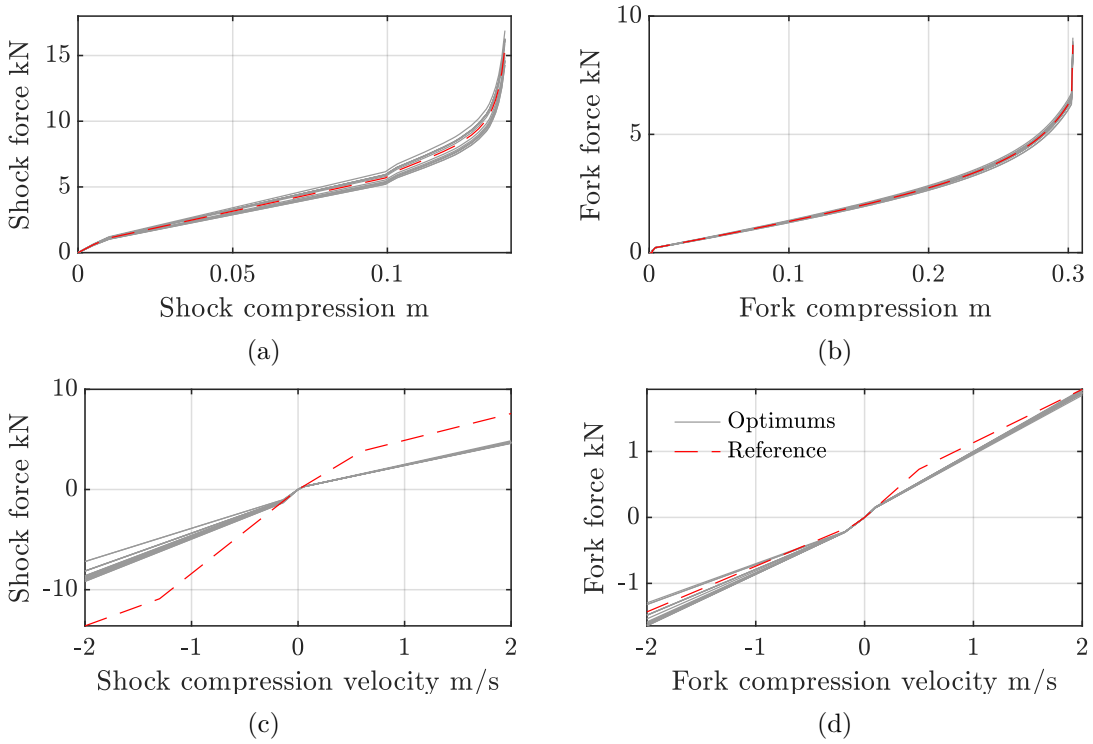

Figure 5.3.2: Optimal stiffness gains and dampings for braking. Larger difference is obtained on rear damping. Low dispersion makes difficult individual distinction.
$\bar{x} = [1.00,\ 1.00,\ 1.04,\ 1.14,\ 1.06,\ 1.04,\ 0.88,\ 0.85,\ 0.98,\ 1.03]$,
$\sigma_x = [0.017,\ 0.057,\ 0.035,\ 0.014,\ 0.015,\ 0.091,\ 0.026,\ 0.012,\ 0.075,\ 0.075]$

that they change together as they move along the Pareto-set.

- Elements in sub-matrix $\mathbf{R}_{vo} = \{R(i,j) : i \leq 10,\ 11 \leq j \leq 12\}$, show the correlation between design variables and objectives. Among both columns there is a negative correlation, which arises from the definition of a Pareto-set solution, i.e. *it improves at least one objective function and worsens at least one of the others.* Positive correlation of a variable with $J1$, indicates that as it increases, comfort worsens, or equivalently, as we move rightward in the Pareto-front, the variable increases.

- Elements in sub-matrix $\mathbf{R}_o = \{R(i,j) : 11 \leq i \leq 12,\ 11 \leq j \leq 12,\ i \neq j\}$, shows the correlation between objectives. In the three situations, the terms are -1, which means that as one increases the other decreases. This is the trade-off between comfort and road holding.

To simplify explanations, we describe changes as we move from comfort optimum to road holding optimum (increase in $J1$ and decrease in $J2$).

Figure 5.3.5 shows that in whoops, the variables with higher correlation to performance are c_6 followed by c_2, which correspond to high speed compression damping coefficients on shock and fork, respectively. It is a reasonable result since high speeds are recurrent

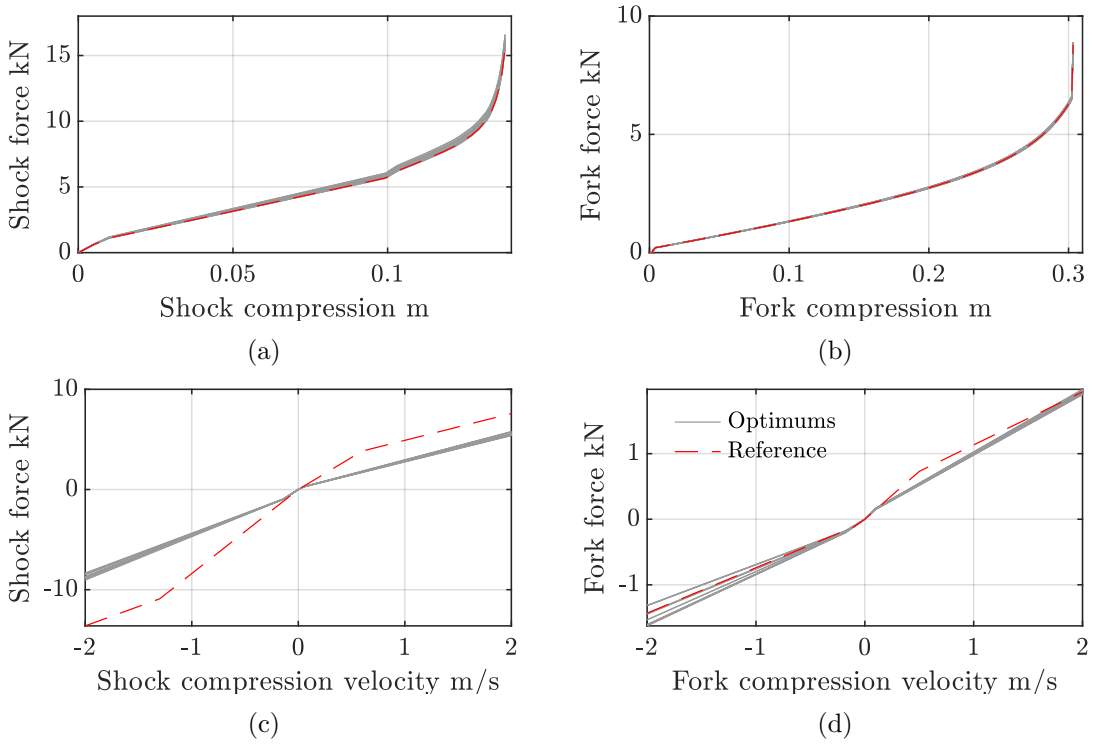

Figure 5.3.3: Optimal stiffness gains and dampings for accelerating. Solutions are close to reference, except on rear damping. Overlapping of solution makes difficult individual distinction. $\bar{x} = [1.00,\ 1.03,\ 1.11,\ 1.16,\ 0.93,\ 1.05,\ 0.85,\ 1.01,\ 0.82,\ 1.08]$, $\sigma_x = [0.007,\ 0.021,\ 0.043,\ 0.015,\ 0.047,\ 0.089,\ 0.011,\ 0.022,\ 0.005,\ 0.026]$

on this section. The correlation of c_6 with $J1$ is positive, while the correlation of c_2 with $J1$ is negative, meaning that as high speed compression damping in the fork decrease, chassis acceleration increases, and comfort worsens. This result, together with the rest of the negative correlations of $J1$ are non-intuitive, since increasing damping or stiffness, increases the force transmitted to the chassis, but it results in a reduction on the acceleration. Important correlations ($> |0.7|$) are also found with c_1, c_3, c_4, c_5, c_7 and k_2 implying that performance in whoops is the result of the combination of several variables.

Between variables, high correlations ($> |0.9|$) are found on the pairs c_1-c_3, c_2-c_4, c_2-k_2 and c_7-k_2. From the first two pairs, it can be implied that, in the fork, the asymmetry ratio should be maintained in low damper speeds and increased at high speeds, since the correlations are positive and negative respectively. The third pair has a positive correlation meaning that high speed compression in the fork should increase as rear stiffness increases. Contrarily, the fourth pair has a negative correlation meaning that as rear stiffness increase, low speed extension damping in the shock should decrease. Low correlation $< |0.1|$ is found only in the pair c_8-k_1, implying that high speed extension damping in the shock and front stiffness can be modified independently.

In braking, Figure 5.3.6, the variables highly correlated to performance are c_7 and k_2

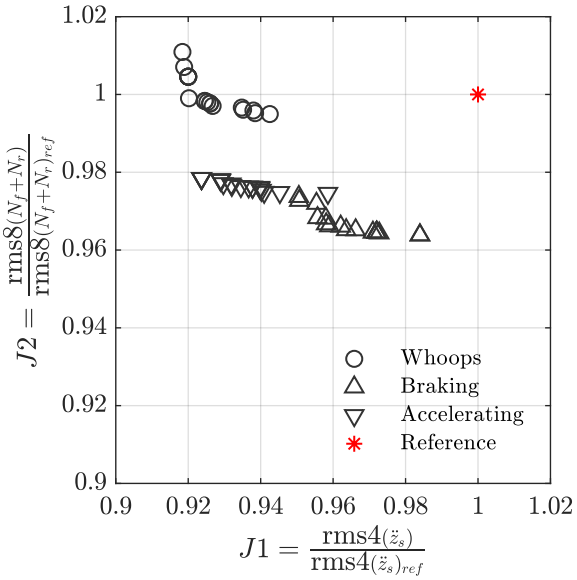

Figure 5.3.4: Comparison of Pareto Fronts

and followed by c_8 with a correlation of 0.85. These variables are low speed extension, elastic gain and high speed extension of the shock, respectively. c_7 and c_8 are negatively correlated to $J1$, implying that a decrease in extension damping in the rear worsens comfort. Oppositely, k_2 has a positive correlation. It is interesting to note that braking performance is correlated importantly only to rear parameters of the motorcycle. Among variables, high correlation is found only in the pair c_7-k_2, as on whoops. Low correlation is found between variables c_1 and c_5, which are low speed compression damping in front and rear respectively.

In acceleration, Figure 5.3.7, the variables with larger correlation to performance are c_2, c_3 and c_1, corresponding to high speed compression, low speed rebound and low speed compression dampings of the fork. The three correlations are positive with $J1$ implying that as they increase, comfort worsens. Interestingly, no correlation to acceleration performance is found with c_8 and very low with k_2 and c_7. Contrarily to braking, acceleration performance is correlated importantly only to front parameters. Among variables, high correlations is found in the pairs c_2-c_3 and c_7-k_2. Low correlation is found the pair c_1-c_8 and c_1-k_2.

To analyse the relationships of optimal suspensions between situations, let us consider only the two variables with higher correlation to performance in each situation. Assume again we want to move from optimal comfort to optimal road holding (reduce $J2$ and increase $J1$). According to correlations in whoops, it requires to raise c_6 and decrease c_2. The first change has no major effect on braking nor accelerating, however the second, implies significant worsening in road holding in acceleration. According to correlations in braking, it requires increasing k_2 and reducing c_7, which reduce road holding in whoops

Figure 5.3.5: Correlation matrix on whoops. Plots in the diagonals are histograms. In off-diagonal plots, each circle indicate an optimal value, the line is the least squares, the and number is the correlation between the variables in the column and row.

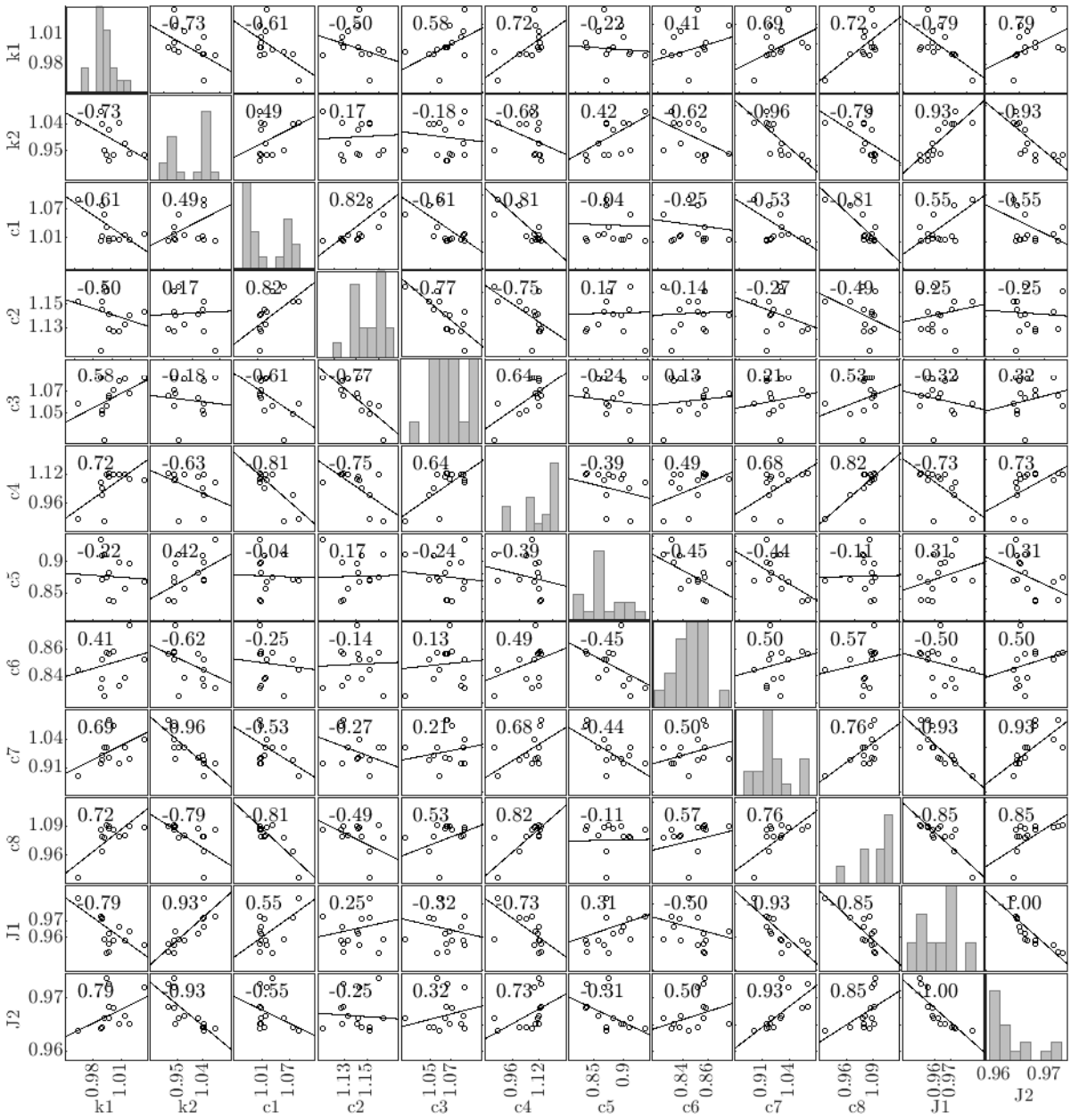

Figure 5.3.6: Correlation matrix on braking. Plots in the diagonals are histograms. In off-diagonal plots, each circle indicate an optimal value, the line is the least squares, the and number is the correlation between the variables in the column and row.

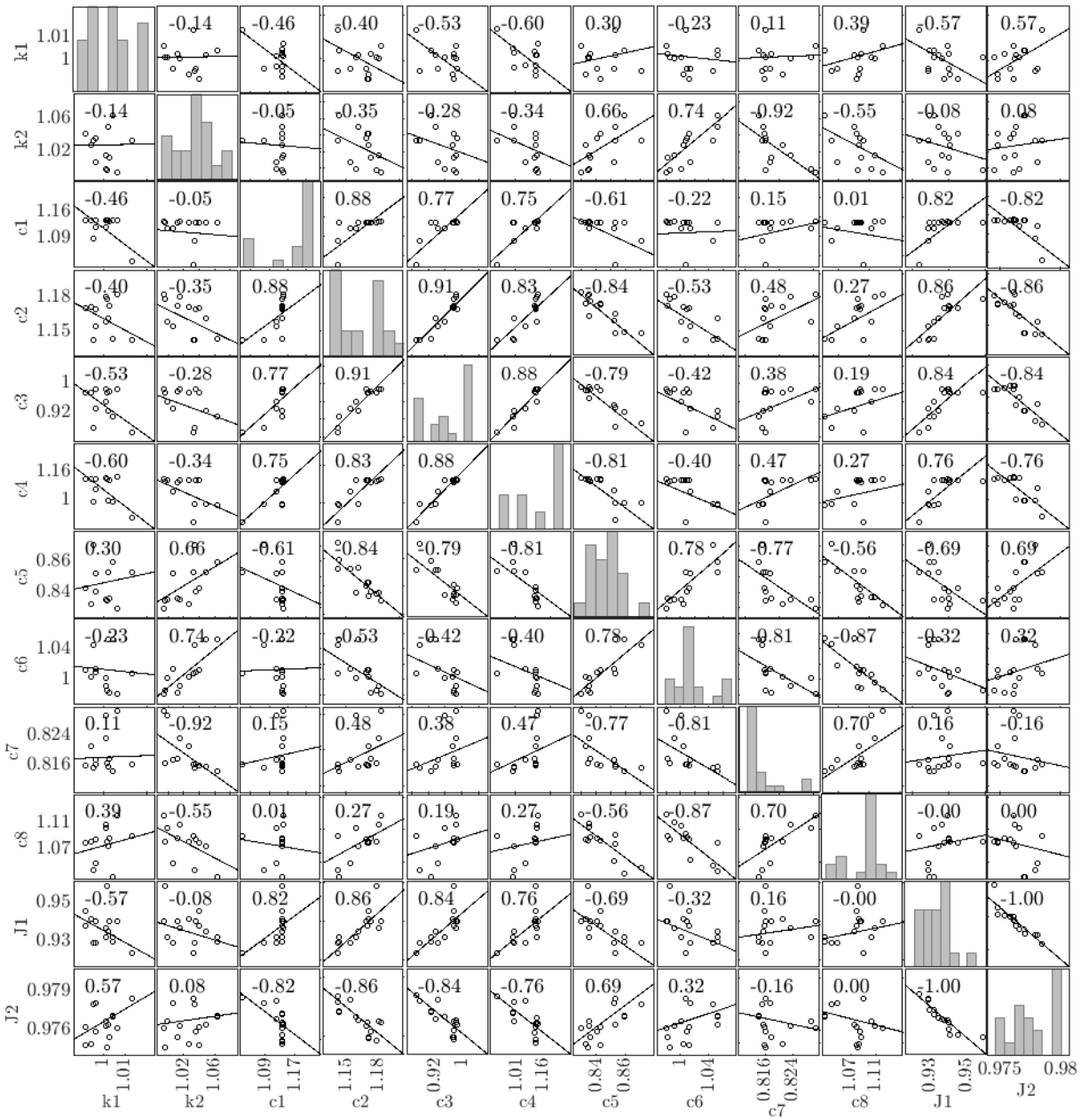

Figure 5.3.7: Correlation matrix on acceleration. Plots in the diagonals are histograms. In off-diagonal plots, each circle indicate an optimal value, the line is the least squares, the and number is the correlation between the variables in the column and row.

and has small effect in acceleration. According to correlations in acceleration, it requires to raise c_2 and c_3, however both imply a reduction of road holding in whoops, but with little effect in braking. The trend with the rest of the variables is similar, performance in whoops is in opposition to performance in braking and accelerating, while performance on these two are lightly correlated.

We understand from this analysis that the optimisation on whoops is complex, since performance is correlated significantly to eight of the ten design variables, and is in conflict with performance in braking and accelerating. On the other hand, optimisation on braking and acceleration are simpler, since performance is correlation to four design variables each and are lightly correlated among them. It is also interesting that in these two manoeuvres the most influencing variables are in the suspension of the wheel that loses load due to horizontal acceleration, i.e. rear in braking and front in accelerating.

Analysing the reference suspension, we noticed that it is closer to the optimal in braking and accelerating than to whoops, which is reasonable considering that in a track there are multiple braking and accelerating zones, and only one whoop section.

Lastly, it would be desirable to verify conclusions for whoops, which requires to develop a rider that can drive realistically for a better matching with the experimental data.

5.4 Summary

In this chapter, we have calculated an optimal suspension to understand its characteristics. To this end, first, we investigated methods to calculate optimal suspensions. Using single-wheel-station and in-plane models we showed that analytical solutions are found only for the simplest cases, while for realistic models the best approach is to optimise numerically. Reviewing numerical optimisations, we concluded that the best methodology is a genetic algorithm due to the complexity of the objective function. Additionally, we determined that a multi-objective optimisation needs to be considered to analyse the relationships between design variables and performance.

Next, we applied this method in a particular class of off-road motorcycle, to obtain the optimal suspensions. For the optimisation, we adapted a validated motorcycle model from the literature for off-road and determined the inputs by comparing against experimental data in three situations of interest: whoops, braking and accelerating. We highlighted the difficulty of simulating transit on whoops. We considered ten parameters of stiffness and damping as design variables, and, as objective functions, comfort and road holding, and we solved it using a genetic algorithm. We found that on the front they are close to the reference suspension, while on the rear, they are softer. Additionally, we found that larger improvement is possible in comfort than road holding.

To understand the characteristics of optimal suspensions, we analysed the correlation between design variables and objectives, where we found three observations not mentioned before in the literature. First, performance in whoops is in conflict with braking and accelerating performance, and is importantly correlated to eight of the ten design variables considered. Second, performance in braking and acceleration are not in conflict between them, and each of them are importantly correlated to four of the ten design variables. Third, variables with higher correlation to performance in braking and acceleration, are in the suspension of the wheel that loses load due to longitudinal inertial force, i.e. rear in braking and front in accelerating.

In this way, we have shown that the optimal suspension is specific for each condition. Optimising for whoops is in detriment of braking and acceleration, while these two have a minor impact on each other, since they depend mainly on a single suspension.

CHAPTER 6

Conclusions and future work

6.1 Conclusions

In this thesis we had determined assessment and calculation procedures for the optimisation of off-road motorcycle suspensions. To this end, we defined performance metrics for assessment based on accelerations and contact forces, we developed an assessment procedure of performance which included a contact forces estimator and a rider model, and we optimised the suspension of a cross motorcycle.

The first task, has been to determine meaningful metrics to assess performance in off-road motorcycles. We examined the literature, finding several definitions of terms. We decided to consider performance as the global behaviour of the vehicle, which depend on comfort and handling. The former, assessed by chassis accelerations, while the latter, we choose to assess it indirectly by road holding through the contact forces. We compared pre-selected indices chosen from the literature and two proposed by us, under weak and strong continuous and impulsive excitations representative of off-road. On one hand, we found out that comfort should be assessed by the fourth order average (rms4), since the levels of chassis accelerations classify as severe according to ISO-2631, instead of the rms. We also found out that considering frequency-weighted or unweighted accelerations as the argument of rms4, makes no to minor difference in the suspension damping that minimises it. On the other hand, we found out that the rms8 is the most appropriate index, since it provides a good estimate of average and peak forces in all situations. rms of the contact force is not a convenient index for these vehicles, since under impulsive excitations is minimised with an excessively low damping.

Experimental assessment of performance with these criteria is not straightforward, particularly because contact forces are not easily measured. With this as a motivation, we developed an estimator of contact forces based on kinematic measurements and inverse dynamics to overcome the difficulty of direct sensing. Measurement errors are partially compensated by considering an overdetermined system and non-physical solutions are reduced by a set of constraint equations that limits the existence of tensile contact forces, and of tangential forces without the corresponding normal one. Tested with experimental data acquired in a motocross track, resulted in contact forces varying consistently with obstacles of the track. Even though the magnitude is not validated, the consistency of the estimation shows that the methodology derived is appropriate for performance comparisons.

The estimator developed requires knowledge of rider forces over the motorcycle, which are not easily obtained since driving is in standing position. For this reason, we studied a suitable description of rider forces. First, in the absence of models for this particular activity, we examined validated models in similar activities, such as off-road cycling and horse riding, finding that they are based on the passive behaviour of the rider. Due to the lack of evidence to support this assumption in our vehicles, we compared a passive rider to a simple rider which represents the fundamental dynamics. When tested with experimental data, we found that the simple model yielded more realistic results than the former, leading to presume that the assumption of passiveness is not valid for off-road motorcycles. We also found that both rider models result in similar contact forces, showing the compensation effect of the estimator. Because of this, we believe that passiveness is not a valid assumption to be used in off-road motorcycles and we provided an alternative method to calculate the rider forces.

Lastly, we calculated an optimal suspension to understand its characteristics. To this end, we determined that the optimisation should be done numerically, with multi-objectives and solved with a genetic algorithm. We applied this method to a cross motorcycle, and optimised stiffness and damping for whoops, braking and acceleration. We found that the optimal solutions are close to the reference suspension in stiffness and front damping, and are slightly lower in rear damping. Improvement is possible particularly in comfort over road holding. We analysed the correlations between optimal solutions and objectives, finding out that performance in whoops is significantly correlated to eight of the ten design variables established, while performance on braking and acceleration are correlated to four each. We also found that performance in whoops is in opposition to braking and accelerating, but these two are not conflict among them. Interestingly as well, we found out that performance in braking and accelerating is mostly correlated to the suspension of the wheel that loses load due to longitudinal acceleration. Briefly, it was shown that optimal suspensions is specific for each condition, and that there is conflict between whoops, and braking and accelerating, while not among the latter two.

Summarising, the main findings and contributions of this thesis are:

- Selection and recommendation of rms4 of frequency-weighted or un-weighted chassis accelerations and rms8 of contact forces as adequate indices to measure performance in off-road motorcycles based on comparative tests.
- A procedure to estimate contact forces in these motorcycles, for experimental assessment.
- Evidence that the rider does not behave passively, and proposed a simple model to estimate the interaction with the motorcycle.
- Outlined optimal suspension parameters for whoops, braking and accelerating; specification of the variables with higher correlation to performance in these situations; description of conflict between whoops performance and braking and accelerating ones, but not among these two.

6.2 Future Work

From the research done, we observed that off-road motorcycles is a relatively unexplored area in scientific terms, and thus, several opportunities for research exist.

On one hand, there are topics pendent from this thesis such as the validation of the estimator and the rider model. This requires measuring forces at the tyres, and at footpegs and handlebar to be contrasted against the estimations. If validated, it could provide a basis for on-board control systems, such as braking assistance or semi active suspensions. Also pendent is the development of a rider controller to drive the motorcycle over whoops to perform more realistic simulations and verify the optimisations obtained here.

On the other hand, there are topics that derive from this thesis such as extension of the optimisations to include other driving situations like jumps or non-motocross terrains like forest or desert. Also, we suggest to investigate the possible effect of friction in the optimal values. Regarding suspension development, we suggest to explore non-linearities in stiffness or damping that might enhance performance, and possibly, resolve the conflict between whoops and braking-accelerating. In the same line, we suggest to explore the benefits of adding an inerter to the suspension. Regarding suspension design, we suggest to develop a simplified methodology to calculate approximately optimal damping and stiffness, to be used by suspension engineers on a routine basis. This could be achieved, for example, by expressing optimal damping coefficients in terms of damping ratios of a single-wheel-station model. Lastly, a significant improvement on the estimation of rider force could be done by measuring accelerations of rider complemented with positions, which can be obtained by visual methods.

6.3 Publications derived from this thesis

Conference publications

- Vasquez F., Lot R., Rustighi E. (2017) Optimisation of off-road motorcycle suspensions. *Proceedings of 15th European Automotive Congress, Madrid, Spain*
- Vasquez F., Lot R., Rustighi E. (2019) Off-road motorcycle tyre force estimation. *Journal of Physics: Conference Series 1264 012020*
- Vasquez F., Lot R., Rustighi E., Pegoraro R.(2019) Rider model for the estimation of tyre forces in off-road motorcycles *Proceedings of 4th Symposium on the dynamics and control of single track vehicles, Padova, Italy*

Journal publications

- Vasquez F., Lot R., Rustighi E., Pegoraro R.(2020) Tyre force estimation for off-road motorcycles *Mechanical Systems and Signal Processing, under review*

Appendices

APPENDIX A

Numerical considerations for index selection.

A.1 Saturation function

The saturation function s is essentially a step function with a continuous and smooth transition between zero and one to reduce numerical issues that may arise from a discontinuous transition. It is defined as,

$$s(y) = \frac{1 + \sin\left(\arctan\left(\frac{y}{y_0}\right)\right)}{2}, \tag{A.1.1}$$

where, y is the argument, and y_0 is a parameter that controls the width of the transition, Figure A.1.1. In particular, 98% of the transition (from 0.01 to 0.99) is $10y_0$ wide.

A.2 Rough road generation

The random road profile is generated based on the procedure described by [87]. The profile $z_g(x)$ is represented by a summation of sinusoidal functions at increasing frequencies,

$$z_g(x) = \sum_{i=1}^{N} A_i \sin(2\pi n_i x + \phi_i), \tag{A.2.1}$$

where, A_i is the amplitude at frequency i and the ϕ_i, is the phase chosen from a uniform probabilistic distribution on the interval $(0, 2\pi)$.

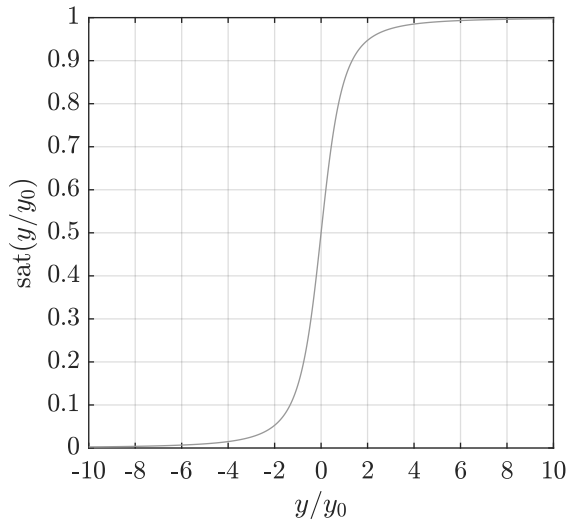

Figure A.1.1: Saturation function. Example values $s(-5y_0) \approx 0.01$, $s(-y_0) \approx 0.146$, $s(0) = 0.5$ and $s(y_0) \approx 0.854$. $s(5y_0) \approx 0.99$

The amplitudes A_i are derived from the discretised definition of the psd, for a given spatial frequency n and frequency step Δn,

$$G_d(n) = \frac{\Psi^2(n, \Delta n)}{\Delta n} \tag{A.2.2}$$

where, $\Psi^2(n_i, \Delta n)$ is the mean-square of the time signal filtered by a band-pass filter at central frequency n_i with bandwidth Δn. For a sinusoidal function, the root-mean-square is related to the amplitude by

$$\Psi^2(n_i, \Delta n) = \frac{A_i^2}{2}. \tag{A.2.3}$$

From Equations A.2.3, A.2.2 and 2.2.15, the road amplitude is written in terms of road class by,

$$A_i = \sqrt{2\Delta n G_d(n_0) \left(\frac{n_i}{n_0}\right)^{-K_r}} \tag{A.2.4}$$

Substituting Equation A.2.4 on A.2.1, and considering that $n_i = i\Delta n$ the road amplitude is described by Equation A.2.5.

$$z_g(x) = \sum_{i=1}^{N} \sqrt{2\Delta n G_d(n_0) \left(\frac{i\Delta n}{n_0}\right)^{-K_r}} \sin(2\pi i \Delta n x + \phi_i) \tag{A.2.5}$$

Figure A.2.1 show the reference power spectral density used to generate road profiles class B and D, and the power spectral density of the generated road.

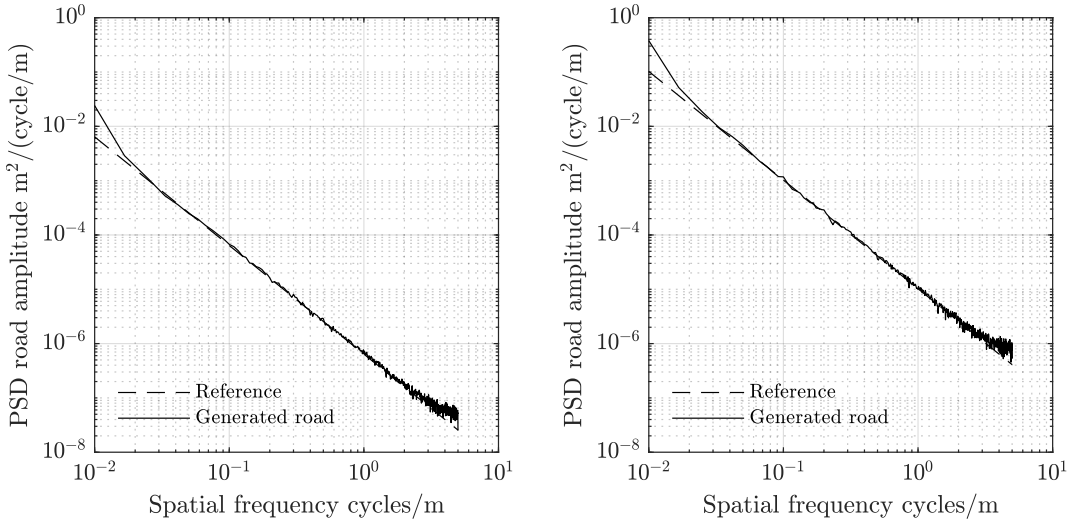

(a) Class B road (b) Class D road

Figure A.2.1: psd of road amplitudes. Class A and D roads built according to ISO 8608, considering the geometric mean of each class as the reference.

A.3 Motorcycle and rider parameters

The numerical parameters considered for the simulation are from a KTM SX-450 2017, a typical motocross motorcycle, Table A.3.1. In particular, its front end is considered. The equivalent mass of the rider m_r and chassis m_c on the front, are estimated as,

$$m_r = M_r b_r / w, \tag{A.3.1}$$

$$m_c = M_c b / w, \tag{A.3.2}$$

where, M_r is total rider mass, b_r is position of rider centre of mass from rear wheel centre, M_c is total chassis mass, b, is chassis centre fo mass from rear wheel centre, and w is wheelbase.

The equivalent rider stiffness k_r and damping c_r on the front, are calculated such that the natural frequency and damping ratio, are the same as with total mass M_r, stiffness K_r and damping C_r, as

$$k_r = m_r K_r / M_r, \tag{A.3.3}$$

$$c_r = m_r C_r / M_r. \tag{A.3.4}$$

The total stiffness and damping are considered from the legs of a cyclist, since are the closest values available in the literature, [54].

The equivalent suspension stiffness and damping are calculated from values at the fork

with a procedure as described by [40],

$$k_s = K_s/\cos(\epsilon)^2, \tag{A.3.5}$$

$$c_s = C_s/\cos(\epsilon)^2, \tag{A.3.6}$$

where, K_s and C_s are stiffness and damping along the fork, and ϵ is the caster angle. The fork parameters are obtained from the company. In absence of tyre parameters, they are estimated from typical values of vehicles [2], the same as the maximum compression values. The bottoming factor of the suspension is estimated from the company data, and for tyre and rider they are assumed as the suspension, therefore, a single value n is considered. Lastly, the constant y_0 is imposed to be 1/10 mm such that 98% of the transition occurs in 1 mm.

Table A.3.1: Data of simulations

Variable	Magnitude	
m_r	24	kg
m_c	57	kg
m_w	12	kg
k_r	26464	N/m
c_r	483	Ns/m
k_s	15961	N/m
c_s	966	Ns/m
k_t	150000	N/m
c_t	100	Ns/m
n	50	-
z_{rM}	0.3	m
z_{sM}	0.3	m
z_{tM}	0.1	m
y_0	10^{-4}	m

A.4 Frequency-weights according to ISO 2631.

In order to weight the frequency components of the accelerations, the standard proposes two methods: using a filter defined as a transfer function or by frequency weights defined in one-third octave bands. We implement them as filters, since it is simpler and clearer.

The standard defines the filter as the product of four transfer functions: high-pass H_h, low-pass H_l, velocity-acceleration transition H_t, and step up H_s,

$$H_h(s) = \left|\frac{1}{1+1/(Q_1 w_1 s)+(w_1/s)^2}\right|, \tag{A.4.1}$$

$$H_l(s) = \left|\frac{1}{1+s/(Q_2 w_2)+(s/w_2)^2}\right|, \tag{A.4.2}$$

Table A.4.1: Parameters of the transfer functions for frequency weightings. Angular frequencies w_i are calculated as $w_i = 2\pi f_i$.

	Band-limiting				Acceleration-velocity transition			Upward step			
Weighting	f_1 Hz	Q_1	f_2 Hz	Q_2	f_3 Hz	f_4 Hz	Q_4	f_5 Hz	Q_5	f_6 Hz	Q_6
W_k	0.4	$\frac{1}{\sqrt{2}}$	100	$\frac{1}{\sqrt{2}}$	12.5	12.5	0.63	2.37	0.91	3.35	0.91

$$H_t(s) = \left| \frac{1+s/w_3}{1+s/(Q_4 w_4)+(s/w_4)^2} \right|, \tag{A.4.3}$$

$$H_s(s) = \left| \frac{1+s/(Q_5 w_5)+(s/w_5)^2}{1+s/(Q_6 w_6)+(s/w_6)^2} \left(\frac{w_5}{w_6}\right)^2 \right|, \tag{A.4.4}$$

where, s is $Q_1, ..., Q_6$ are resonant quality factors and $w_1, ..., w_6$ are corner frequencies, defined in Table A.4.1.

We convert the continuous filter to a discrete filter, using the bilinear transform,

$$s = 2\frac{1 - z^{-1}}{1 + z^{-1}}, \tag{A.4.5}$$

The final transfer function filter, shown in Figure A.4.3, is obtained by combining the four of them as,

$$H(z) = H_h(z)H_l(z)H_t(z)H_s(z). \tag{A.4.6}$$

We test the filter with a signal composed of the sum of sinusoidal functions with unit amplitude,

$$a = \sum_i \sin(2\pi f_i t), \tag{A.4.7}$$

and frequencies f_i chosen from Table A.4.2 which are the nominal frequencies of the one-third octave bands. Figure A.4.3 shows that the filter is implemented correctly.

Table A.4.2: Frequency weights W_k, defined by ISO 2631.

Frequency Hz	Weight	Frequency Hz	Weight	Frequency Hz	Weight
1	0.482	4	0.967	16	0.768
1.25	0.484	5	1.039	20	0.636
1.6	0.494	6.3	1.054	25	0.513
2	0.531	8	1.036	31.5	0.405
2.5	0.613	10	0.988	40	0.314
3.15	0.804	12.5	0.902	50	0.246

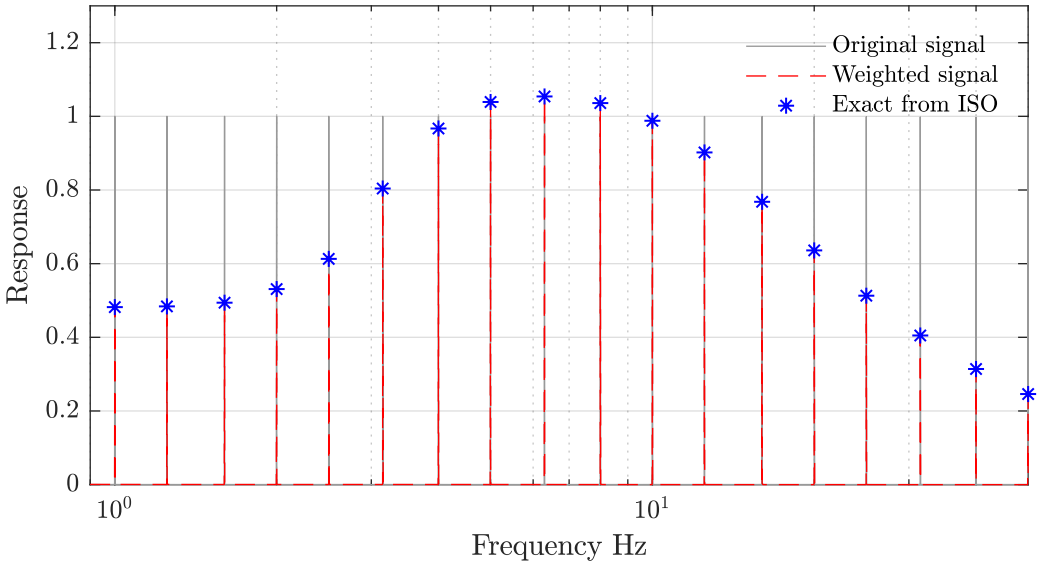

Figure A.4.3: Implemented frequency-weight filter test. The test function composed of the sum of sinusoidal functions at selected frequencies, is filtered with Equation A.4.6, resulting in the weighted signal. It is clear that the amplitudes of this signal match the exact values given by standard ISO 2631 in Table A.4.2.

APPENDIX B

Equations of motion of the estimator

The equations of motion are derived under the four assumptions described in Chapter 2, namely, in plane motion, four bodies with five degrees of freedom, standing rider, and contact point under wheel centres.

We derived an equation per degree of freedom using Newton-Euler equations in the following order. First and second equations are sum of forces acting over all bodies along x_s and z_s respectively; third equation, is sum of torques on all bodies around centre of mass of chassis; fourth equation is sum of forces acting on front wheel along z_f; fifth equation is sum of torques acting on rear wheel and swing arm, around the connecting point between body 2 and 3 (P_{23}). Organizing the equations in matrix form, we get

$$\mathbf{M\ddot{q}} + \mathbf{m_v} = \mathbf{A_w}g + \mathbf{A_s f_s} + \mathbf{A_r f_r} + \mathbf{A_t f_t},$$

where the elements on the matrices are the following:

$$\begin{aligned}
M_{1,1} &= m_4 + m_1 + m_3 \\
M_{1,2} &= 0 \\
M_{1,3} &= \left(\left(S\left(\mu + \alpha_{r0} - \alpha_r\right) - S\left(\mu + \alpha_{r0}\right)\right) l_r + C\left(\mu\right)\left(h - R_r\right) + S\left(\mu\right) b\right) m_1 \\
&\quad + \left(-z_f C\left(\mu + \epsilon\right) + C\left(\mu\right)\left(h - R_f\right) + \left(b - w\right) S\left(\mu\right)\right) m_4 \\
M_{1,4} &= -m_4\, S\left(\mu + \epsilon\right) \\
M_{1,5} &= -l_r\, m_1\, S\left(\mu + \alpha_{r0} - \alpha_r\right) \\
M_{2,2} &= m_4 + m_1 + m_3
\end{aligned}$$

$$
\begin{aligned}
M_{2,3} = & \left(\left(C\left(\mu+\alpha_{r0}-\alpha_r\right)-C\left(\mu+\alpha_{r0}\right)\right) l_r+\left(-h+R_r\right) S\left(\mu\right)+C\left(\mu\right) b\right) m_1 \\
& +\left(z_f S\left(\mu+\epsilon\right)+\left(R_f-h\right) S\left(\mu\right)+\left(b-w\right) C\left(\mu\right)\right) m_4 \\
M_{2,4} = & -m_4 C\left(\mu+\epsilon\right) \\
M_{2,5} = & -l_r m_1 C\left(\mu+\alpha_{r0}-\alpha_r\right) \\
M_{3,3} = & \Big(\left(-2 C\left(\alpha_r\right)+2\right) {l_r}^2+\left(\left(-2 R_r+2 h\right) S\left(\alpha_{r0}-\alpha_r\right)+2 C\left(\alpha_{r0}-\alpha_r\right) b+\right. \\
& \left.\left(-2 h+2 R_r\right) S\left(\alpha_{r0}\right)-2 b C\left(\alpha_{r0}\right)\right) l_r+{R_r}^2-2 R_r h+b^2+h^2\Big) m_1 \\
& +\Big(\left(z_f\right)^2+\left(\left(2 b-2 w\right) S\left(\epsilon\right)+\left(2 R_f-2 h\right) C\left(\epsilon\right)\right) z_f+{R_f}^2 \\
& -2 R_f h+b^2-2 b w+h^2+w^2\Big) m_4+I_1+I_2+I_3+I_4 \\
M_{3,4} = & \left(\left(R_f-h\right) S\left(\epsilon\right)+\left(w-b\right) C\left(\epsilon\right)\right) m_4 \\
M_{3,5} = & \Big(\left(C\left(\alpha_r\right)-1\right) {l_r}^2+\left(\left(-h+R_r\right) S\left(\alpha_{r0}-\alpha_r\right)-C\left(\alpha_{r0}-\alpha_r\right) b\right) l_r\Big) m_1 \\
& -I_1-I_2 \\
M_{4,4} = & m_4 \\
M_{4,5} = & 0 \\
M_{5,5} = & {l_r}^2 m_1+I_1+I_2
\end{aligned}
$$

$$
\begin{aligned}
m_{v1,1} = & \Big(\left(\left(C\left(\mu+\alpha_{r0}-\alpha_r\right)-C\left(\mu+\alpha_{r0}\right)\right) l_r+\left(-h+R_r\right) S\left(\mu\right)+C\left(\mu\right) b\right)\left(\dot{\mu}\right)^2 \\
& -2\left(\dot{\alpha_r}\right) C\left(\mu+\alpha_{r0}-\alpha_r\right)\left(\dot{\mu}\right) l_r+\left(\dot{\alpha_r}\right)^2 C\left(\mu+\alpha_{r0}-\alpha_r\right) l_r\Big) m_1 \\
& +\Big(\left(z_f S\left(\mu+\epsilon\right)+\left(R_f-h\right) S\left(\mu\right)+\left(b-w\right) C\left(\mu\right)\right)\left(\dot{\mu}\right)^2-2 C\left(\mu+\epsilon\right)\left(\dot{z_f}\right)\dot{\mu}\Big) m_4 \\
m_{v2,1} = & \Big(\left(\left(-S\left(\mu+\alpha_{r0}-\alpha_r\right)+S\left(\mu+\alpha_{r0}\right)\right) l_r-S\left(\mu\right) b+\left(-h+R_r\right) C\left(\mu\right)\right)\left(\dot{\mu}\right)^2 \\
& +2\left(\dot{\alpha_r}\right) S\left(\mu+\alpha_{r0}-\alpha_r\right)\left(\dot{\mu}\right) l_r-\left(\dot{\alpha_r}\right)^2 S\left(\mu+\alpha_{r0}-\alpha_r\right) l_r\Big) m_1 \\
& +\Big(\left(z_f C\left(\mu+\epsilon\right)+S\left(\mu\right)\left(w-b\right)+\left(R_f-h\right) C\left(\mu\right)\right)\left(\dot{\mu}\right)^2+2 S\left(\mu+\epsilon\right)\left(\dot{z_f}\right)\dot{\mu}\Big) m_4 \\
m_{v3,1} = & \Big(\Big(2 S\left(\alpha_r\right) {l_r}^2+\left(2 S\left(\alpha_{r0}-\alpha_r\right) b+\left(-2 h+2 R_r\right) C\left(\alpha_{r0}-\alpha_r\right)\right) l_r\Big)\left(\dot{\alpha_r}\right)\dot{\mu} \\
& +\Big(-S\left(\alpha_r\right) {l_r}^2+\left(-S\left(\alpha_{r0}-\alpha_r\right) b+\left(h-R_r\right) C\left(\alpha_{r0}-\alpha_r\right)\right) l_r\Big)\left(\dot{\alpha_r}\right)^2\Big) m_1 \\
& +\left(2 z_f+\left(2 b-2 w\right) S\left(\epsilon\right)+\left(2 R_f-2 h\right) C\left(\epsilon\right)\right)\left(\dot{z_f}\right)\left(\dot{\mu}\right) m_4+I_1\ddot{\mu}_1+I_4\ddot{\mu}_4 \\
m_{v4,1} = & \left(-z_f+\left(w-b\right) S\left(\epsilon\right)+\left(h-R_f\right) C\left(\epsilon\right)\right)\left(\dot{\mu}\right)^2 m_4 \\
m_{v5,1} = & \Big(-S\left(\alpha_r\right) {l_r}^2+\left(-S\left(\alpha_{r0}-\alpha_r\right) b+\left(h-R_r\right) C\left(\alpha_{r0}-\alpha_r\right)\right) l_r\Big)\left(\dot{\mu}\right)^2 m_1-I_1\ddot{\mu}_1
\end{aligned}
$$

$$
\begin{aligned}
A_{w1,1} = & 0 \\
A_{w2,1} = & m_4+m_1+m_3 \\
A_{w3,1} = & \left(\left(C\left(\mu+\alpha_{r0}-\alpha_r\right)-C\left(\mu+\alpha_{r0}\right)\right) l_r+\left(-h+R_r\right) S\left(\mu\right)+C\left(\mu\right) b\right) m_1 \\
& +\left(z_f S\left(\mu+\epsilon\right)+\left(R_f-h\right) S\left(\mu\right)+\left(b-w\right) C\left(\mu\right)\right) m_4
\end{aligned}
$$

$$A_{w4,1} = -\, m_4\, C\left(\mu + \epsilon\right)$$
$$A_{w5,1} = -\, l_r\, m_1\, C\left(\mu + \alpha_{r0} - \alpha_r\right)$$

$$\mathbf{A_r} = \begin{bmatrix} -1 & 0 & -1 & 0 \\ 0 & -1 & 0 & -1 \\ A_{r3,1} & A_{r3,2} & A_{r3,3} & A_{r3,4} \\ 0 & 0 & 0 & 0 \\ 0 & 0 & 0 & 0 \end{bmatrix} \qquad \mathbf{A_s} = \begin{bmatrix} 0 & 0 \\ 0 & 0 \\ 0 & 0 \\ -1 & 0 \\ 0 & -1 \end{bmatrix}$$

$$A_{r3,1} = \; S\left(\mu\right) x_{3p} - C\left(\mu\right) z_{3p}$$
$$A_{r3,2} = \; C\left(\mu\right) x_{3p} + S\left(\mu\right) z_{3p}$$
$$A_{r3,3} = \; S\left(\mu\right) x_{3h} - C\left(\mu\right) z_{3h}$$
$$A_{r3,4} = \; C\left(\mu\right) x_{3h} + S\left(\mu\right) z_{3h}$$

$$\mathbf{A_t} = \begin{bmatrix} -S\left(\mu\right) & -S\left(\mu\right) & -C\left(\mu\right) & -C\left(\mu\right) & C\left(\mu\right) \\ -C\left(\mu\right) & -C\left(\mu\right) & S\left(\mu\right) & S\left(\mu\right) & -S\left(\mu\right) \\ A_{t3,1} & A_{t3,2} & A_{t3,3} & A_{t3,4} & A_{t3,5} \\ C\left(\epsilon\right) & 0 & S\left(\epsilon\right) & 0 & 0 \\ 0 & A_{t5,2} & 0 & A_{t5,4} & A_{t5,5} \end{bmatrix}$$

$$A_{t3,1} = \; -z_f S\left(\epsilon\right) - b + w$$
$$A_{t3,2} = \; C\left(\alpha_{r0}\right) l_r - l_r\, C\left(\alpha_{r0} - \alpha_r\right) - b$$
$$A_{t3,3} = \; z_f C\left(\epsilon\right) - h$$
$$A_{t3,4} = \; S\left(\alpha_{r0}\right) l_r - l_r\, S\left(\alpha_{r0} - \alpha_r\right) - h$$
$$A_{t3,5} = \; -S\left(\alpha_{r0}\right) l_r + l_r\, S\left(\alpha_{r0} - \alpha_r\right) + h$$
$$A_{t5,2} = \; l_r\, C\left(\alpha_{r0} - \alpha_r\right)$$
$$A_{t5,4} = \; l_r\, S\left(\alpha_{r0} - \alpha_r\right) + R_r$$
$$A_{t5,5} = \; -l_r\, S\left(\alpha_{r0} - \alpha_r\right) - R_r$$

The equations are derived using the following MBSymba [49, 70] code:

```
> interface(displayprecision=3, rtablesize=50):

> with(LinearAlgebra):
> q := [x__s(t),z__s(t), mu(t), z__f(t), alpha__r(t)]:

> PDEtools[declare](q,u,prime=t,quiet):

> alias(C=cos,S=sin):
```

Frames:

```
> T__R := ground:

> _gravity := make_VECTOR(ground,0,0,g):

> T__3 := T__R *  translate(b,0,-h)  * translate(x__s(t), 0, z__s(t) )

> * rotate('Y',mu(t)) :

> T__3 * translate(-b, 0, h - R__r) * rotate('Y', alpha__r0) * translate(l__r,0,0):

> P__S := project( origin(%), T__3):

> T__2 := T__3 * translate(comp_X(P__S), 0, comp_Z(P__S))

> * rotate('Y', alpha__r0 - alpha__r(t)) * translate(-l__s, 0, 0):

> T__1 := T__2 * translate(-(l__r - l__s), 0, 0):

> T__4 := T__3 * translate(w - b, 0, h - R__f) * rotate('Y', epsilon)

> * translate(0, 0, -z__f(t) ):
```

Bodies

```
> rear_wheel := make_BODY(T__1, m__1, 0, 0, 0):  show(rear_wheel):

> swing_arm := make_BODY(T__2, 0, 0, I__2, 0):  show(swing_arm):

> chassis := make_BODY(T__3, m__3, 0, I__3, 0):  show(chassis):

> front_wheel := make_BODY(T__4, m__4, 0, 0, 0):  show(front_wheel):
```

Points

```
> cp_front := project(CoM(front_wheel),T__R) + make_VECTOR(T__R, 0, 0, R__f):

> cp_rear  := project(CoM(rear_wheel ),T__R) + make_VECTOR(T__R, 0, 0, R__r):

> P__3h := make_POINT(T__3, x__3h, 0, z__3h):  handlebar

> P__3p := make_POINT(T__3, x__3p, 0, z__3p):  footpeg
```

Forces

```
> front_cont := make_FORCE(T__3, -B__f, 0, N__f, cp_front, front_wheel):

> rear_cont := make_FORCE(T__£, D__r - B__r, 0, N__r, cp_rear , rear_wheel):

> leg_force := make_FORCE(T__R, -flx, 0, -flz, P__3p, chassis):

> arm_force := make_FORCE(T__R, -fax, 0, -faz, P__3h, chassis):

> front_susp := make_FORCE(T__4, 0, 0, S__f, origin(T__4), front_wheel,
chassis):

> rear_susp := make_TORQUE(T__2, 0, TS__r, 0,  swing_arm, chassis):
```

Equations of motion of all motorcycle

```
> all_bike := {rear_wheel, swing_arm, chassis, front_wheel, rear_cont, front_con
leg_force, arm_force}:

> eqnsN__A := newton_equations(all_bike):

> eqnsN__Ax := comp_X(eqnsN__A):

> eqnsN__Az := comp_Z(eqnsN__A):

> eqnsE__A := euler_equations(all_bike, origin(T__3)):

> eqnsN__Ay := combine(comp_Y(eqnsE__A),'trig'):
```

Equation of motion of Front Wheel

```
> front     := {front_wheel, front_cont, front_susp}:

> eqnsN__4  := newton_equations(front):

> eqnsN__4z := collect(comp_Z(project(eqnsN__4,T__4)),m__4):
```

Equation of motion of Rear Wheel + Swing arm

```
> rear_swing_arm     := {rear_wheel, swing_arm, rear_cont, rear_susp}:

> eqnsE__12  := euler_equations(rear_swing_arm, P__S):

> eqnsE__12y := combine(comp_Y(eqnsE__12),'trig'):
```

Solution

```
> all_eqns := [eqnsN__Ax, eqnsN__Az, eqnsN__Ay, eqnsN__4z, eqnsE__12y]:

> x__m := [N__f, N__r, B__f, B__r, D__r ]:

> GenerateMatrix(all_eqns, x__m):

> A1:= combine(%[1],'trig'):

> b1:= -%%[2]:
```

APPENDIX C

Instrumentation of experimental motorcycle.

The instrumented motorcycle carries sensors detailed in Table C.0.1. Sampling frequency is 1600Hz.

Table C.0.1: Description of sensors of experimental motorcycle. Vertical and lateral and longitudinal are with respect to the body in which they are mounted.

Name	Magnitude	Direction	Location
FbAob	Acceleration	Along shock	Shock upper mount
FbAun	Acceleration	Along shock	Shock lower mount
FbHub	Length	Along shock	Shock
FzgPhiNick	Angle	Lateral	Seat
GaAlat	Acceleration	Front wheel axis	Front wheel
GaAlon	Acceleration	Forward	Front wheel
GaAob	Acceleration	Along fork	Steering head
GaAun	Acceleration	Along fork	Front wheel
GaFw	Length	Along Fork	Fork
HaALonRe	Acceleration	Forward	Rear wheel
HaAverRe	Acceleration	Vertical	Rear wheel
HeAlat	Acceleration	Lateral	Rear seat
HeAver	Acceleration	Vertical	Rear seat
MoAlat	Acceleration	Lateral	Engine
MoAlon	Acceleration	Longitudinal	Engine
MoAver	Acceleration	Vertical	Engine
RdVVo	Angular speed	Wheel axis	Front wheel
RdVHi	Angular speed	Wheel axis	Rear wheel
StkAver	Acceleration	Vertical	Steering head
V_GPS	Speed	Forward	Seat

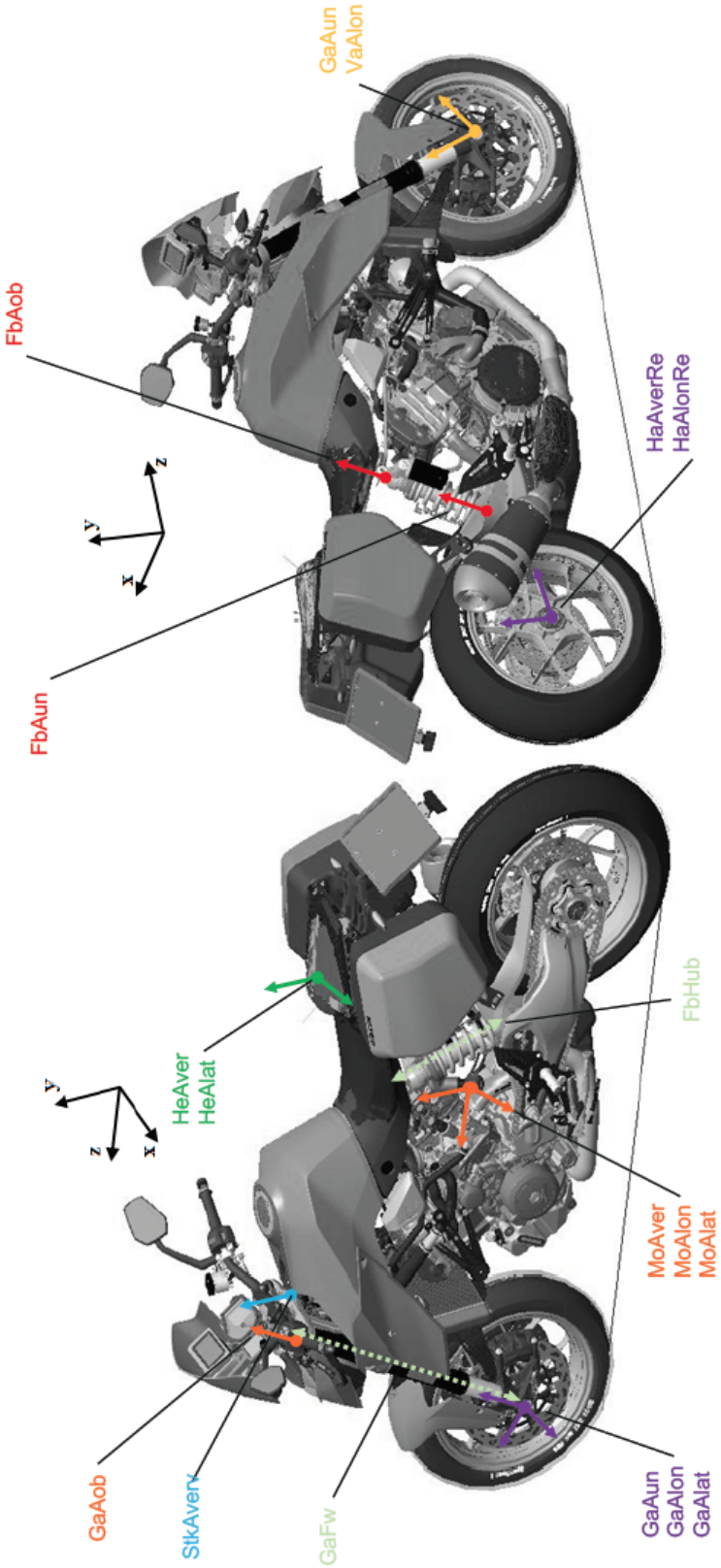

Figure C.0.2: Location of sensors in experimental motorcycle.

APPENDIX D

Equations of motion of passive rider

The equations of motion of the passive rider model are derived under the assumptions detailed in Chapter 4 using the following MBSymba [49, 70] code:

```
> interface(displayprecision=3, rtablesize=50):
```

Coordinates

```
> q := [x__7(t), z__7(t)]:
> u := [x__s(t), z__s(t), mu(t)]:
> PDEtools[declare](q,u,prime=t,quiet); alias(C=cos,S=sin):
```

Frames and points

```
> T__R := ground:

> _gravity := make_VECTOR(ground,0,0,g):

> T__3 := T__R * translate(x__s(t) + x__03, 0, z__s(t) + z__03 ) * rotate('Y',
mu(t)) :

> T__7 := T__R * translate(x__07, 0, z__07) * rotate('Y', theta__07 ) *
translate(x__7(t) , 0, z__7(t)):

> G7 := make_POINT(T__7, g7x, 0, g7z):

> P__3h := make_POINT(T__3, x__3h, 0, z__3h):  handlebar

> P__3p := make_POINT(T__3, x__3p, 0, z__3p):  footpeg

> P__7s := make_POINT(T__7, x__7s, 0, 0):  shoulder

> P__7c := make_POINT(T__7, x__7c, 0, 0):  hip (cadera)
> PS := project(P__7s, T__R): shoulder point in ground coordinates

> PC := project(P__7c, T__R): cadera (hip) point in ground coordinates

> ua := < uax, 0, uaz, 0 > / l__arm:

> va := <   0, 1,   0, 0 > :

> wa := < wax, 0 , waz, 0 > / l__arm:

> T__arm := < ua | va | wa | < comp_X(PS), 0, comp_Z(PS), 1 > >:

> ul := < ulx, 0, ulz, 0 > / l__leg:

> vl := <   0, 1,   0, 0 > :

> wl := < wlx, 0, wlz, 0 > / l__leg:

> T__leg := < ul | vl | wl | < comp_X(PC), 0, comp_Z(PC), 1 > >:
```

Bodies and forces

```
> rider := make_BODY(G7, m[7], 0, I[7], 0):

> arm_force := make_FORCE(T__arm, 0, 0, F__a, PS, rider):

> leg_force := make_FORCE(T__leg, F__lt, 0, F__l, PC, rider):

> hip_torque := make_TORQUE(T__R, 0, F__lt * l__leg, 0, rider ):
```

Implicit equations of motion

```
> collect_list := [ diff(x__7(t),t,t), diff(z__7(t),t,t), m[7], g, F__a,
F__l]:

> rider_system := {rider, arm_force, leg_force, hip_torque}:

> eqnsN := newton_equations( rider_system ):

> dyn_eqnsN1 := collect([comp_X(eqnsN), comp_Z(eqnsN)], collect_list):

> eqnsN_Y := comp_Y( euler_equations(rider_system, G7)):

> flt1 := F__lt = collect(solve(%, F__lt), collect_list):

> dyn_eqnsN0 := collect(subs(%, dyn_eqnsN1), collect_list):
```

Expressions for arm and leg lengths, vectors, unit vectors and forces

```
> v__sh := project(join_points(P__7s, P__3h), T__R): Shoulder to handlebar

> v__cp := project(join_points(P__7c, P__3p), T__R): Cadera to footpeg
> l__armi := sqrt(dot_prod(v__sh,v__sh)):

> l__legi := sqrt(dot_prod(v__cp,v__cp)):

> lengthi := l__arm = l__armi, l__leg = l__legi, v__arm = diff(l__armi,t),
v__leg = diff(l__legi,t):

> v__shx := project(rotate('Y',Pi/2, v__sh ),ground):

> v__cpx := project(rotate('Y',Pi/2, v__cp ),ground):

> unit_vectors := uax = comp_X(v__shx), uaz = comp_Z(v__shx), wax = comp_X(v__sh
waz = comp_Z(v__sh), ulx = comp_X(v__cpx), ulz = comp_Z(v__cpx), wlx = comp_X(v__
wlz = comp_Z(v__cp):

> forces :=  F__a =   c__a *  v__arm + k__a * (l__arm - l__arm0 - l__armp),

> F__l =   c__l *  v__leg + k__l * (l__leg - l__leg0 - l__legp) :
```

Explicit equations of motion

```
> subs(forces,dyn_eqnsN0):  subs(lengthi,%):  subs(unit_vectors,%):  dyn_eqns:=%
```

Initial conditions in rider frame

```
> P7 := project(origin(T__7), T__R):

> V7 := velocity(P7, T__R):

> P7_c := [ comp_X(P7), comp_Z(P7) ]  :

> V7_c := [ comp_X(V7), comp_Z(V7) ]  :

> Pg70 := [ x__g70,  z__g70]:

> Vg70 := [vx__g70, vz__g70]:

> P7_Pg := op(combine( solve(P7_c - Pg70 ,  [op(q)] ), trig)):

> op( combine(solve(V7_c - Vg70  ,  [op( diff(q,t)) ]))):

> V7_Vg := subs( P7_Pg, %):

> X7i := < rhs(op(1,%%%)); rhs(op(2,%%%)); rhs(op(1,%)); rhs(op(2,%)) >:
```

First order formulation

```
> fo_vars, fo_eqns := first_order(dyn_eqns, q, t):

> A2, b2 := GenerateMatrix(fo_eqns, diff(fo_vars,t)):
```

Motorcycle forces over rider - f___r

```
> fl_tr := project(leg_force,T__R):

> fa_tr := project(arm_force,T__R):
> Flx1 := comp_X(fl_tr):

> Flz1 := comp_Z(fl_tr):

> Fax1 := comp_X(fa_tr):

> Faz1 := comp_Z(fa_tr):

> f8_i := [Flx1, Flz1, Fax1, Faz1]:

> subs(flt1, f8_i):  subs(forces, %):  subs(unit_vectors, %):  subs(lengthi,
%):  fr := %:
```

APPENDIX E

FastBike implementation

FastBike is a multibody code developed at the Department of Mechanical Engineering of the University of Padova and has been validated experimentally in several works [79–82].

The motorcycle model considers six bodies: front and rear wheel, chassis (includes frame, engine and tank), front chassis (includes fork, handlebar and steering column), swingarm and front unsprung mass. The degrees of freedom considered are: forward, downward and rightward translations, yaw, roll and pitch angle, steering angle, front suspension and swingarm compressions and rear and front wheel rotations, as shown in Figure E.0.1.

External torques are on the steering and front and rear wheels are applied by the rider to control the motorcycle. Additionally, forces and torques can be applied on the centre of mass. The equations of motion are derived symbolically using MBSymba [48, 49], and implemented in a Simulink block, as shown in Figure E.0.2

For off-road, we added the rider in standing position, using the simple rider model derived in Chapter 4. We apply this forces over the centre of mass of the motorcycle and added the torques arising from the translation of the forces from the handlebar and footpeg to the centre of mass. Additionally, we added pitch and vertical controls used only for whoops simulations. The simulink model is shown in Figure E.0.3

The suspension forces are described in terms of the design variables. For the elastic forces, a look-up table, which contains the measured relation of force against displacement are multiplied by the elastic gains. The damping forces are described using four damping coefficients and two knee velocities, for which we used a look-up table. Additionally,

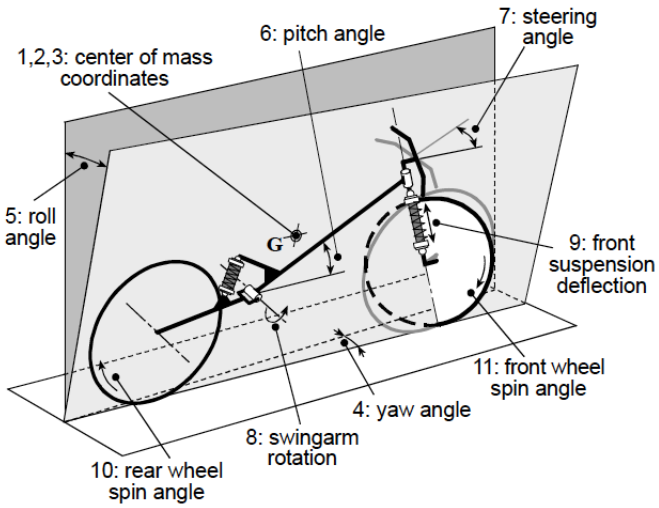

Figure E.0.1: FastBike's degrees of freedom, reproduced from [80].

on the rear wheel, the relationship between shock compression and swingarm rotation is considered, as seen in Figure E.0.4

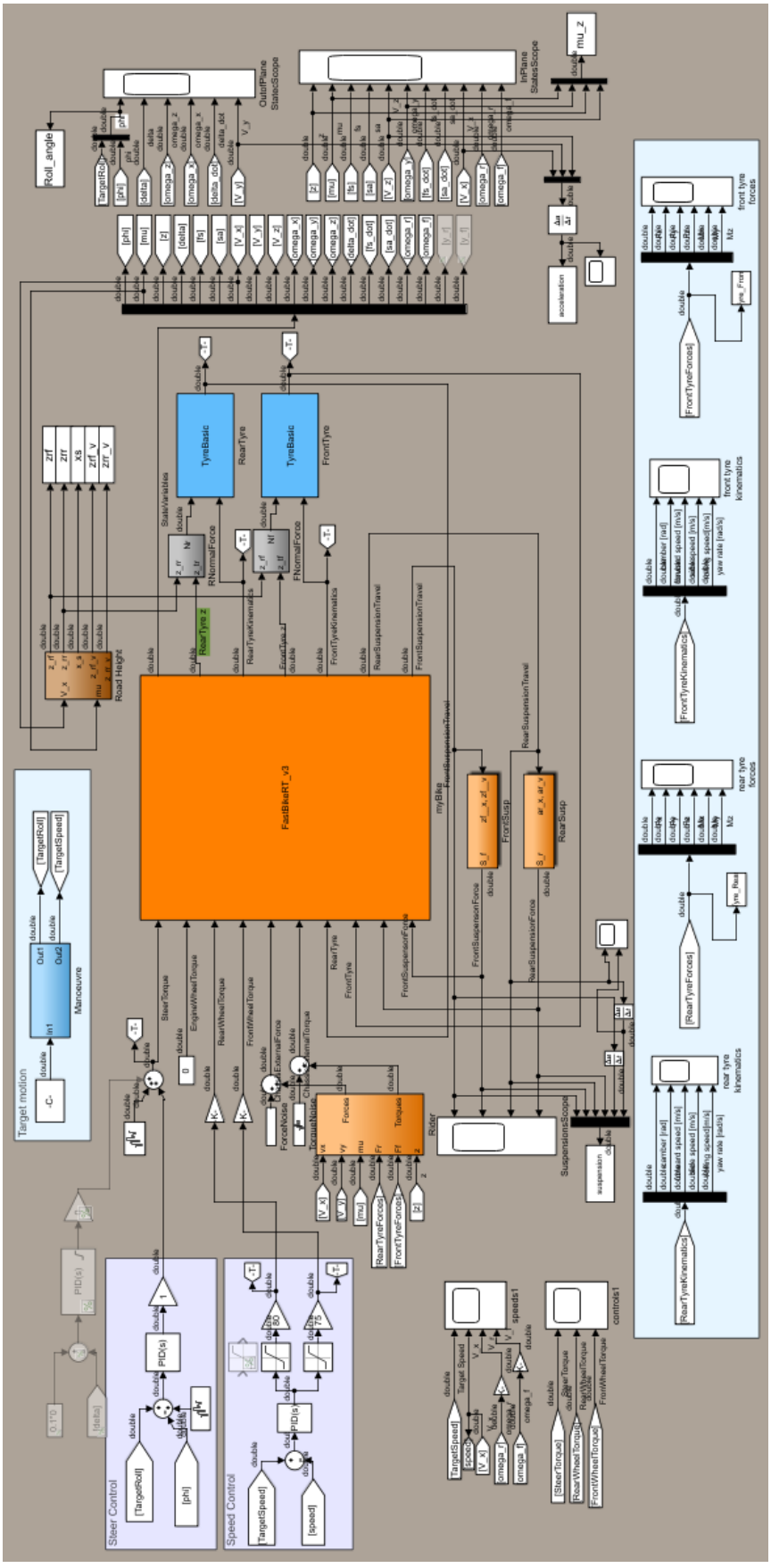

Figure E.0.2: FastBike implemented in Simulink. FastBikeRT v3 block (big orange block) is the main block, which accepts several intpus to calculate the motion. Rider block is shown at its left and suspension blocks, at its bottom.

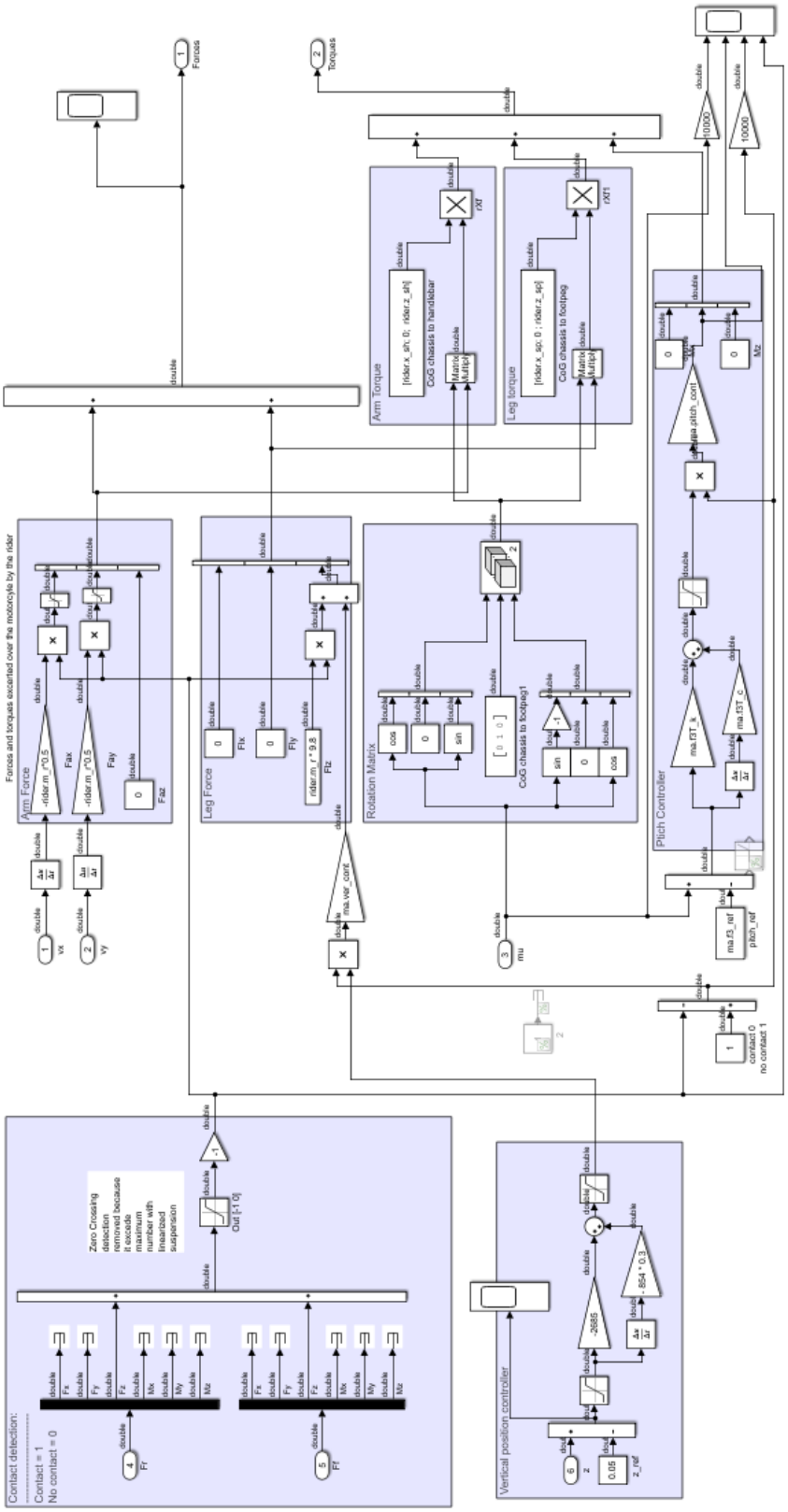

Figure E.0.3: Rider block in Simulink. It considers a standing rider acting over footpeg and handlebars only, and a pitch and vertical controls used only for whoops simulations.

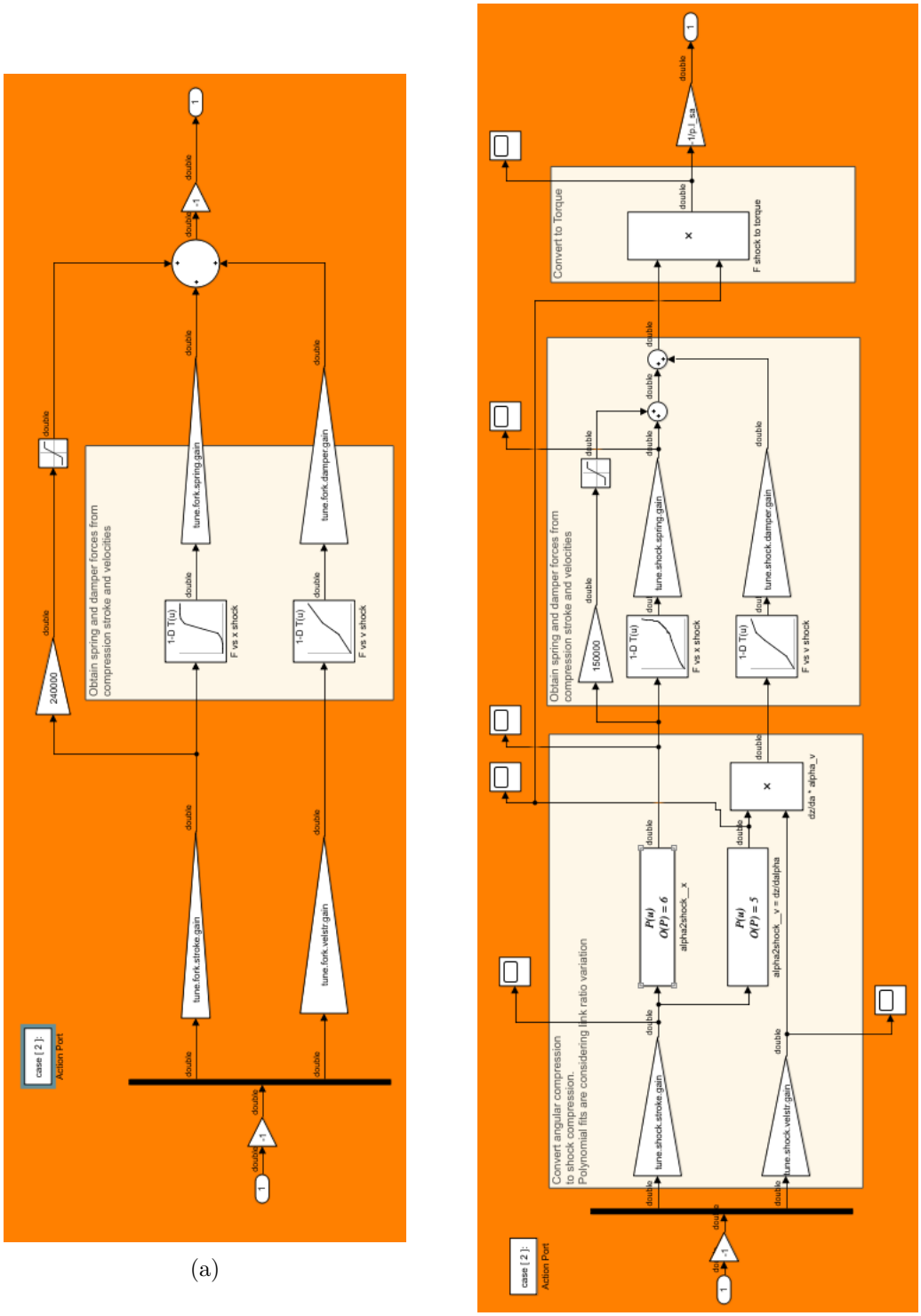

(a) (b)

Figure E.0.4: Suspension blocks in Simulink. a) front suspension block, b) rear suspension block. It considers a standing rider acting over footpeg and handlebars only, and a pitch and vertical controls used only for whoops simulations.

Bibliography

[1] International Organization for Standardization (2016) ISO 8608, Mechanical vibration - Road surface profiles - Reporting of measured data, The Organization, .

[2] Limebeer, D. and Massaro, M. (2018) Dynamics and optimal control of road vehicles, Oxford University Press, .

[3] Mastinu, G. and Ploechl, M., (eds.) (2014) Road and Off-road Vehicle System Dynamics Handbook, CRC Press, Inc., .

[4] Guiggiani, M. (2014) The science of vehicle dynamics, Springer, .

[5] Guillespie, T. (1992) Fundamentals of vehicle dynamics, Society of Automotive Engineers, .

[6] International Organization for Standardization (1997) ISO 2631-1, Mechanical vibration and shock-Evaluation of human exposure to whole-body vibration-Part 1: General requirements, The Organization, .

[7] International Organization for Standardization (2001) ISO 5349-1, Mechanical vibration — Measurement and evaluation of human exposure to hand-transmitted vibration — Part 1: General requirements, The Organization, .

[8] British Standards Institution (1987) BS 6841, Measurement and evaluation of human exposure to whole-body mechanical vibration and repeated shock, The Organization, .

[9] Verein Deutcher Ingenieure VDI 2057, Human exposure to mechanical vibrations whole-body vibration (2002).

[10] Goncalves, J. and Ambrosio, J. (2005) Road Vehicle Modeling Requirements for optimisation of ride and handling. *Multibody system dynamics,* **13**, 3–13.

[11] Zou, L. and Nayfeh, Z. (2003) Structured H2 optimisation of vehicle suspensions based on multi-wheel models. *Vehicle System Dynamics: International Journal of Vehicle Mechanics and Mobility,* **40**, 351–371.

[12] Deprez, K., Moshou, D., and Ramon, H. (2005) Comfort improvement of a nonlinear suspension using global optimization and in situ measurements. *Journal of Sound and Vibration,* **284**, 1003–1014.

[13] Zehsaz, M., Sadeghi, M., Ettefagh, M., and Shams, F. (2011) Tractor cabin's passive suspension parameters optimization via experimental and numerical methods. *Journal of Terramechanics,* **48**, 439–450.

[14] Özcan, D., Sönmez, U., and Güvenç, L. (2012) Optimisation of the Nonlinear Suspension Characteristics of a Light Commercial Vehicle. *International Journal of Vehicular Technology,.*

[15] Els, P. and Uys, P. (2003) Investigation of the applicability of the Dynamic-Q optimisation algorithm to vehicle suspension design. *Mathematical and Computer Modelling,* **37**, 1029–1046.

[16] Georgiou, G., Verros, G., and Natsiavas, S. (2007) Multi-objective optimization of quarter-car models wih a passive or semi-active suspension system. *Vehicle System Dynamics: International Journal of Vehicle Mechanics and Mobility,* **45**, 77–92.

[17] Jonasson, M. and Roos, F. (2008) Design and evaluation of an active electromechanical wheel suspension system. *Mechatronics,* **18**, 218–230.

[18] Verros, G., Natsiavas, S., and Papadimitriou, C. (2005) Passive and Semi-active suspensios under random road excitation. *Journal of Vibration and control,* **11**, 581–606.

[19] Sheibe, F. and Smith, M. (2009) Analytical solutions for optimal ride comfort and tyre grip for passive vehicle suspensions. *Vehicle System Dynamics,.*

[20] Genta, G. and Campanile, P. (1989) An approximated approach to the study of motor vehicle suspensions with nonlinear shock absorber. *Meccanica,.*

[21] Baumal, A., McPhee, J., and Calamai, P. (1998) Application of genetic algorithms to the design optimization of an active vehicle suspension system. *Computer methods in applied mechanics and engineering,* **163**, 87–94.

[22] Goga, V. and Kl'ucik, M. (2012) Optimisation of vehicle suspension parameters with use of evolutionary computation. *Procedia Engineering,* **48**, 174–179.

[23] Pintado, P. and Benitez, F. G. (1988) Vehicle suspension optimisation. *Mathematical Computational Modelling,* **11**, 946–949.

[24] Gobbi, M., Mastinu, G., and Doniselli, C. (1999) Optimising a car chassis. *Vehicle System Dynamics: International Journal of Vehicle Mechanics and Mobility,* **32**, 149–170.

[25] Gobbi, M., Mastinu, G., Doniselli, C., Guglielmetto, L., and Pisino, E. (1999) Optimal and Robust Design of a Road Vehicle Suspension System. *Vehicle System Dynamics,* **33**, 3–22.

[26] Biral, F., Bortoluzzi, D., Cossalter, V., and Lio, M. D. (2003) Experimental Study of Motorcycle Transfer Functions for Evaluating Handling. *Vehicle System Dynamics: International Journal of Vehicle Mechanics and Mobility,* **39**, 1–25.

[27] Frendo, F., Sisi, A., Guiggiani, M., and Piazza, S. D. (2006) Analysis of motorcycle models for the evaluation of the handling performances. *Vehicle System Dynamics: International Journal of Vehicle Mechanics and Mobility,* **44**, 181–191.

[28] Cossalter, V. and Sadauckas, J. (2007) Elaboration and quantitative assessment of manoeuvrability for motorcycle lane change. *Vehicle System Dynamics: International Journal of Vehicle Mechanics and Mobility,* **44**, 903–920.

[29] Thompson, A. (1983) Suspension design for optimum road holding. *SAE Technical Paper 830663,*.

[30] Gobbi, M., Haque, I., Papalambros, P., and Mastinu, G. (2005) Optimisation and integration of ground vehicle systems. *Vehicle System Dynamics: International Journal of Vehicle Mechanics and Mobility,* **43**, 437–453.

[31] Sharp, R. and Crolla, D. (1987) Road Vehicle Suspension System Design - a review. *Vehicle System Dynamics,*.

[32] Jazar, R. (2017) Vehicle Dynamics, Springer, 3rd edition.

[33] van Vliet, M. Computer Aided Analysis and Design of Off-Road Motorcycle Suspensions PhD thesis Concordia University (October, 1983).

[34] Thompson, A. (1969) Optimum Damping in a Randomly Excited Non-Linear Suspension. *Proceedings of the Institution of Mechanical Engineers: Automobile Division,*.

[35] Dodds, C. and Robson, J. (1973) The description of road surface roughness. *Journal of Sound and Vibration,*.

[36] Robson, J. and Kamash, M. (1977) Road Surface Description in Relation to Vehicle Response. *Vehicle System Dynamics,* **6**, 153–157.

[37] Gobbi, M. and Mastinu, G. (2001) Analytical description and optimization of the dynamic behaviour of passively suspended road vehicles. *Journal of Sound and Vibration,*.

[38] Dixon, J. (2007) The shock absorber handbook, Professional Engineering Publishing and John Wiley & Sons, .

[39] Metwalli, S. (1986) Optimum Nonlinear Suspension Systems. *Journal of Mechanisms, Transmissions, and Automation in Design,*.

[40] Cossalter, V. (2006) Motorcycle Dynamics, Lulu, .

[41] Catania, G., Leonelli, L., and Mancinelli, N. (2010) Optimization of the damping parameters of a sport motorcycle. *Information not found,*.

[42] Tey, J., Ramli, R., Khengb, C., Chongc, S., and Abidind, M. (2014) Identification of vehicle suspension parameters by design optimization. *Engineering Optimization,* **46**(5), 669–686.

[43] Gadvi, B., Savsani, V., and V.Patel (2016) Multi-Objective Optimization of Vehicle Passive Suspension System using NSGA-II, SPEA2 and PESA-II. *Procedia Technology,* **23**, 361–368.

[44] Acosta, M., Kanarachos, S., and Blundell, M. (2017) Virtual Tyre Force Sensors: An Overview of Tyre Model-based and Tyre Model-less State Estimation Techniques. *Proceedings of the Institution of Mechanical Engineers, Part D: Journal of Automobile Engineering,* **(in press)**, (in press).

[45] Teerhuis, A. P. and Jansen, T. (2012) Motorcycle state estimation for lateral dynamics. *Vehicle System Dynamics,* **50**, 1261–1276.

[46] Slimi, H., Arioui, H., and Mammar, S. (2013) Motorcycle lateral Dynamic Estimation and Lateral Tire-Road Forces Reconstruction Using Sliding Mode Observer. *IEEE Intelligent Transportation System Conference,* pp. 821–826.

[47] Shabana, A. (2005) Dynamics of Multibody Systems, Cambridge University Press, 3rd edition.

[48] Lot, R. and da Lio, M. (2004) A Symbolic Approach for Automatic Generation of the Equations of motion of Multibody Systems. *Multibody System Dynamics,* **12**(2), 147–172.

[49] Lot, R. and Massaro, M. (2017) A Symbolic Approach to the Multibody Modeling of Road Vehicles. *International Journal of Applied Mechanics,* **09**(05).

[50] Wang, E. and Hull, M. (1997) A dynamic system model of an off-road cyclist. *Journal of Biomechanical Engineering,* **119**, 248–253.

[51] Popov, A., Rowell, S., and Meijaard, J. (2010) A review on motorcycle and rider modelling for steering control. *Vehicle System Dynamics: International Journal of Vehicle Mechanics and Mobility,*.

[52] Massaro, M. (2011) A nonlinear virtual rider for motorcycles. *Vehicle System Dynamics: International Journal of Vehicle Mechanics and Mobility,*.

[53] Lot, R., Massaro, M., and Sartori, R. (2008) Advanced motorcycle virtual rider. *Vehicle System Dynamics: International Journal of Vehicle Mechanics and Mobility,* **46**, 215–224.

[54] Wilczynski, H. (1994) A dynamic system model for estimating surface-induced frame loads during off-road cycling. *Journal of Mechanical Design,* **116**, 816 – 822.

[55] Cocq, P., Muller, M., Clayton, H., and van Leeuwen, J. (2013) Modelling biomechanical requirements of a rider for different horse-riding techniques at trot. *Journal of Experimental Biology,* **216**, 1850–1861.

[56] Els, P., Theron, N., Uys, P., and Thoresson, M. (2007) The ride comfort vs handling compromise for off-road vehicles. *Journal of Terramechanics,* **44**, 303–317.

[57] Liguori, C., Paciello, V., Paolillo, A., Pietrosanto, A., and Sommella, P. (2013) Characterization of motorcycle suspension systems: Comfort and handling performance evaluation. In *IEEE Instrumentation and Measurement Technology Conference* pp. 444–449.

[58] Thoresson, M., Uys, P., Els, P., and Snyman, J. (2009) Efficient optimisation of a vehicle suspension system, using a gradient-based approximation method, Part1: Mathematical modelling. *Mathematical and Computer Modelling,* **50**, 1421–1436.

[59] Naud, A. and Snyman, J. (2003) Optimisation of road vehicle passive suspension systems. Part 1. Optimisation algorithm and vehicle model. *Applied Mathematical Modelling,* **27**, 249–261.

[60] Uys, P., Els, P., and Thoresson, M. (2007) Suspension settings for optimal ride comfort of off-road vehicles travelling on roads with different roughness and speeds. *Journal of Terramechanics,* **44**, 163–175.

[61] Cossalter, V., Doria, A., and Lot, R. (2000) Optimum suspension design for motorcycle breaking. *Vehicle System Dynamics: International Journal of Vehicle Mechanics and Mobility,* **54**, 175–198.

[62] Lozoya-Santos, J., Cervantes-Muñoz, D., Tudon-Martinez, J. C., and Ramirez-Mendoza, R. (2015) Off-Road Motorbike Performance Analysis Using a Rear Semi-active EH Suspension. *Shock and Vibration,*.

[63] Moreno-Ramirez, C. and Tomas-Rodriguez, M. (2014) Non linear optimization of a sport motorcycle's suspension interconnection system. In *UKACC International Conference on Control (CONTROL).*

[64] Els, P. (2005) The applicability of ride comfort standards to off-road vehicles. *Journal of Terramechanics,* **42**, 47–64.

[65] Durbin, T., Smith, M., Wilson, R., and Rhee, S. (2004) In-use activity measurements for off-road motorcycles and all-terrain vehicles. *Transportation Research Part D,.*

[66] www.mathworks.com. (May, 2019).

[67] www.planetmath.org/ProofOfGeneralMeansInequality. (May, 2020).

[68] Acosta, M., Kanarachos, S., and Fitzpatrick, M. (2017) Accurate Virtual Sensing of Vertical Tire Forces for Enhanced Handling Dynamics. In *IEEE 978-1-5386-1127-2/17.*

[69] Delvecchio, D., Spelta, C., and Savaresi, S. M. (2011) Estimation of the Tire Vertical Deflection in a Motorcycle Suspension via Kalman-Filtering Techniques. In *IEEE 978-1-4577-1063-6/11.*

[70] www.multibody.net. (May, 2019).

[71] www.maplesoft.net. (May, 2019).

[72] Lawson, C. and Hanson, J. (1974) Solving Least-Sqaures Problems, Prentice Hall, .

[73] www.design-simulation.com/wm2d.

[74] Simpson, K., Ciapponi, T., and Wang, H. (2000) Exercise and sport science, Lippincott William & Wilkins, 1st edition.

[75] Cheli, F., Mazzoleni, P., Pezzola, M., Ruspini, E., and Zappa, E. (2003) Vision-based measuring system for rider's pose estimation during motorcycle riding.. *Mechanical Systems and Signal Processing,.*

[76] https://youtu.be/NTqFmdJxWmI. (May, 2019).

[77] DeCarbon, C. (1950) Théorie mathématique et réalisation pratique de la suspension amortie des vehicules terrestres. *Communication au 3 Congrès Technique Internationale de l'Automobile, Paris,.*

[78] Walls, J., Houbolt, J., and Press, H. (1954) Some measurements and power spectra of runaway roughness. *N.A.C.A. Technical note 3305,.*

[79] Cossalter, V. and Lot, R. (2002) A Motorcycle Multi-Body Model for Real Time Simulations Based on the Natural Coordinates Approach. *Vehicle System Dynamics,* **37**, 423–448.

[80] Cossalter, V., Lot, R., and Maggio, F. (2003) A Multibody Code for Motorcycle Handling and Stability Analysis with Validation and Examples of Application. *SAE Technical Paper,*.

[81] Lot, R., Cossalter, V., and Maggio, F. (2007) An Integrated Multi-Body Software for the Design of Motorcycles. *Proc. of the 11th European Automotive Conference EAEC 2007„*.

[82] Cossalter, V., Dalla Tore, G., Lot, R., and Massaro, M. (2009) An Advanced Multibody Code for the Analysis of Motorcycle Dynamics. *Proc. of 3rd Internation Conference of Mechanical Engineering and Mechanics,*.

[83] Vasquez, F., Lot, R., Rustighi, E., and Pegoraro, R. (2019) Tyre force estimation for off-road motorcycles. *In press,*.

[84] Park, K. I. (2018) Fundamentals of Probability and Stochastic Processes with Applications to Communications, Springer, .

[85] Soong, T. (2004) Fundamentals of probability and statistics for engineers, John Wiley & Sons, .

[86] www.mathworks.com/help/gads/gamultiobj.html. (August, 2019).

[87] Agostinacchio, M., Ciampa, D., and Olita, S. (2014) The vibrations induced by surface irregularities in road pavements - a Matlab approach. *European Transport Research Review,* **6**, 267–275.